UNIVERSITÀ
DEGLI STUDI
DI BRESCIA

DIPARTIMENTO DI MEDICINA MOLECOLARE E TRASLAZIONALE

DOTTORATO DI RICERCA IN GENETICA MOLECOLARE,
BIOTECNOLOGIE E MEDICINA SPERIMENTALE
Ciclo XXXVI

Settori Scientifici Disciplinari
BIO/13 Biologia Applicata
MED/27 Neurochirurgia

Molecular characterization of human glioblastoma: longitudinal follow-up of plasmatic microRNAs levels by droplet digital PCR

Dottor Carmine Antonio Donofrio

Supervisore:
Ch.ma Prof.ssa Giuseppina De Petro
Università degli Studi di Brescia, Brescia, I.

Co-Supervisori:
Ch.mo Prof. Alessandro Salvi
Università degli Studi di Brescia, Brescia, I.

Ch.mo Prof. Franco Servadei
Humanitas University di Milano, Milano, I

a.a. 2022/2023

ABSTRACT

In uno studio longitudinale prospettico caso-controllo sono stati analizzati, mediante droplet digital PCR, microRNA plasmatici, in particolare miR 21-5p, miR 23b-3p e miR 34a-5p, in qualità di biomarcatori periferici di astrocitomi IDH-mutati e glioblastomi IDH-wildtype grado 4 (secondo la quinta edizione della classificazione dei tumori del sistema nervoso centrale dell'Organizzazione Mondiale della Sanità).

L'espressione plasmatica di miR 21-5p, miR 23b-3p e miR 34a-5p è stata documentata sia nei volontari sani sia nei pazienti al momento della diagnosi. Sono stati registrati livelli circolanti di miR 34a-5p significativamente più elevati nei pazienti rispetto ai volontari sani, identificando un cut-off diagnostico assoluto di 1.25 copie/μL. Inoltre, è stato possibile riconoscere due gruppi di pazienti, rispettivamente con alte e basse concentrazioni plasmatiche assolute di miRNA al momento della diagnosi.

miR 21-5p, miR 23b-3p e miR 34a-5p hanno mostrato lo stesso andamento longitudinale nel tempo con un progressivo aumento a 1 e 3 mesi dopo l'intervento chirurgico, momento in cui sono state registrate le concentrazioni massime, seguito da una graduale diminuzione a 6 e 12 mesi dall'intervento.

Correlazioni significative dei livelli plasmatici di ciascun miRNA sono state identificate tra il momento della diagnosi e 1 mese dopo l'intervento chirurgico e, più interessante, è stata riscontrata una correlazione reciproca tra le concentrazioni di miR 21-5p e miR 23b-3p a ciascun *timing point* e tra miR 21-5p e miR 34a-5p al momento della diagnosi. Una *network analysis* ha evidenziato alcune possibili vie molecolari di interazione tra questi miRNA nel contesto patologico dei gliomi, come i meccanismi di controllo del ciclo (E2F1, E2F3, RB1, CDK6) e della crescita cellulare (PTEN, PIK3R1, IGF1R). Infine, livelli elevati di miRNA circolanti sono risultati predittori affidabili di sopravvivenza globale e sopravvivenza libera da malattia. Nonostante la novità dei risultati descritti nel nostro lavoro, si rendono necessari ulteriori futuri studi che prendano in analisi più ampie coorti di pazienti per supportare i nostri dati.

1. INTRODUCTION

1.1 Liquid biopsy and glioblastoma

The identification of circulating biomarkers for 'liquid biopsy' is gradually surging in popularity in the oncology research fields due to its potential huge clinical applications for population screening, tumor monitoring and delivery of targeted therapies deriving from tumor molecular profiling. Liquid biopsies are "non-invasive" procedures based on sampling and analysing circulating tumour cells, tumour DNA, cell-free RNA, extracellular vesicles, tumour-educated platelets, proteins and metabolites derived from various biological fluids[1,2]. MicroRNAs (miRNAs), a family of small non-coding RNAs, are deregulated in patients affected by cancer. Detection of tumour-specific peripheral biomarkers may be also useful in managing patients affected by primary brain tumours[3-7].

Glioblastoma (GBM) is the most frequent primary malignant brain tumour in adults, accounting for approximately 15% of all intracranial neoplasms and 45-50% of all primary malignant brain tumours. The annual incidence of GBM is between 3.19 and 3.55 cases per 100000 people *per* year in Europe and USA. GBM preferentially affects older adults, with a peak of incidence between 55 and 85 years[8,9]. These malignant brain tumours progress rapidly and clinical presentation largely depends on their location. They may manifest with focal neurological deficits, behavioural alterations, neurocognitive impairment, seizures and signs or symptoms of increased intracranial pressure, such as headaches, nausea and vomiting. The gold standard of treatment for GBM is surgical resection followed by concurrent conformal radiotherapy (RT) and chemotherapy[10-13]. Nevertheless, GBM has a dismal prognosis, with the highest mortality rate within 15-18 months after diagnosis, and a 5-year overall survival (OS) lower than 5%[8,9].

Despite growing efforts, no peripheral biomarker has been validated for GBM. Different circulating factors have been explored in the context of GBM, but variable and sometimes conflicting results have been reported[5,6,14-16]. miRNA levels in serum and plasma are more stable, reproducible and consistent among individuals in comparison with other circulating nucleic acids[17,18]. Furthermore, there is a lack of studies that take into consideration the major revisions of the fifth edition of the World Health Organization (WHO) Classification of Tumours of the Central Nervous System (CNS)[13,19]. The revised classification of adult-type, diffuse astrocytic gliomas distinguishes **astrocytoma, IDH-mutant WHO grade 4** from **GBM, IDH-wildtype WHO grade 4**. Molecular parameters have been added as biomarkers of grading in addition to histological features, such as microvascular proliferation and/or necrosis. Astrocytomas IDH-mutant WHO grade 4 are diagnosed in case of *CDKN2A/B* homozygous deletion, and GBM IDH-wildtype WHO grade 4 in case of *TERT* promoter mutation, *EGFR* amplification or +7/-10 signature (combined gain of chromosome 7 and loss of chromosome 10)[13,19,20].

1.2 microRNAs and their role in cancer

In the context of circulating biomarkers, our interest focused on miRNAs, small non-coding RNAs, typically 20-23 nucleotides in length[21-25]. They are synthesized by RNA pol II as *primary miRNA* (*pri-miRNAs*), then processed into *precursor miRNAs* (*pre-miRNAs*) and *miRNA duplex* by consecutive ribonuclease cleavages – Drosha-Pasha complex, Dicer in the cell nucleus and cytoplasm respectively (**Figure 1**).

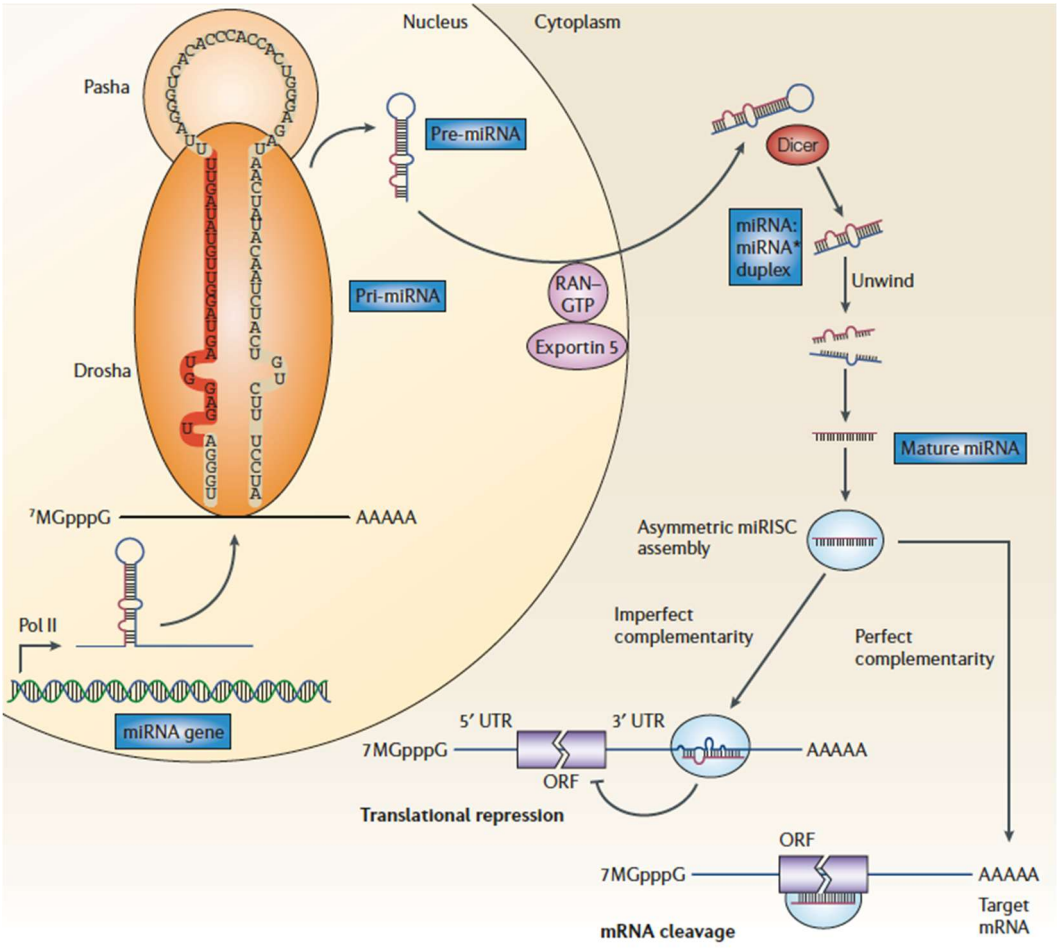

Figure 1 – The biogenesis of miRNAs; from Esquela-Kersher 2006[21].

miRNAs act mainly as post-transcriptional regulators of gene expression and particularly as 'silencers' of messenger RNAs (mRNA)[21-28]. The base pairing of miRNAs to target mRNAs depends primarily on 7-8 nucleotides at their 5′ end, known as 'seed region'. Consequently, each miRNA may target many mRNAs and each mRNA can be targeted by multiple miRNAs altering the cellular phenotype[25,26,29]. Depending on the degree of complementarity of their pairing, miRNAs exert their regulatory effect in two ways: i) mRNA degradation, and ii) translation inhibition. miRNAs that bind with perfect or nearly perfect complementarity to mRNA sequences induce the cleavage and degradation of mRNA transcripts by ribonucleases in the miRNA-associated induced-silencing complex (miRISC). miRNAs that pair with imperfect complementary sites within the 3′ untranslated

regions of their mRNA targets repress the target-gene expression post-transcriptionally, by blocking translation initiation and/or elongation[21,29] (**Figure 1**).

miRNAs are expressed both in physiological and pathological conditions. They exhibit a causal role in tumorigenesis of a wide variety of human cancers, acting either as *onco-miRNAs* or *tumour-suppressor miRNAs*. miRNAs are detectable in tumour tissues and biological fluids, such as peripheral blood, because released by tumour and/or microenvironment cells[17,21,23-25,27,28,30]. Three major potential pathways have been hypothesized for miRNAs to enter the circulation: i) energy-free passive release from damaged cells consequent to apoptosis or necrosis into circulation; ii) active and selective secretion mediated by the RNA-binding protein dependent pathway; iii) active and selective secretion facilitated by extra-cellular vesicles[18,31] (**Figure 2**).

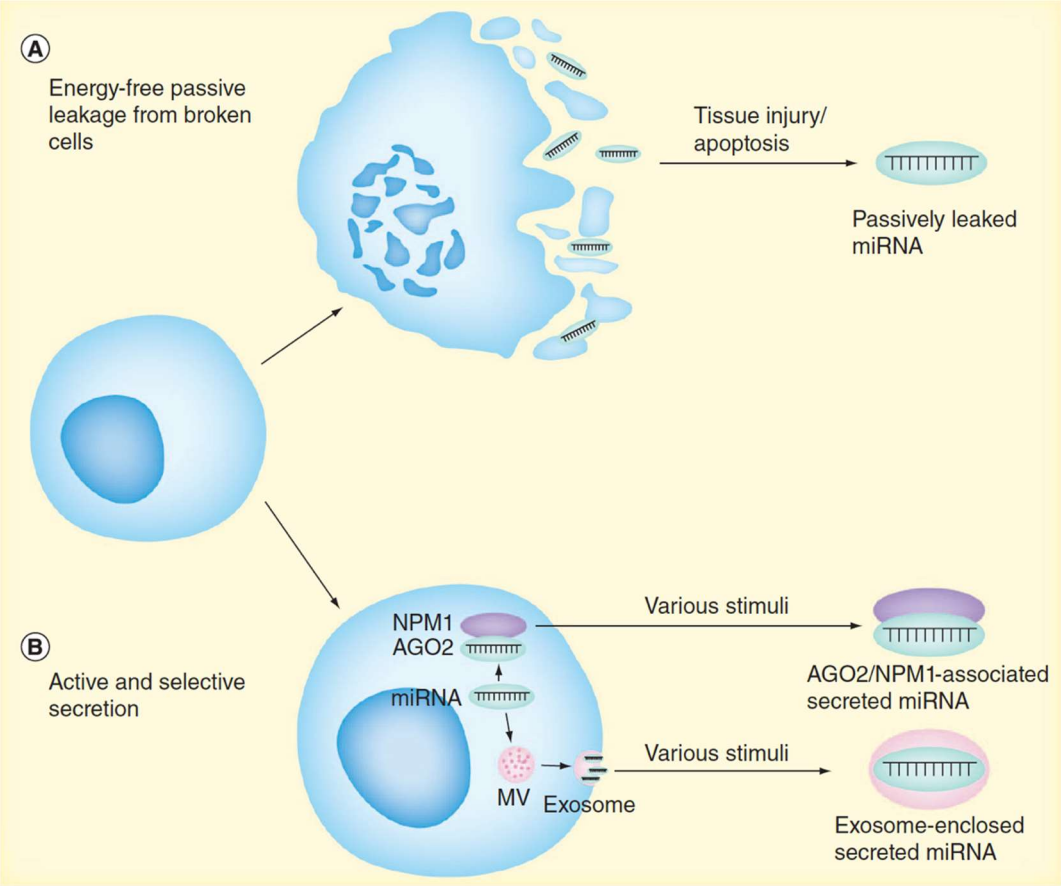

Figure 2 – Sources of circulating miRNAs; from Redova 2013[18].

1.3 Detection of circulating miRNAs by droplet digital polymerase chain reaction (ddPCR)

Measurements of circulating transcripts' expression levels, especially miRNAs, may be challenging because of their low concentrations.

miRNAs can be detected and quantified by reverse transcriptase polymerase chain reaction (PCR) achieved by real-time quantitative PCR (qPCR) or digital PCR.

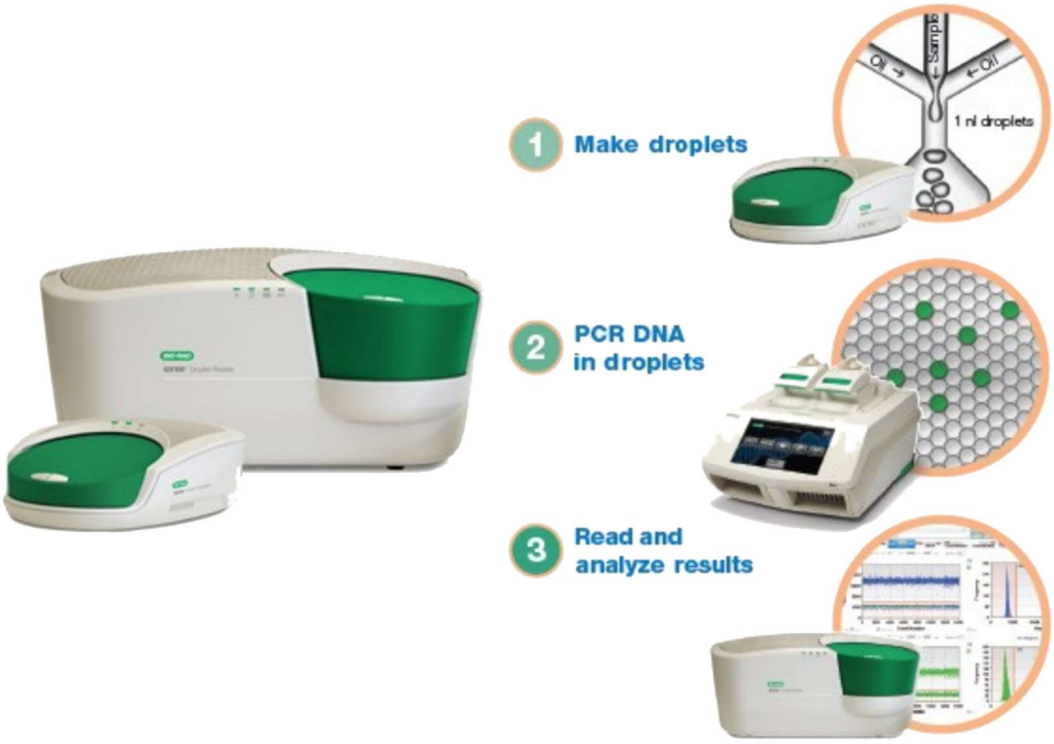

Figure 3 – ddPCR workflow (Bio-Rad Laboratories, Inc.; Hercules, CA, USA).

Digital PCR builds on traditional PCR amplification steps (denaturation, annealing and extension cycles) and intercalating dye and fluorescent probe-based detection methods to provide a highly sensitive absolute quantification of nucleic acids without the need for endogenous controls and standard curves. Particularly, the droplet digital PCR (ddPCR) is a method (**Figure 3**) based on water-oil emulsion droplet technology[32]. The sample is partitioned into 20,000 nanoliter-sized droplets. Template molecules are distributed randomly among droplets, such that some droplets have no template molecules and others have one or more (at most few). Each droplet undergoes PCR amplification and fluorescence analysis separately. The droplets are then individually counted and scored as *positive* or *negative* by passing in a single stream through a fluorescence detector. Due to the random nature of the partitioning, the fluorescence data after amplification – the ratio between the number of positive events (positive droplets) and the total number of independent events (the total number of droplets) – are well fitted by a Poisson distribution – a function that relates the probability of a given number of events occurring independently in a given sample when the average rate of occurrence is known – to determine the absolute copy number of the target DNA molecule (copies/µL) in the input reaction mixture.

2. AIMS OF THE STUDY

This study is aimed to develop a new line of research in neuro-oncology focusing on circulating biomarkers in GBM.

The discovery of miRNAs, both cellular and extracellular miRNAs has revealed their great potential as novel and robust diagnostic and prognostic cancer biomarkers. miRNAs can effectively control tumorigenesis by affecting different signal transduction pathways[15,33]. Data obtained from tissue biopsies (mainly by RNA-sequencing technology) have been catalogued in the OncomiR Cancer database (OMCD) www.oncomir.umn.edu/omcd, where only 5 cases of GBM have been reported[34]. Liquid biopsies are not included in the OMCD and their results in patients affected by GBM are extremely variable, in part due to challenges of carrying out accurate measurements of transcripts' expression levels[5,6,15,16].

The primary objective of our study was to correlate the circulating levels of non-coding RNAs in patients affected by GBM with clinical, neuroradiological and pathological tumour features in order to identify the possible role of peripheral GBM biomarkers as early and reliable predictors of tumour response to treatments (surgery, radiotherapy and chemotherapy), tumour recurrence and patients' survival. We focused on circulating miRNAs[4,17,18,30] selected according to literature review, analysing their plasmatic levels both in patients affected by GBM and healthy volunteers:

- **miR 21-5p**, an *onco-miRNA* highly expressed in cell cultures, tumour tissue and serum or plasma derived from patients affected by GBM[14,15,35-44];
- **miR 23b-3p**, overexpressed in GBM tissue and cell cultures[45-48];
- **miR 34a-5p**, a *tumour suppressor miRNA* investigated in cell cultures, tumour tissue and serum or plasma of patients with GBM[15,37,39,44,49-53].

3. MATERIALS AND METHODS

3.1 Study population

Twenty-three patients presenting with diffuse high-grade astrocytic gliomas (**Figure 4**) operated at the Neurosurgical Department of the ASST Cremona between April and December 2021 were prospectively included in the study.

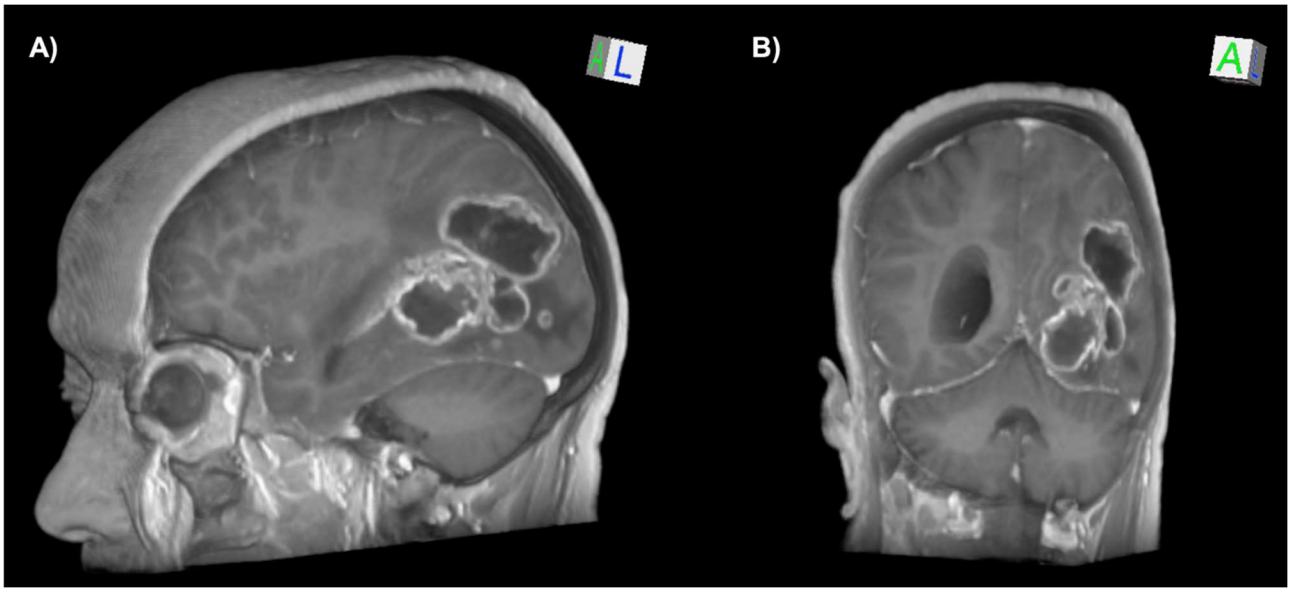

Figure 4 – Diffuse high-grade astrocytic glioma appearance on T1-weighted post-contrast sequences: **A**) 3D sagittal reconstruction; **B**) 3D coronal reconstruction.

The patients' inclusion criteria were: age older than 18 years, prognosis greater than six months, Karnofsky performance status (KPS) ≥70 and pathological report consistent with **GBM IDH-wildtype WHO grade 4** or **astrocytoma IDH-mutant WHO grade 4**[13,19]. Furthermore, 32 healthy volunteers were enrolled in the study.

All the procedures were conducted in accordance with the ethical standards of the institutional research committee and with the 1964 Helsinki declaration and its later amendments. Informed consent was obtained from all patients and healthy volunteers. The local ethics committee approved the study (protocol number 32219, dated 2 October 2019).

3.2 Preoperative clinical, neuroradiological and surgical features

Clinical, neuroradiological and surgical characteristics were collected and recorded in an anonymized database.

The clinical features included: age at diagnosis, gender, KPS, modified Rankin scale (mRS) and medical therapies. According to KPS, used to quantify general well-being and independence in daily life activities, patients were classified as “independent” (KPS ≥90) or “dependent” (KPS ≤80). Similarly, they were categorized as “presenting” (mRS > 2) or “non-presenting” (mRS ≤ 2) significant disabilities in keeping with mRS, a specific score for neurological pathological conditions[54]. Therapies with steroids (dexamethasone) and anti-epileptic drugs (i.e. levetiracetam, lacosamide) at the time of diagnosis were registered.

Tumour location, volume, contrast enhancement and necrosis were assessed by two independent investigators on preoperative magnetic resonance imaging (MRI) images.

3.3 Treatments

3.3.1 Surgery

All patients underwent microsurgical fluorescence-guided tumour resection by craniotomy or frameless neuronavigated robotic-assisted biopsy, in keeping with the patient’s and tumour’s characteristics. They were administered an oral solution of 5-aminolevulinic acid (5-ALA, 20 mg/Kg of body weight) between 2 and 4 hours prior to surgery. Tumour fluorescence intensity was assessed under microscopic blue light (wavelength: 375-440 nm) and defined as “absent”, “faint” or “strong”[55] (**Figure 5**).

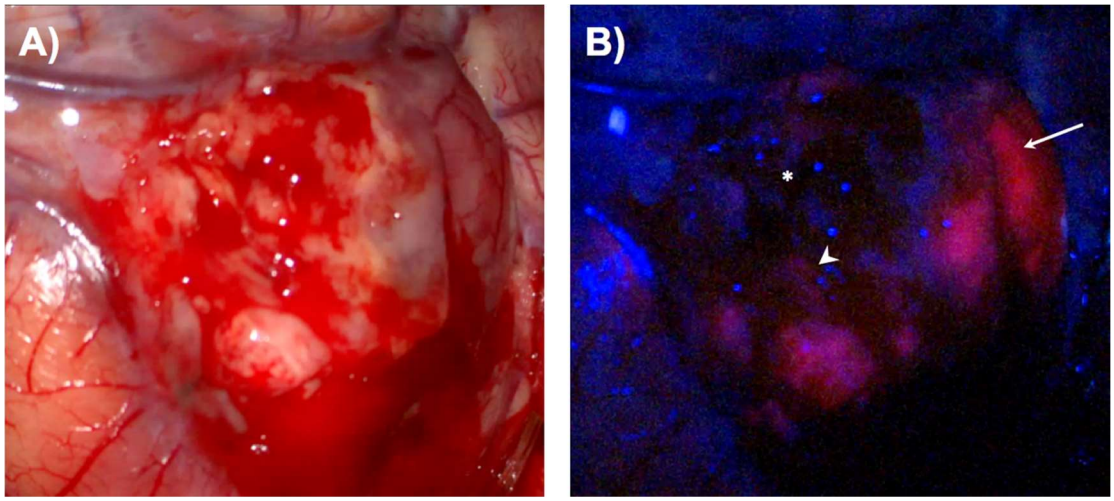

Figure 5 – Fluorescence-guided (5-ALA) microscopic tumour resection (Zeiss; Oberkochen, Germany): **A**) intraoperative microscopic tumour appearance under white light (10x); **B**) intraoperative microscopic tumour appearance under blue light (wavelength: 375-440 nm): “absent” (white asterisk), “faint” (white arrowhead) and “strong” (white arrow) tumour fluorescence intensity (10x).

3.3.2 Adjuvant therapies: radiotherapy and chemotherapy

One month after surgery, patients with newly diagnosed GBM IDH-wildtype WHO grade 4 or astrocytoma IDH-mutant WHO grade 4 underwent conformal RT and concomitant chemotherapy with temozolomide, an alkylating agent that add methyl groups to the purine and pyrimidine groups particularly inducing the formation of O^6-methylguanine (O^6MeG), which leads to DNA double-strand breaks, chromosomal aberrations and ultimately cell death[56-58].

RT was delivered following a standard or hypo-fractionated protocol. The standard RT protocol was based on 2 Gy per daily fraction, 5 days per week, over 6 weeks, for a total dose of 60 Gy. The hypo-fractionated RT protocol was reserved to patients older than 70 or with postoperative KPS lower than 70 and was planned to reach a total dose of 40 Gy in 15 fractions over 3 weeks[12]. RT was delivered to the gross tumor volume with a 2-to-3-cm margin for the clinical target volume. Concomitant temozolomide was administered at a dose of 75 mg per square meter of body-surface area per day, 7 days per week from the first until the last day of RT, however for no longer than 49 days[10,11]. After a 4-week break, patients clinically and neurologically fit for chemotherapy were administered up to 12 cycles of adjuvant chemotherapy with temozolomide following a 5-day schedule every 28 days at a dose of 150 mg per square meter of body-surface area for the first cycle, increased to 200 mg per square meter of body-surface area per day, until unacceptable toxicity, tumour progression, recurrence or death[10,11].

Patients experiencing tumour recurrence during adjuvant temozolomide and those with recurrent GBM were operated and then started on regorafenib, an oral inhibitor of several kinases involved in tumour angiogenesis (VEGFR1-3, TIE2), oncogenesis (KIT, RET, RAF1, BRAF), interactions between tumour and microenvironment (PDGFR, FGFR), and tumour immunity (CSF1R). Regorafenib was administered at a dose of 160 mg per day, 7 days per week for the first 3 weeks every 4-week cycle, 4 weeks after surgery in case of operation. Dose reduction, to 120 mg or 80 mg per day, or treatment discontinuation were adopted in case of toxicity[59].

3.4 Pathology

The histological diagnosis followed the fifth edition of the WHO Classification of Tumours of the CNS[19]. Tumour tissue was fixed in buffered 10% formalin for 24-48 hours, dehydrated in graded alcohols and paraffin embedded following the standard protocols. Serial 3-μm thick sections were obtained from paraffin tumour blocks and mounted on glass slides, then underwent deparaffinization (by rinsing into a bath of xylene twice for 5 minutes each) and hydration (by rinsing into ethanol baths at reducing concentrations 100%, 90% and 70% and distilled water three times for 5 minutes each) before staining.

3.4.1 Histology

Serial sections were stained with hematoxylin and eosin (H&E). GBM typically appear as highly cellular tumours, usually composed of poorly differentiated, sometimes pleomorphic, tumour cells with nuclear atypia and brisk mitotic activity. Prominent microvascular proliferation and/or necrosis are essential diagnostic features (**Figure 6**).

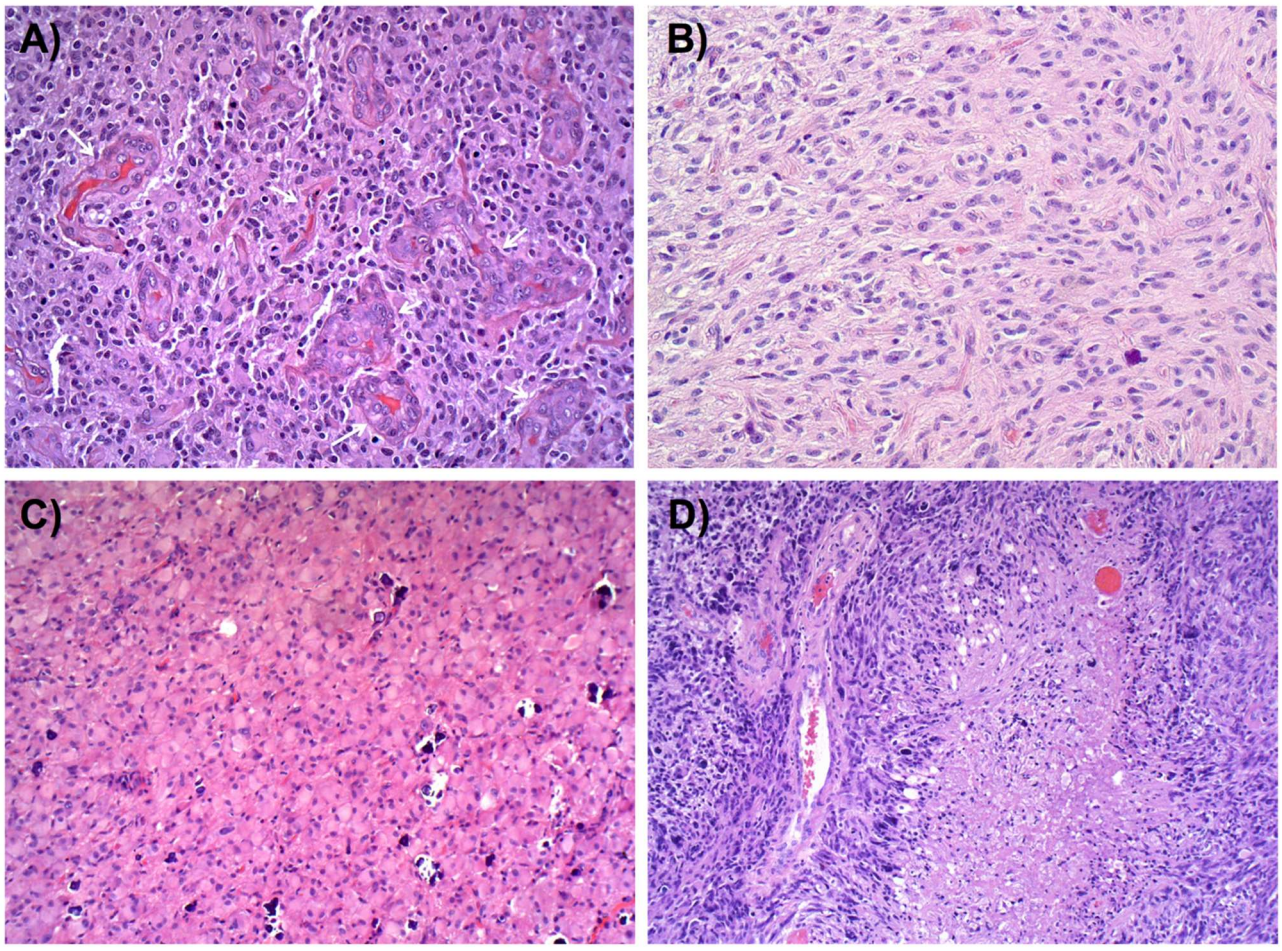

Figure 6 – GBM's morphological features: **A**) microvascular proliferation (white arrows; H&E – 20x); **B**) tumour cells with spindle features (H&E – 20x); **C**) tumour cells with epithelioid features and microcalcifications (H&E – 10x); **D**) necrosis (H&E – 10x).

3.4.2 Immunohistochemistry

Immunohistochemical (IHC) analyses were performed using the BOND Polymer Refine Detection system on the LEICA BOND III staining platform (Leica Biosystem; Wetzlar, Germany) for primary antibodies directed against the following antigens: synaptophysin (clone 27G12; 1:200), neurofilament (clone 2F11; 1:500), NeuN (A60; 1:500), GFAP (clone GA.5; 1:400), SOX10 (clone BC34; 1:200), EMA (clone E29; 1:500), CD34 (clone QBEnd/10; 1:1000), ATRX (polyclonal; 1:400), IDH1 R132H (clone H09; 1:50) and p53 (clone DO-7; 1:100). Otherwise, Roche's antibodies ready

to use were detected on the platform BenchMark ULTRA using the UltraView Universal DAB Detection Kit (Roche; Basel, Switzerland) for: Ki-67 (clone 30-9; prediluted) with the Ultraview Amplification Kit; BRAF (clone VE1; prediluted) and OLIG 2 (clone EP112; prediluted) with the Optiview Amplification Kit.

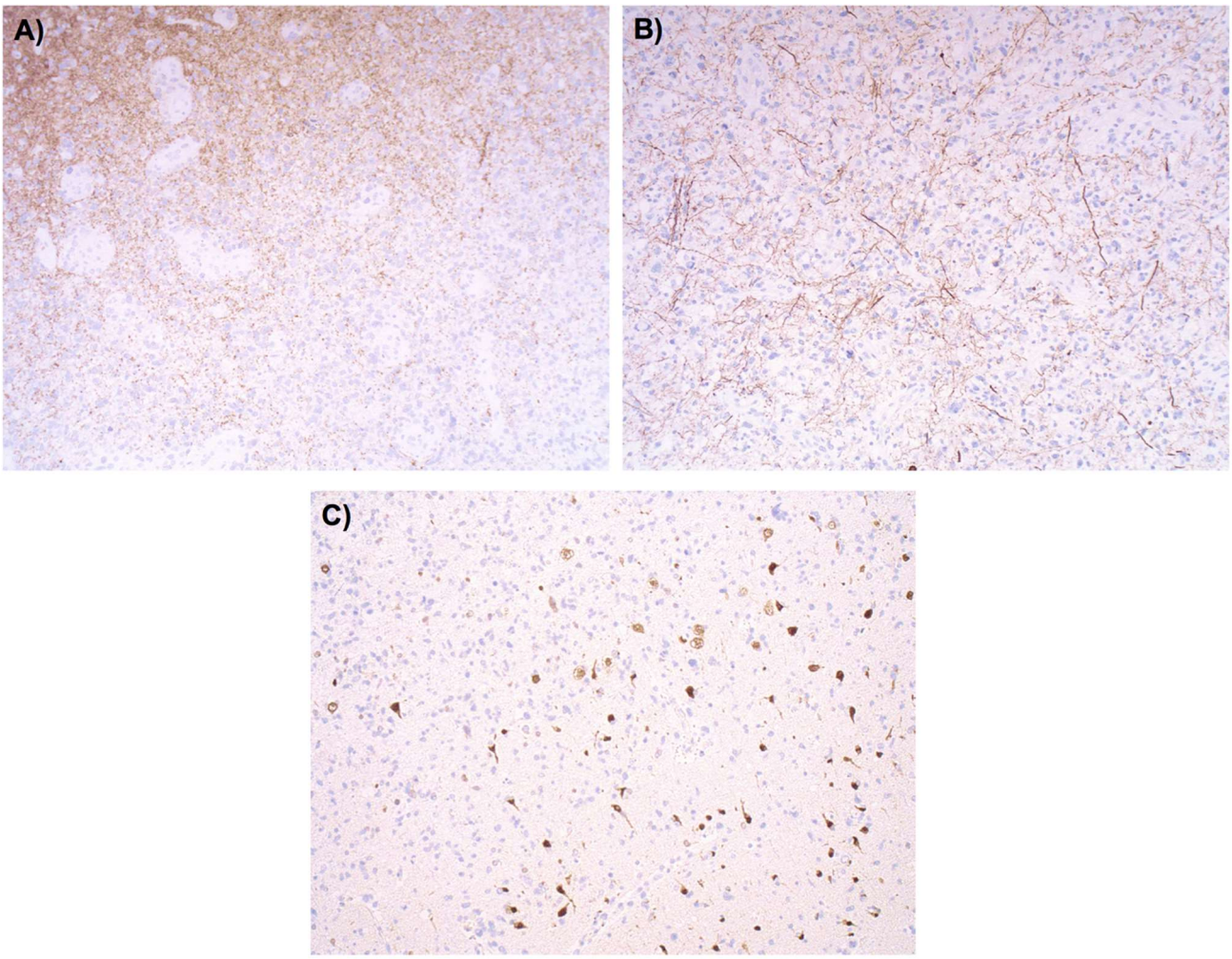

Figure 7 –GBM infiltration (synaptophysin, neurofilament, NeuN negative) of brain tissue (synaptophysin, neurofilament, NeuN positive): **A**) IHC for synaptophysin (10x); **B**) IHC for neurofilament (10x); **C**) IHC for NeuN (10x).

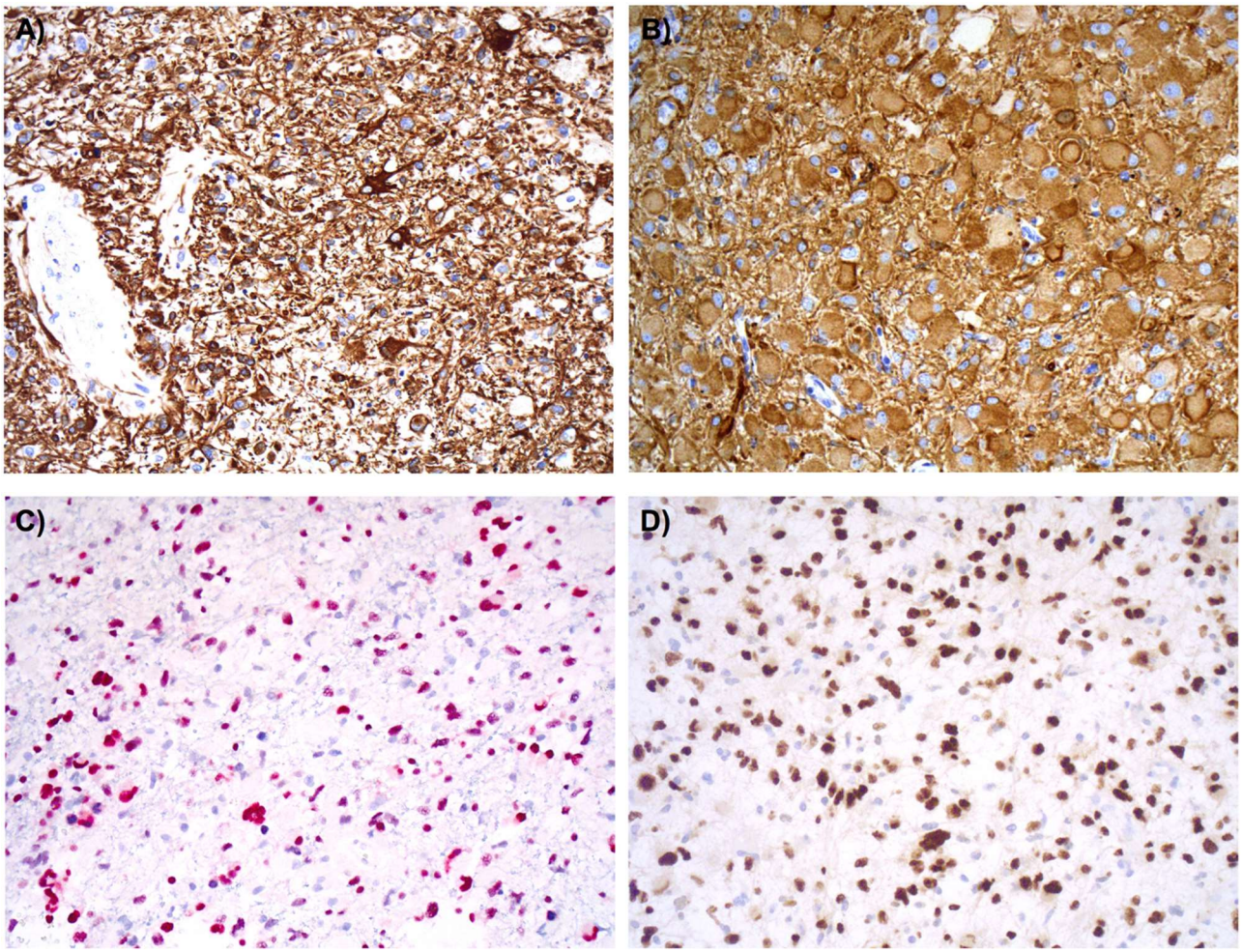

Figure 8 – **A**, **B**) GFAP expression in GBM: (IHC – 20x); **C**) SOX10 positivity in GBM (IHC – 20x); **D**) Olig2 positivity in GBM (IHC – 20x).

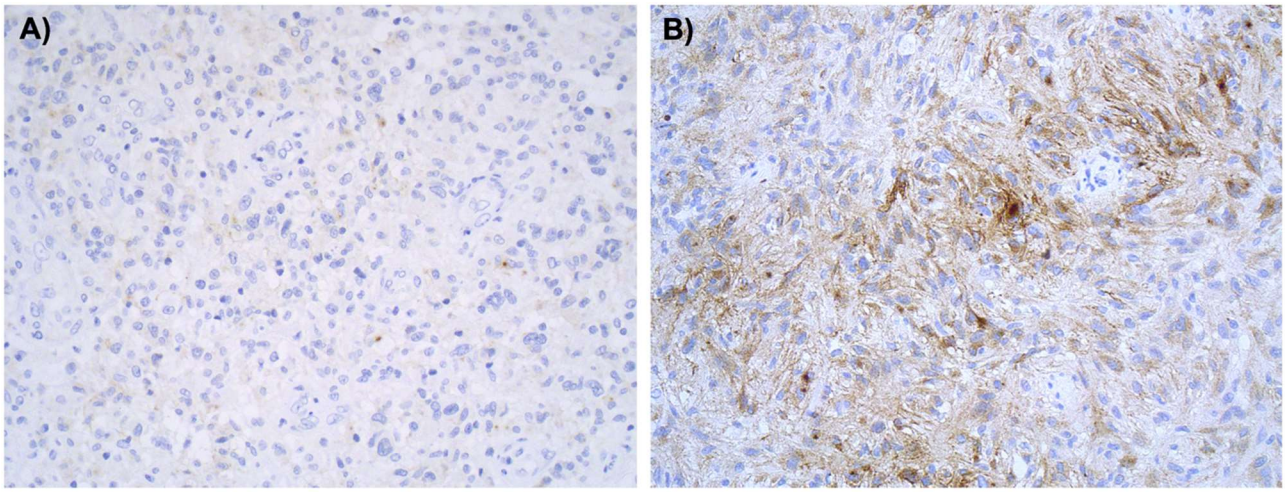

Figure 9 – EMA expression in GBM: **A**) negative (IHC – 20x); **B**) positive (IHC – 20x).

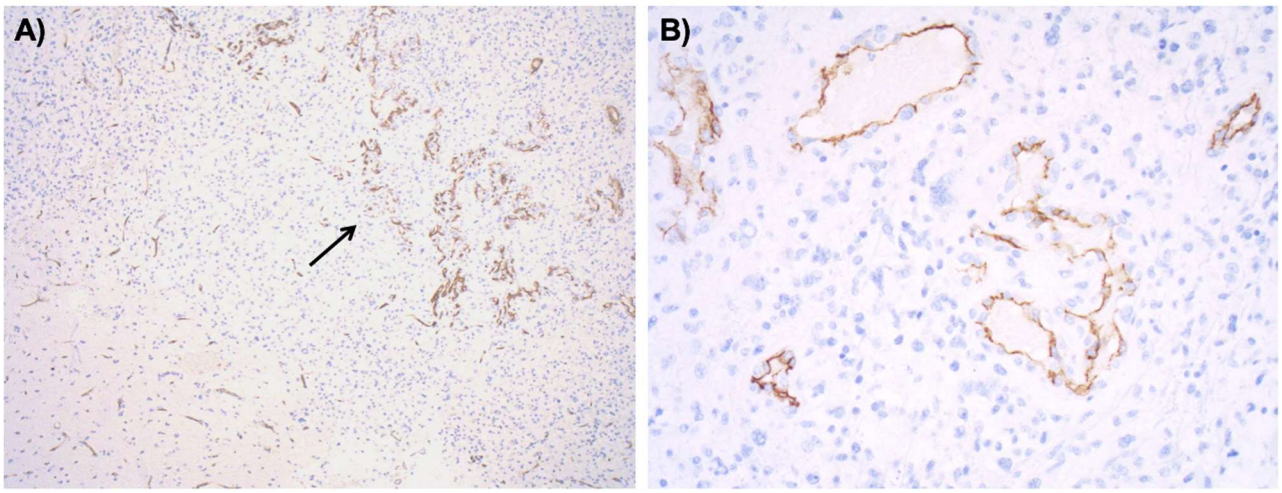

Figure 10 – GBM microvascular proliferation: **A**) vascular patterns in normal brain tissue and tumour (black arrow) (CD34; IHC – 4x); **B**) microvascular tumour proliferation (CD34; IHC – 20x).

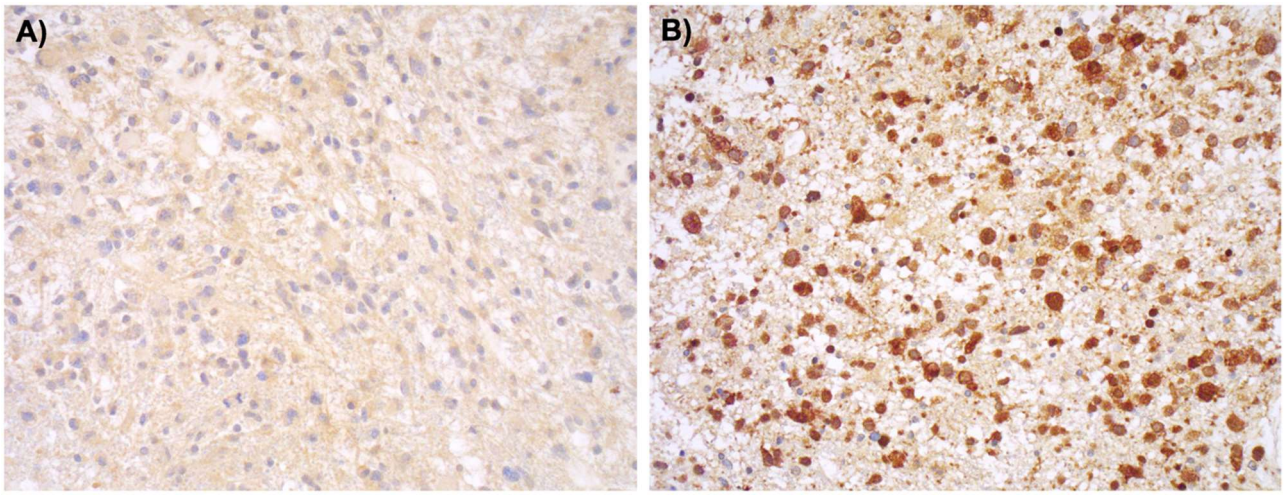

Figure 11 – IDH1 R132H status in GBM: **A**) IDH1 wild-type (negative; IHC – 20x); **B**) IDH1 mutant (positive; IHC – 20x).

The stainings for ATRX and p53 underwent semi-quantification by two expert neuropathologists. ATRX expression was classified as "lost" or "retained" (**Figure 12**), while p53 as "absent", "intermediate", or "strong" (**Figure 13**). ATRX is a chromatin remodelling protein and its loss of function causes microsatellite instability and telomere maintenance impairment but also increased tumour sensitivity to alkylating agents and RT[60].

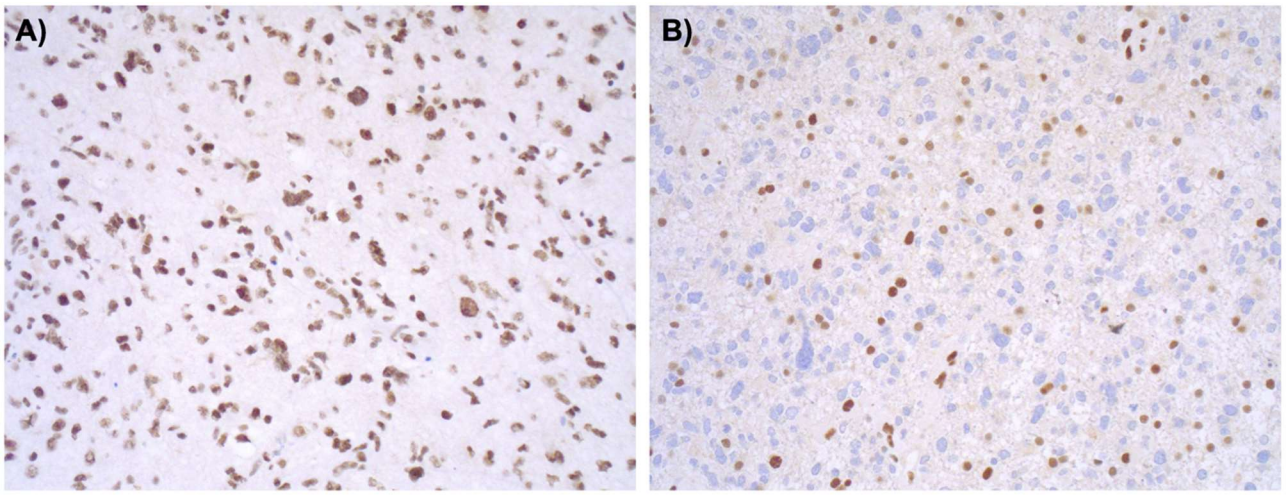

Figure 12 – ATRX expression in GBM: **A**) retained nuclear expression (IHC – 20x); **B**) lost nuclear expression (IHC – 20x).

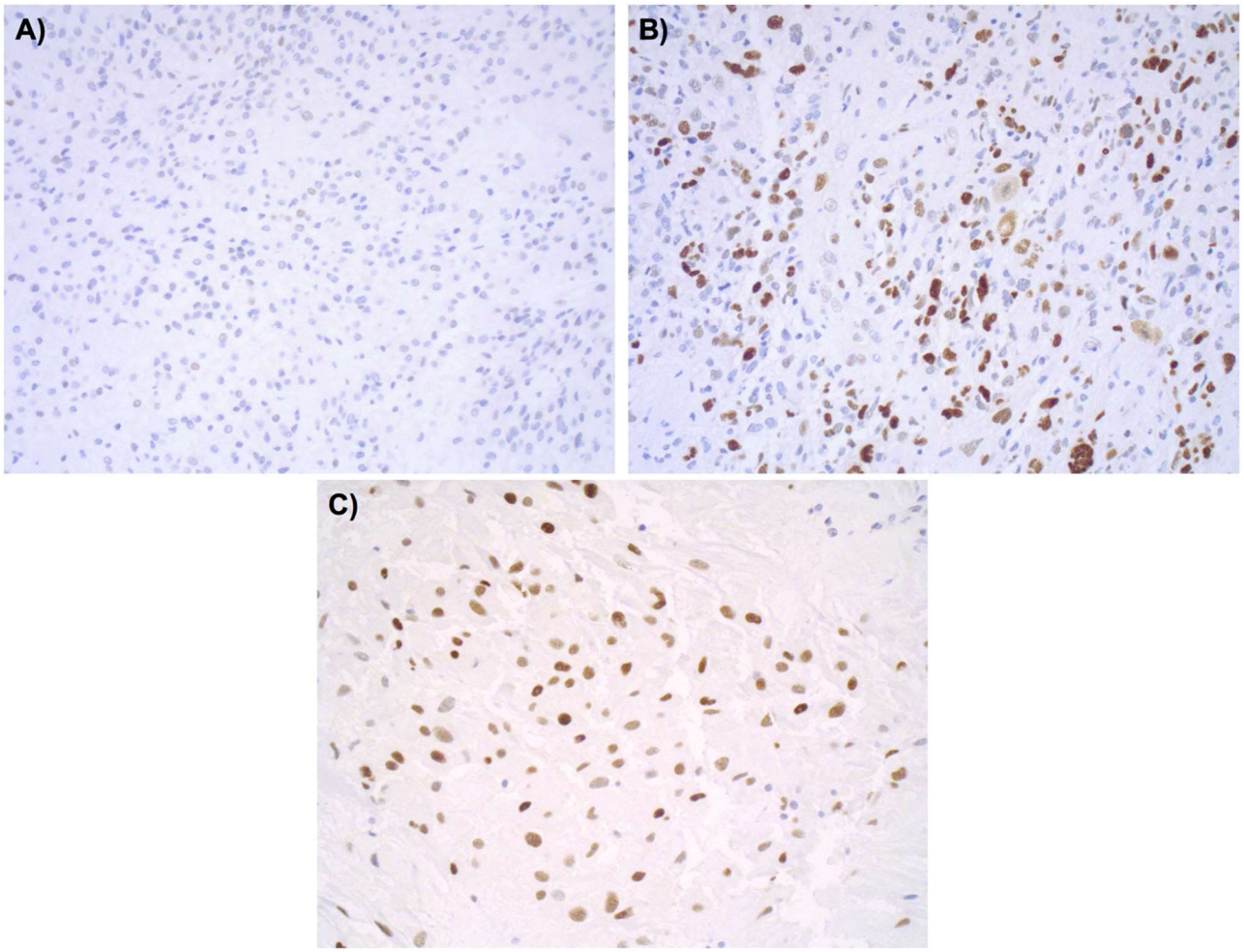

Figure 13 – p53 status in GBM: **A**) negativity (IHC – 10x); **B**) "intermediate" positivity (IHC – 20x); **C**) "strong" positivity (IHC – 20x).

The Ki-67 proliferative index was evaluated by counting the number of positive cells in at least 1000 tumour cells focusing on hot-spot tumour areas (**Figure 14**).

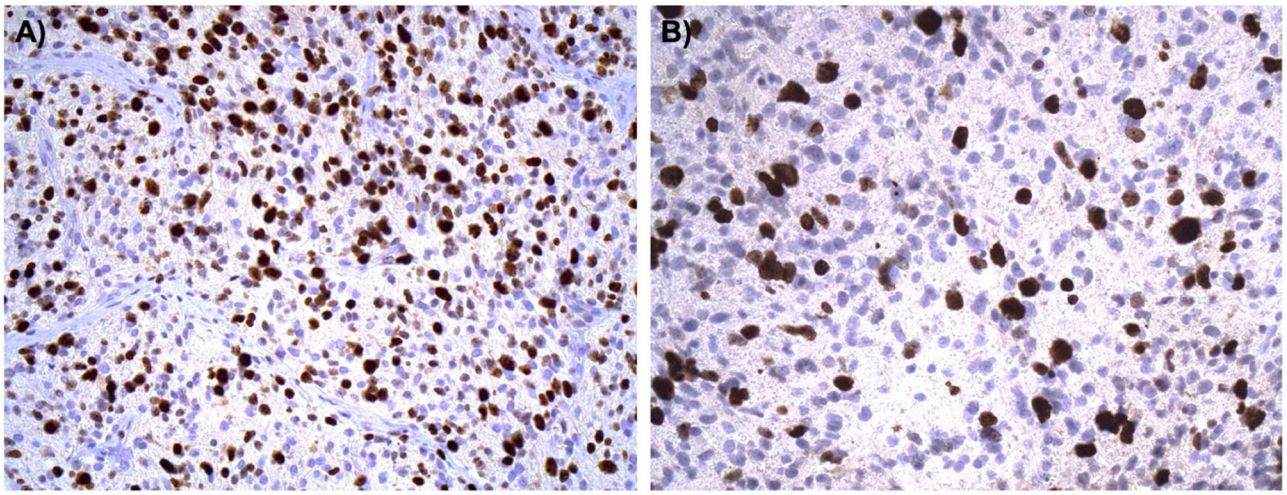

Figure 14 – Ki67 labelling: **A**) IHC – 10x; **B**) IHC – 20x.

3.4.3 Determination of IDH mutations and MGMT promoter methylation status

The most representative tumour area was circled on a reference H&E-stained section. Five serial 5-μm thick sections were cut from formalin-fixed and paraffin-embedded tissue for DNA extraction. Genomic DNA was isolated from the selected tumour area using the Promega Maxwell DNA FFPE Preparation Kit (Promega; Madison, WI, USA).

A Real Time PCR was performed on the platform RT800-96 (EasyPGX® qPCR instrument 96, Diatech Pharmacogenetics SRL, Jesi, Italy) to detect mutations on *IDH1* (codon 105: G105G; codon 132: R132H, R132C, and R132S/G/L/I/V) and *IDH2* (codon 140: R140G/W/Q/L; codon 172: R172K and R172G/W/T/M/S). *Isocitrate dehydrogenase 1* (*IDH1*) on chromosome 2q33 and *IDH2* on chromosome 15q26.1 encode for enzymes that function as homodimers and catalyse a reversible oxidative decarboxylation reaction of isocitrate to alpha-ketoglutarate to generate NADPH from NADP+, providing defence from oxidative damage and supporting cell fitness. Glioma-associated *IDH* mutations lead to a gain of function: synthesis of (D)-2-hydroxyglutarate causes epigenetic shift, DNA repair deficiencies, RNA demethylases, histone modification, and metabolism changes that all favour the gliomagenesis process[61,62].

The *O^6-methylguanine methyltransferase* (*MGMT*) promoter methylation status was assessed by pyrosequencing (Pyromark Q961.D, kit MGMT plus, Diatech Pharmacogenetics SRL; Jesi, Italy). According to the percentage of MGMT promoter methylation status, tumours were grouped in un-methylated (< 9%), and methylated (methylated 9-29%; hyper-methylated > 29%)[63]. *MGMT* sited on chromosome 10q26.3 encodes for an enzyme that transfers methyl groups at the O^6 site of guanine (O^6MeG) to a cysteine residue in its catalytic pocket, thus finally avoiding cell death promoted by alkylating agents, such as temozolomide. The *MGMT* expression is mainly regulated by epigenetic modifications, especially the methylation of CpG island in the promoter region, that reduces the transcription of MGMT increasing tumour chemosensitivity[56,58,64].

3.5 Extent of tumour resection analysis

Early postoperative MRI was routinely performed within 48 hours of surgery to assess the extent of tumour resection – near total (NTR) or subtotal (STR) if the tumour removal was greater or lesser than 95%, respectively[65] – and postoperative contrast enhancement of surgical cavity classified as "absent", "linear" or "nodular" (**Figures 15-17**).

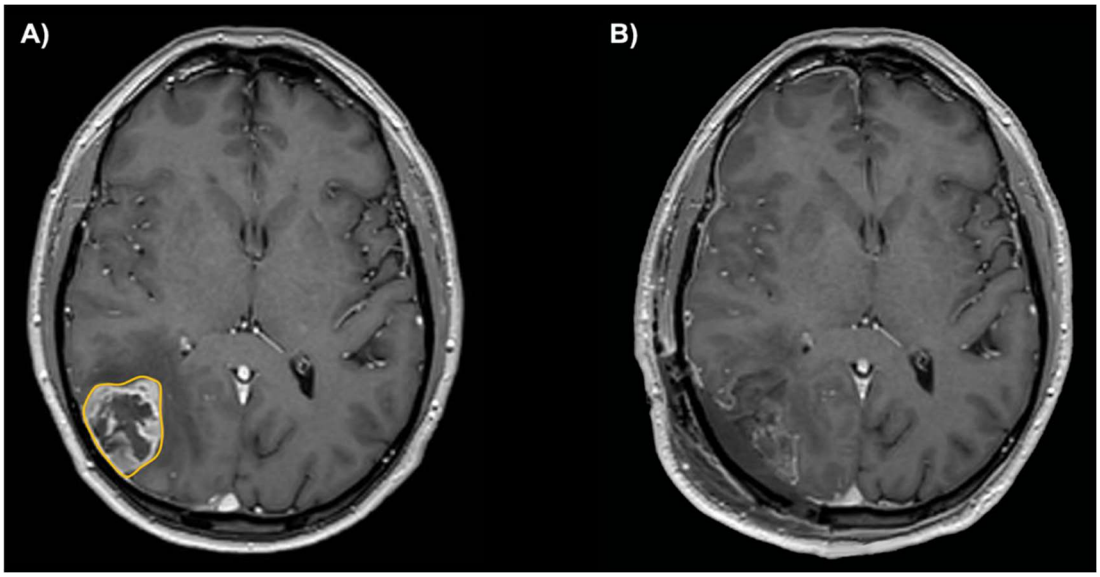

Figure 15 – Preoperative (**A**) and postoperative (**B**) T1-weighted post-contrast axial images showing *NTR* with *absence of pathological enhancement* of surgical cavity.

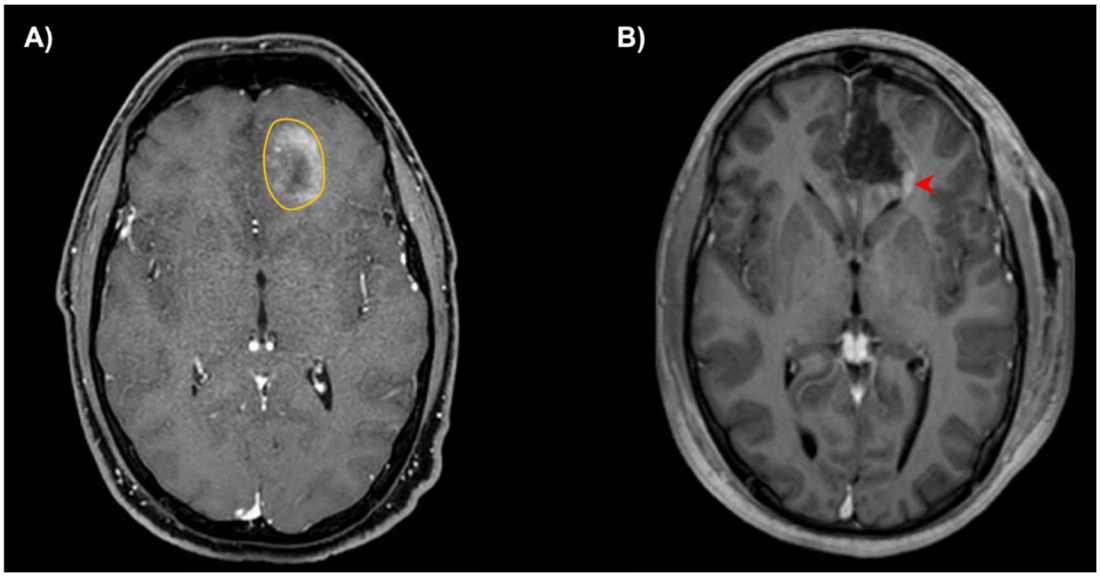

Figure 16 – Preoperative (**A**) and postoperative (**B**) T1-weighted post-contrast axial images showing *NTR* with *linear enhancement* (red arrowhead) of surgical cavity.

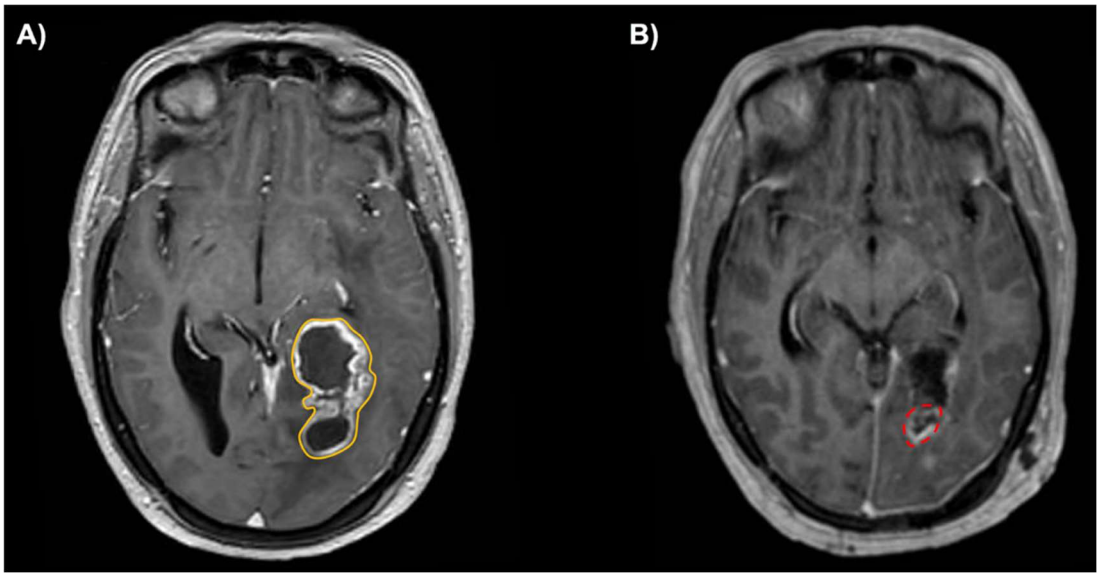

Figure 17 – Preoperative (**A**) and postoperative (**B**) T1-weighted post-contrast axial images showing *NTR* with *nodular enhancement* (dotted red area) of surgical cavity.

Tumour volumes were assessed on T1-weighted contrast enhanced volumetric images, retrieved from the institution's digital archive system and stored as DICOM files. The imaging analysis was carried out using OsiriX MD (Osirix MD 9.0®, Pixmeo, Swiss). Tumour volume, expressed in cubic centimetres (cc), was computed with the Region of Interest (ROI) methodology. Tumour and postoperative pathologic enhancement of surgical cavity were segmented on axial images, then multiplied by the slice thickness through the software[66,67] (**Figures 18-19**).

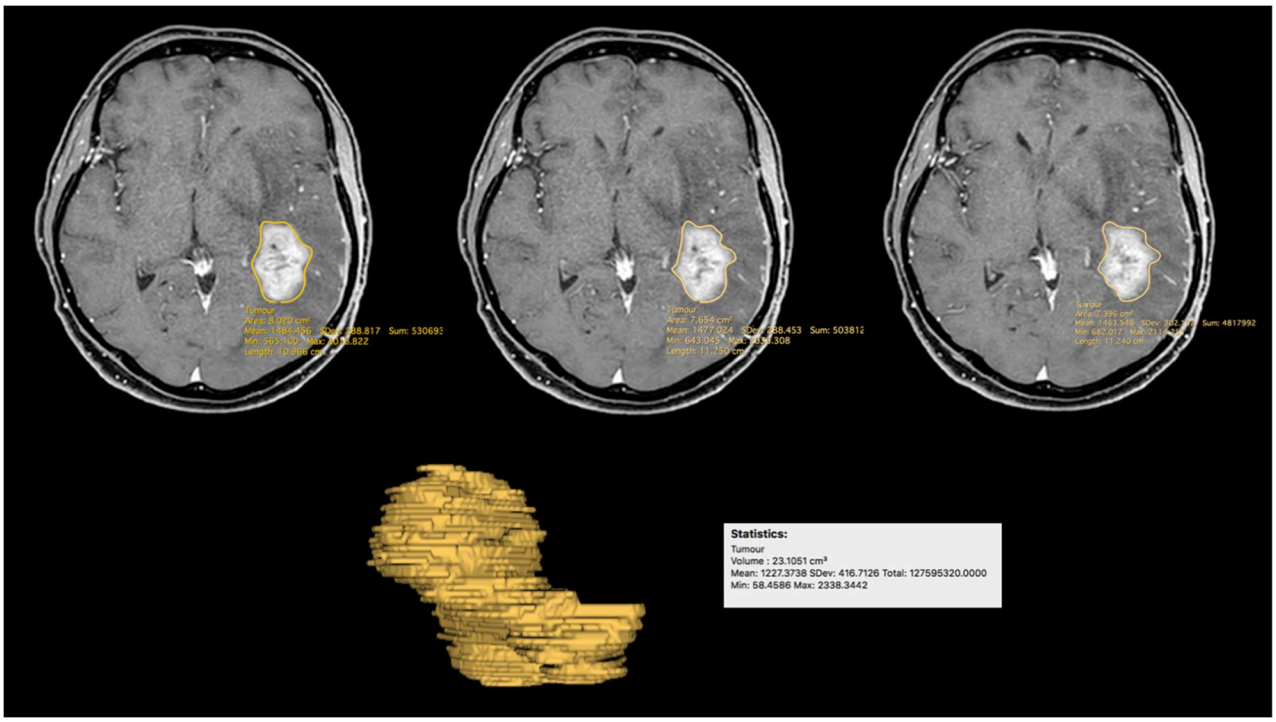

Figure 18 – Preoperative tumour volume computation by Osirix (Osirix MD 9.0®, Pixmeo, Swiss).

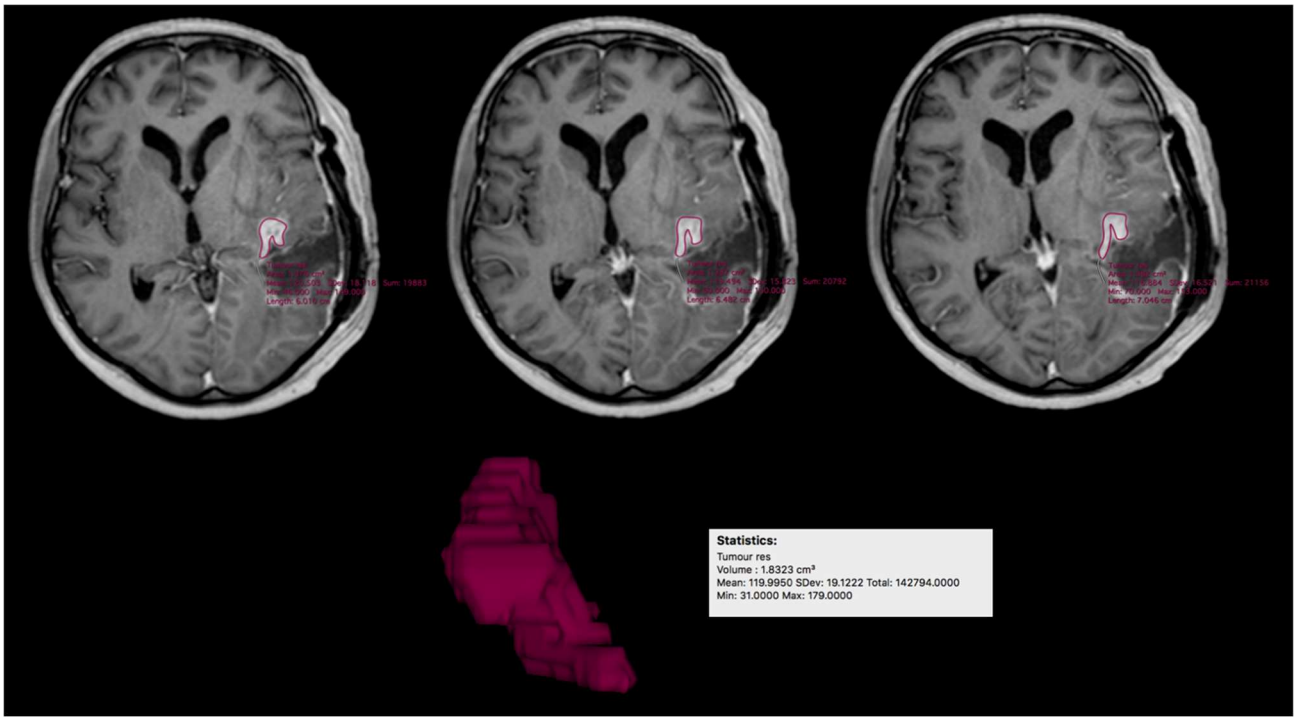

Figure 19 – Postoperative residual tumour volume computation by Osirix (Osirix MD 9.0®, Pixmeo, Swiss).

The percentage of tumour resection was computed according to the formula:

$$\frac{(\boldsymbol{preoperative\ tumour\ volume - postoperative\ tumour\ remnant\ volume})}{preoperative\ tumour\ volume} \times \mathbf{100}$$

3.6 Peripheral blood and tumour samples collection

Peripheral blood samples were collected at diagnosis (before surgery) and regularly over the follow-up (1, 3, 6 and 12 months after surgery), specifically in 23 patients at diagnosis, 16 patients 1 month after surgery, 8 patients 3 months after surgery, 9 patients 6 months after surgery and 5 patients 12 months after surgery (**Figure 20**).

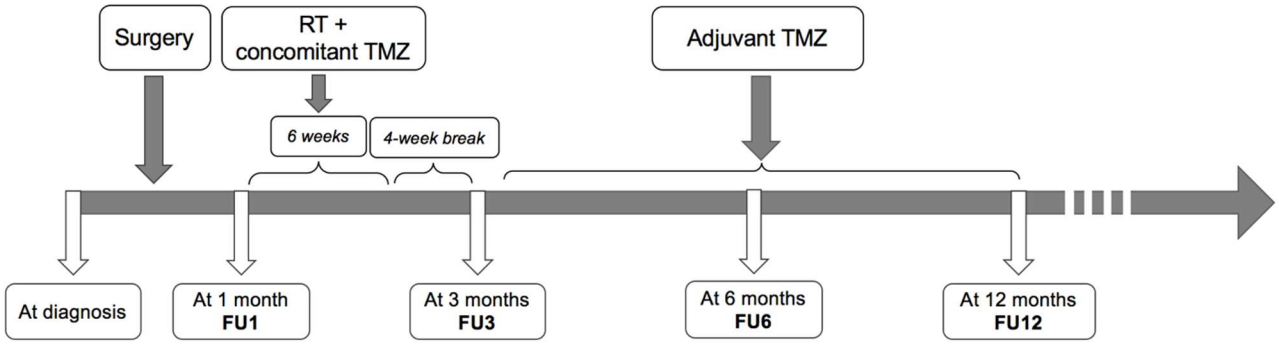

Figure 20 – Timing line of blood samples' collection reporting the standard adjuvant therapy scheme (see paragraph: "*Adjuvant therapies: radiotherapy and chemotherapy*").

Plasma (5), buffy coat (1) and whole blood (4) aliquots were obtained by processing the peripheral blood samples collected in EDTA-coated collection tubes (BD Vacutainer® K2E 10.8mg), while serum aliquots (4) by processing the peripheral blood samples gathered in serum-specific collection tubes containing an inert gel (BD Vacutainer® SST™ II Advance 8.5 mL). The aliquots were then frozen at – 80°C.

Plasma aliquots were obtained within 30 minutes from the withdrawal by: 1) spinning the peripheral blood at 3000 rpm for 10 minutes at 4°C; 2) collecting and further centrifuging the supernatant at 4000 rpm for 20 minutes at 4°C. Buffy coat was achieved from the white interphase obtained after the first centrifugation of peripheral blood (1) in the plasma processing.

The serum-specific collection tubes were kept at room temperature for 60 minutes after the withdrawal to allow the coagulation process. Serum aliquots were obtained by spinning the peripheral blood at 3000 rpm for 15 minutes at 20°C and collecting the upper phase.

Furthermore, representative tumour tissue samples were taken during surgery and fresh frozen at – 80°C.

3.7 Quantification of circulating miRNA levels in plasma

3.7.1 Total RNA isolation from plasma

Total RNA was isolated from 200 μL of plasma by means of the miRNeasy Mini Kit (Qiagen), which combines phenol/guanidine-based lysis of samples and silica membrane-based purification of total RNA, including small RNAs. According to the manufacturer's instructions, plasma samples were lysed in 1 mL of QIAzol Lysis Reagent (Qiagen) and 2.5 μL of 5 nM synthetic cel-miR-39-3p (Integrated DNA Technologies) from *C. elegans* were added to each sample as spike-in. After the addition of 200 μL of chloroform and centrifugation at 12000 g for 15 minutes at 4°C, the lysate was separated into the upper aqueous phase containing RNA, the white interphase containing DNA, and the lower organic phase. The upper aqueous phase was transferred into a new tube and the miRNeasy kit protocol was followed by using the miRNeasy MinElute spin columns, which allow total RNA to bind to the membrane and remove phenol or other contaminants. RNA was eluted from the spin columns in 35 μL of nuclease-free water. Total RNA concentration was measured using a NanoDrop spectrophotometer (Thermo Fisher Scientific, Inc.; Waltham, MA, USA) and RNA quality was assessed using the 260/280 ratio.

3.7.2 Droplet digital PCR (ddPCR) workflow

Circulating levels of miR-21-5p, miR 23b-3p and miR 34a-5p were quantified using the specific TaqMan microRNA assays (Thermo Fisher Scientific, Inc.; Waltham, MA, USA): miR 21-5p assay (ID 000397); miR 23b-3p assay (ID 000400); miR 34a-5p assay (ID 000426). Each assay employs the target-specific stem-loop primer during the reverse transcription to produce a template, which is then quantified in ddPCR using the specific TaqMan probe.

For each miRNA, 2.5 μL of purified total RNA were reversed transcribed using the TaqMan microRNA Reverse Transcription kit (Thermo Fisher Scientific, Inc.; Waltham, MA, USA) in a 7.5 μL reaction containing 0.075 μL of dNTPs, 0.500 μL of 50 U/μL MultiScribe™Reverse Transcriptase, 0.750 μL of 10X Reverse Transcription Buffer, 0.095 μL of RNase Inhibitor, 2.08 μL of nuclease-free water and 1.5 μL of specific stem-loop primers. The reverse transcription reaction was performed at 16°C for 30 minutes, followed by incubation at 42°C for 30 minutes and 85°C for 5 minutes.

The ddPCR experiments were performed according to the QX200 TaqMan ddPCR protocol. For each miRNA, 1.33 μL of reverse transcription product, 11 μL of 2X ddPCR Supermix for probes (Bio-Rad Laboratories, Inc.; Hercules, CA, USA) and 1.1 μL of specific 20X TaqMan PCR probe assay (Thermo Fisher Scientific, Inc.; Waltham, MA, USA) were mixed to obtain a final volume of 22 μL. 20 μL of the ddPCR assay mixture and 70 μL of droplet generation oil for probes (Bio-Rad Laboratories, Inc.; Hercules, CA, USA) were loaded into a disposable droplet generator cartridge (Bio-Rad Laboratories, Inc.; Hercules, CA, USA). Once the droplet generation process has been completed by the QX200 droplet generator (Bio-Rad Laboratories, Inc.; Hercules, CA, USA), 45 μL of the mix containing the droplets were transferred to a 96-well PCR plate (Bio-Rad Laboratories,

Inc.; Hercules, CA, USA) using a multichannel pipette. The plate was heat-sealed with foil and placed in a conventional thermal cycler set as follows: 95°C for 10 minutes, 40 cycles of 94°C for 30 seconds followed by 58°C for 1 minute, 98°C for 10 minutes, 4°C for 40 minutes and a 4°C indefinite hold. A negative control, containing all components of the reaction except for the template, was included in each ddPCR experiment for every miRNA assay. Following the PCR amplification step, the plate containing the droplets was loaded into the QX200 Droplet Reader (Bio-Rad Laboratories, Inc.; Hercules, CA, USA) and the results were analysed using QuantaSoft Software, version 1.7 (Bio-Rad Laboratories, Inc.; Hercules, CA, USA), with Absolute Quantification (ABS) set as the type of experiment. For each plate, the total number of droplets (positive and negative) was verified; one-dimension plot (1-D plot) was used to manually set the threshold and distinguishing the positive droplets, which contained at least one copy of the target miRNA and exhibited high fluorescence, from the negative droplets with very low fluorescence (**Figure 21**). The fraction of positive droplets was fitted by the software to a Poisson distribution to determine the concentration of each target miRNA in copies/μL.

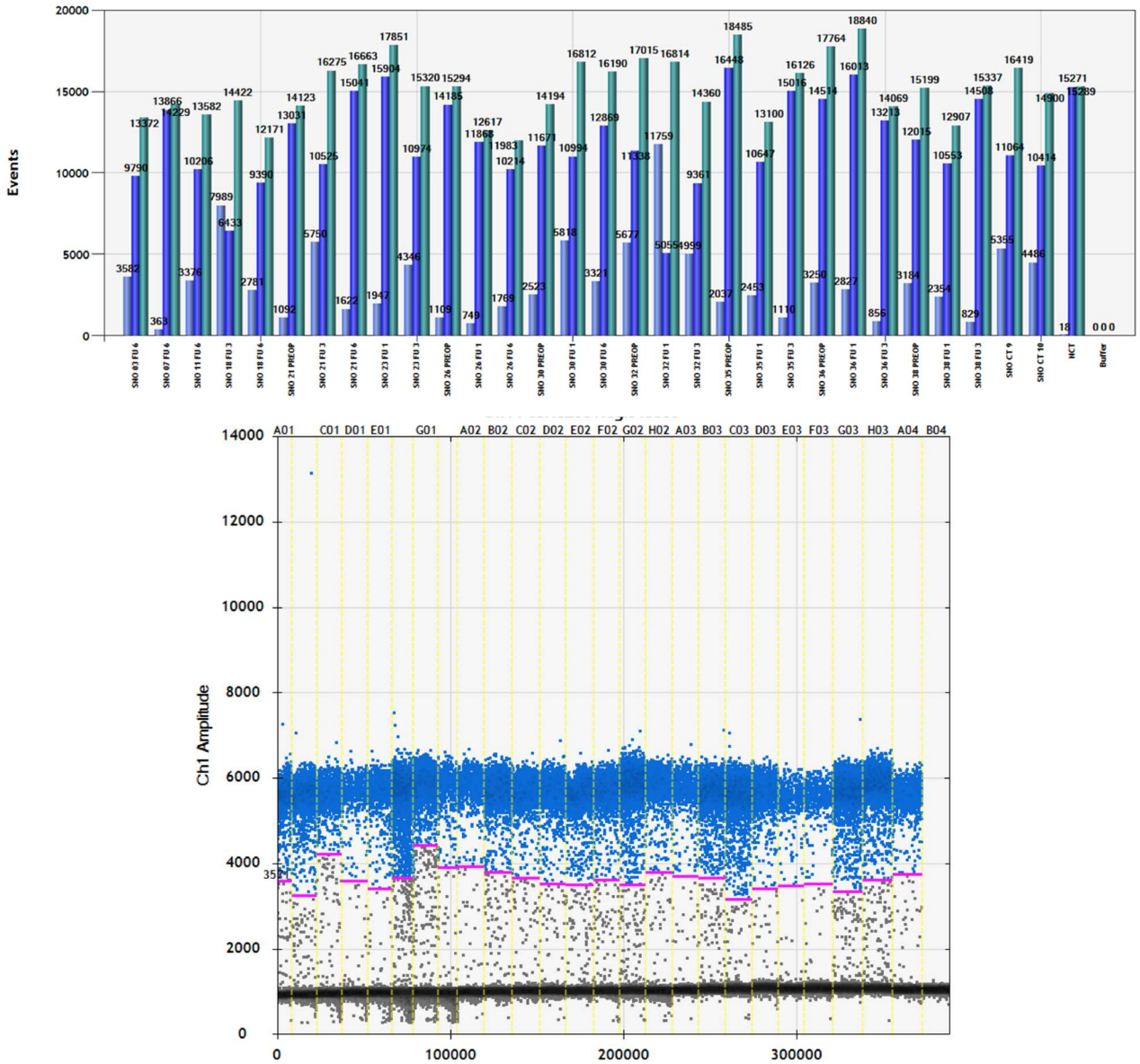

Figure 21 – Illustrative outputs obtained with QuantaSoft Software (version 1.7; Bio-Rad Laboratories, Inc.; Hercules, CA, USA): A) histograms depicting the number of droplets (positive, negative, total); B) 1-D plot.

3.8 Computation of miRNAs' plasmatic concentrations changes

The percentage of change of miRNAs' plasmatic concentrations between different timing points was calculated according to the following formula:

$$\Delta\,[miR_{T2} - miR_{T1}] = \frac{[miR_{T2}] - [miR_{T1}]}{[miR_{T1}]} \times 100$$

The concentrations were defined as *increased* or *stable/decreased* if their variation was greater or lower than 10%.

3.9 miRNA network creation

The miRNet Version 2.0 (https://www.mirnet.ca/miRNet/home.xhtml) allowed the creation of miRNA-centric networks for systems-level interpretation of miRNA functions and gene regulations[68].
The process started selecting "miRNAs" as module of input. Thereafter in the *Upload section* "*H. sapiens*" was selected as *Organism*, "*miRBase ID*" as *ID type* and "*Genes (miRTarBase v8.0)*" as *Targets*; "*hsa-miR-21-5p; hsa-miR-23b-3p; hsa-miR-34a-5p*" were entered in the *miRNA list*. In the Network Builder we set the *Degree cutoff* at *1.0* and applied it to all the network nodes.

3.10 Statistical analysis

Categorical variables were reported as numbers (percentages) and compared with either the Pearson's chi-square test with Yates' correction or Fisher's exact test as appropriate. Continuous variables were expressed as means (± standard deviation, SD) or medians (interquartile range, IQR) and compared with the unpaired Student's *t* test or Mann-Whitney U test as appropriate, after confirmation of normality of distribution by histograms' visual inspection and the Shapiro-Wilk test.
The correlations of plasmatic miRNA concentrations with patients' and tumours' variables were reported either as Pearson's or rho Spearman's correlation coefficients (*r*) in case of linear and non-linear associations, respectively. The results of linear regression were reported as adjusted R^2 estimates on included figures.
Receiver operating characteristics (ROC) curves were generated to assess sensitivity, specificity and predictive power of each miRNA for GBM. The area under curve (AUC) values ranged from 0

to 1: values around 0.5 indicated an equal distribution among healthy volunteers and GBM patients; values between 0.5 and 1 suggested that miRNAs' levels were higher in GBM patients; values between 0 and 0.5 indicated that miRNA were higher in healthy volunteers[3,35]. The cut-off values were identified according to the Youden index (YI)[69,70].

Hierarchical cluster analysis with Ward's methods and K-means cluster analysis were performed to classify patients affected by GBM according to their miRNAs' plasmatic levels.

Multivariate linear regression analysis was used to determine which variables independently predicted plasmatic miRNA levels at different timing points. Results of multivariate modelling were expressed as odds ratios (OR), 95% confidence interval (CI) after adjustment for covariates and *p* for significance.

The overall survival (OS) and recurrence free survival (RFS) analyses were performed according to the Kaplan-Meier method from the date of surgery to the date of death, tumour recurrence/progression or end of observation. Censoring was applied to the last follow-up date for patients who remained alive. The log-rank test was used to compare survivals[70].

The Cox regression analysis was adopted to determine which variables independently predicted OS and RFS. Results of multivariate modelling were expressed as hazard ratios (HR), 95% confidence interval (CI) after adjustment for covariates and *p* for significance.

A two-tailed probability (*p*) value ≤ 0.05 was considered statistically significant.

Statistical analysis was performed using the package SPSS for Windows, Version 23.0 (SPSS Inc.; Chicago, IL, USA).

4. RESULTS

4.1 Patients' and tumour's features

The mean age at diagnosis was 57.9 years (± 9.6) with a male prevalence (60.9%). Eighteen patients (78.3%) were "independent" in daily life activities (KPS ≥90) and 21 (91.3%) did not present significant neurological disabilities (mRS ≤ 2). Steroids and anti-epileptic drugs were preoperatively administered in 21 (91.3%) and 10 cases (43.5%), respectively (see **Appendix** – **Table 1**).

Lesions were left-sided in 11 cases (47.8%), right-sided in 9 cases (39.1%) and sited along the midline in 3 cases (13.1%). The preoperative brain MRI showed tumour contrast enhancement in all cases and necrosis in 87.0% of them. The mean tumour volume was 33.8 cc (± 19.1); 10 patients (43.5%) presented a tumour volume smaller than 30.0 cc.

Nineteen (82.6%) were newly diagnosed tumours. Intraoperative "strong" tumour fluorescence was recorded in all but one (95.7%) surgeries. The pathological report was consistent with GBM IDH-wildtype WHO grade 4 in 22 cases (95.7%) and astrocytoma IDH-mutant WHO grade 4 in the remaining one (4.3%). Twelve cases (52.2%) showed un-methylated MGMT, 4 (17.4%) methylated MGMT and the remaining 7 (30.4%) hyper-methylated MGMT, with no statistical difference in their distribution (p=0.119). ATRX expression was "retained" (in the cell nucleus) in 20 cases (87.0%) and "lost" in 3 cases (13.0%, p<0.001). p53 tumour expression was classified as "absent" in 2 cases (8.7%), "intermediate" in 13 cases (56.5%) and "strong" in 8 cases (34.8%, p=0.028). The mean Ki67% was 41.3 (±19.8).

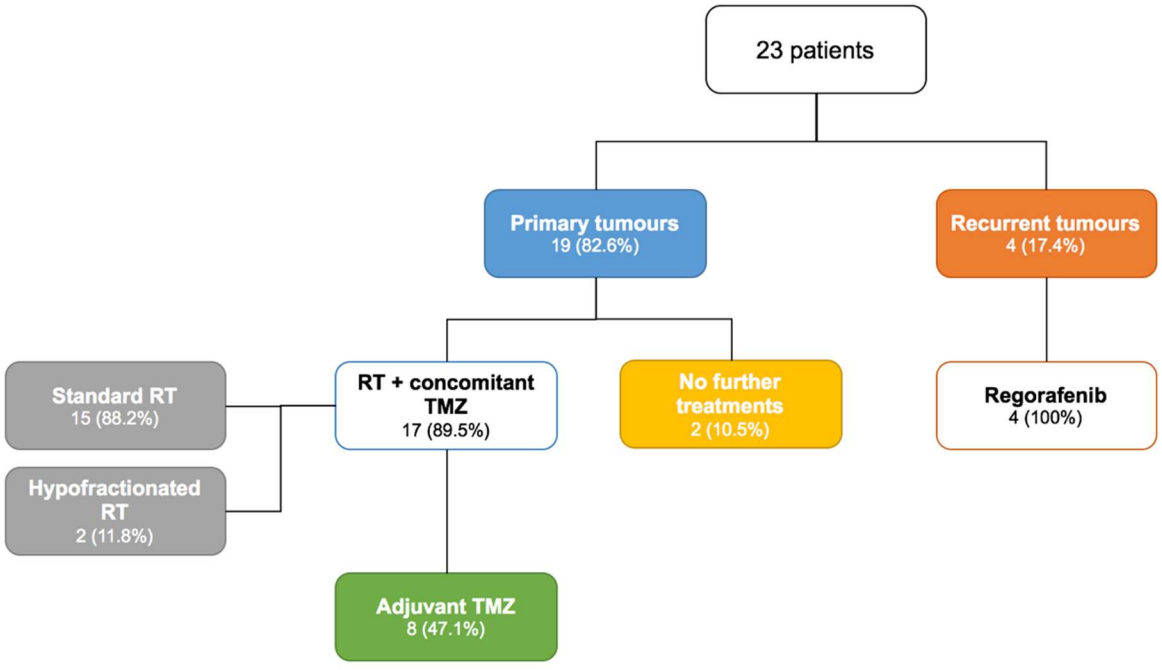

Figure 22 – Flow chart showing patients' distribution according to adjuvant therapies (RT: radiotherapy; TMZ: temozolomide).

Seventeen out of 19 patients (89.5%) operated for newly diagnosed tumours were treated with RT and concomitant temozolomide. The RT protocol was standard in 15 (88.2%) and hypo-fractionated in the remaining 2 (11.8%). Overall, 12 patients (52.2%) were suitable for adjuvant chemotherapy. Eight of them were started on temozolomide, 3 of which were treated with regorafenib at tumour recurrence, and 4 presenting with recurrent GBM were treated with regorafenib (**Figure 22**).

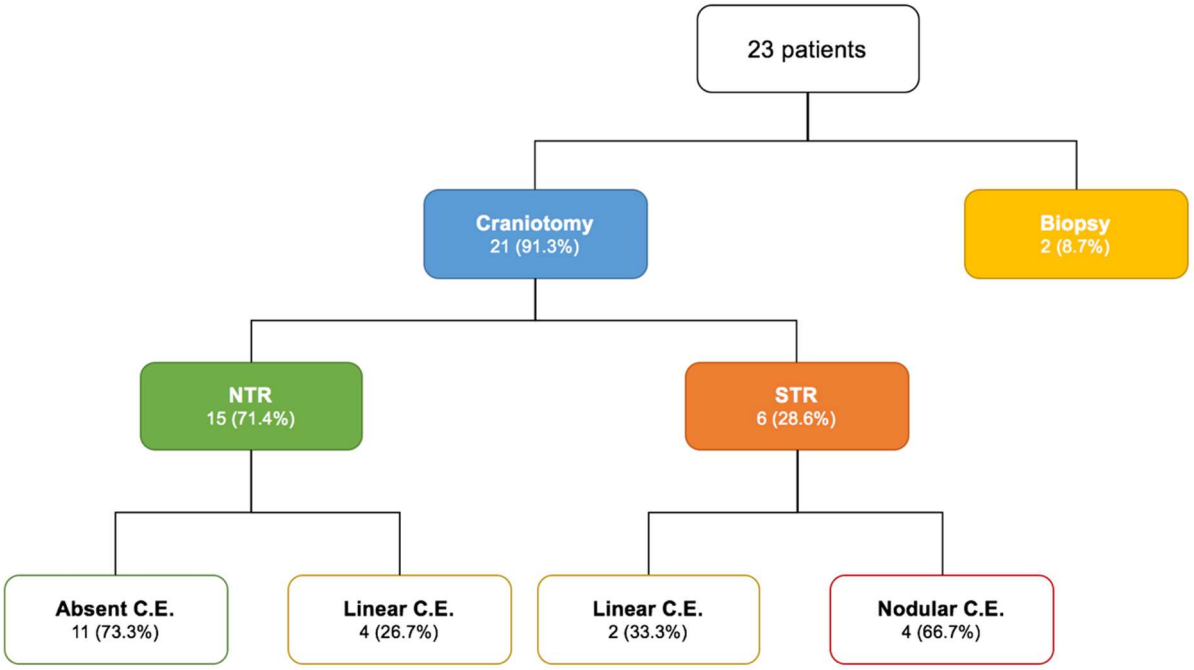

Figure 23 – Flow chart showing patients' distribution according to the extent of tumour resection (C.E.: contrast enhancement of surgical cavity; NTR: near-total resection; STR: subtotal resection).

Craniotomy was performed in 21 patients (91.3%) and NTR was achieved in 15 of them (71.4%). In case of STR (6, 28.6%), the pathologic contrast enhancement of surgical cavity was "linear" in 2 (33.3%) and "nodular" in 4 (66.7%) cases (**Figure 23**) with a mean tumour remnant volume of 5.88 cc (±3.74). The mean percentage of tumour resection was 99.3% (±1.0) and 80.7% (±7.9) in case of NTR and STR, respectively (see **Appendix** – **Table 2**).

4.2 Results of ddPCR assays

Overall, the ddPCR assays provided a mean of 16265.48 total droplets (±2045.53; median: 16342.00, IQR 15147.00-17716.00) showing similar results for each miRNA (miR 21-5p: 15643.15 ± 1808.62; miR 23b-3p: 16728.15 ± 2134.99; miR 34a-5p: 16429.80 ± 2041.81; **Figure 24**).

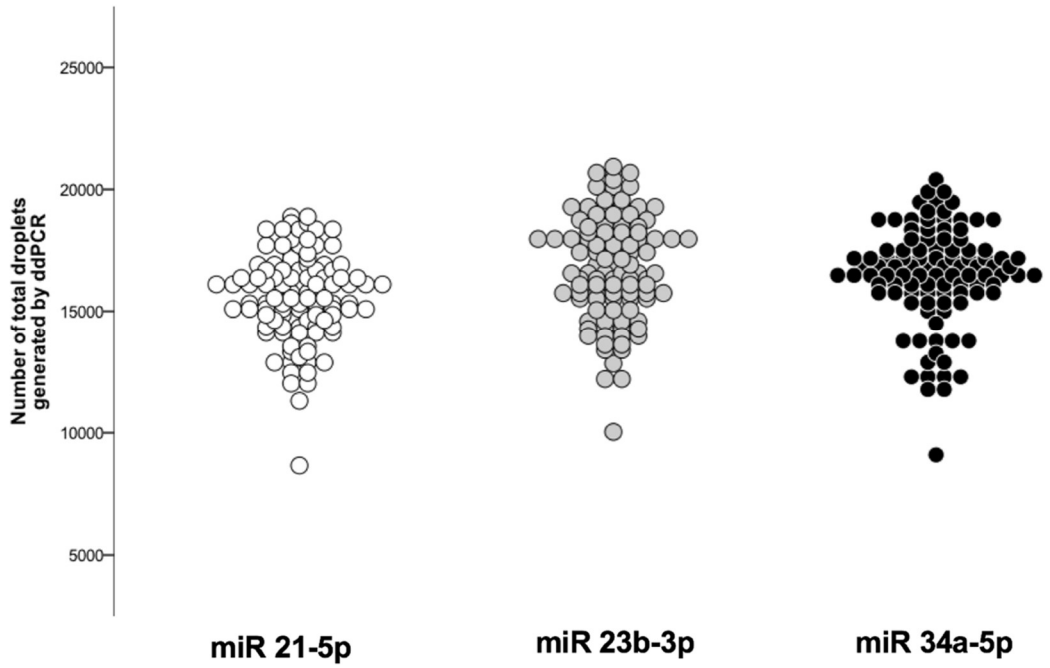

Figure 24 – Dot plots showing the total number of droplets generated by ddPCR for miR 21-5p (**A**), miR 23b-3p (**B**) and miR 34a-5p (**C**).

The mean number of positive droplets detected by ddPCR was 650.80 (±1443.36; median: 56.00, IQR 13.00-429.00). The mean number of positive droplets was greater for miR 21-5p (1783.18 ± 2054.95) followed by miR 23b-3p (129.29 ± 222.63) and miR 34a-5p (22.14 ± 29.95) (**Figure 25**).

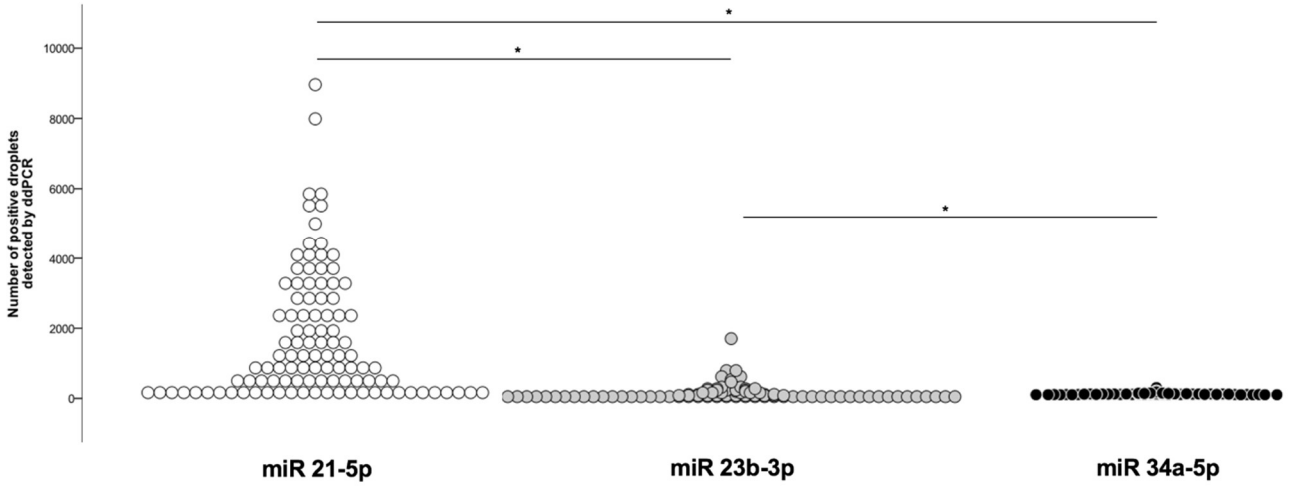

Figure 25 – Dot plots showing the number of positive droplets detected by ddPCR for miR 21-5p (**A**), miR 23b-3p (**B**) and miR 34a-5p (**C**) (*: p<0.001).

4.3 miRNAs' plasmatic concentrations in healthy volunteers and patients

miR 21-5p, miR 23b-3p and miR 34a-5p were all detectable in healthy volunteers with a mean plasmatic concentration of 114.28 copies/μL (± 125.41), 4.43 copies/μL (± 5.40) and 0.68 copies/μL

(± 0.62), respectively. Patients presented on average 115.49 copies/μL (± 132.57) of miR 21-5p, 7.18 copies/μL (± 10.15) of miR 23b-3p and 1.28 copies/μL (± 1.10) of miR 34a-5p at diagnosis. Healthy volunteers showed significantly lower mean circulating levels of miR 34a-5p than patients at diagnosis (0.68 vs. 1.28 copies/μL; *p*=0.012) (**Figure 26**).

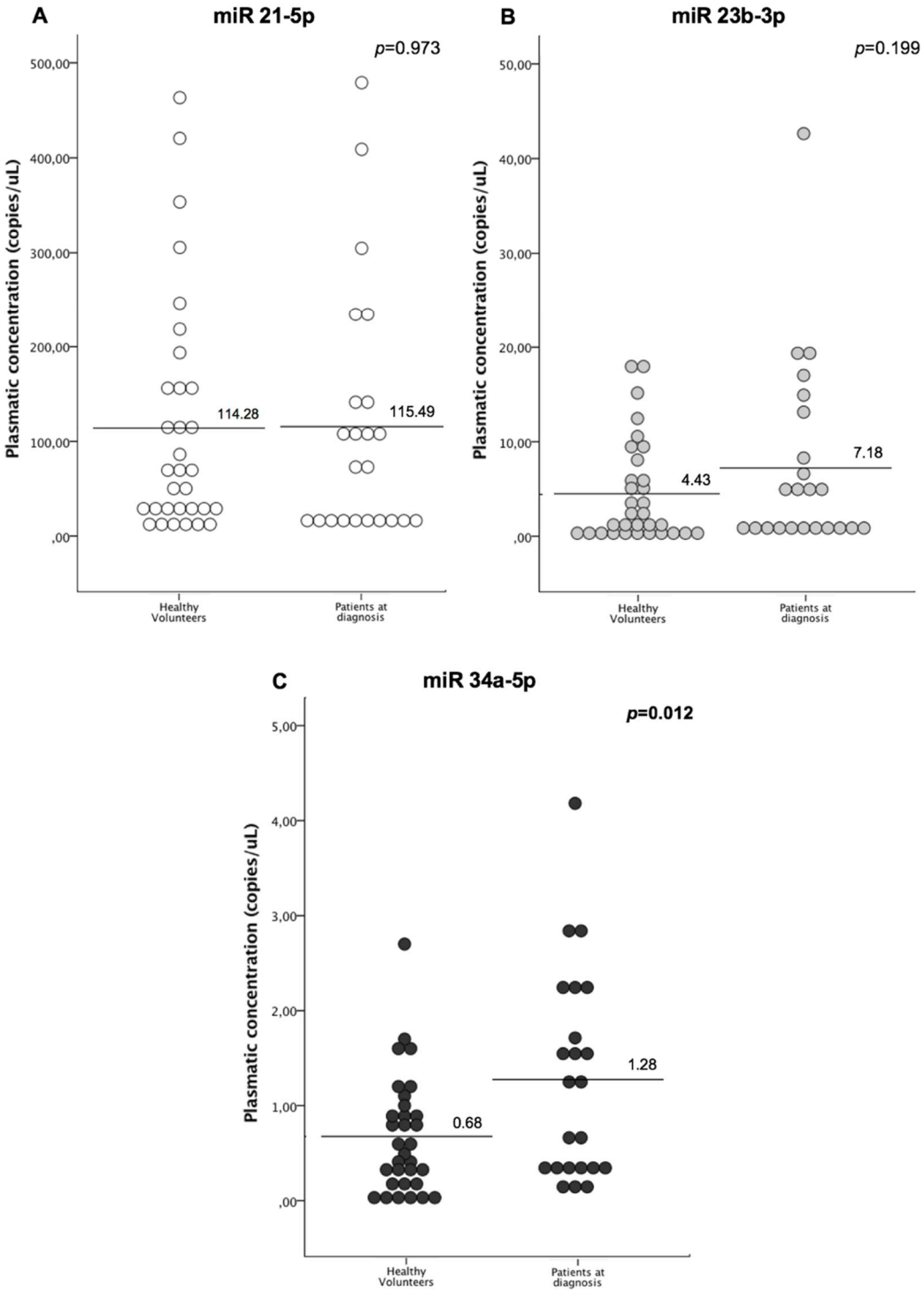

Figure 26 – Dot plots showing plasmatic concentrations of miR 21-5p (**A**), miR 23b-3p (**B**) and miR 34a-5p (**C**) in healthy volunteers and patients at diagnosis (mean values represented by lines).

The diagnostic efficacy of the tested miRNAs in distinguishing patients affected by GBM from healthy individuals was evaluated using the ROC curve analysis (**Figure 27**). The AUC was 0.484 for miR 21-5p (95% C.I. 0.326 – 0.643, *p*=0.844), 0.537 for miR 23b-3p (95% C.I. 0.375-0.700, *p*=0.639) and 0.664 for miR 34a-5p (95% C.I. 0.515-0.814, *p*=0.039). The cut-off value for miR 34a-5p was 1.25 copies/μL (sensitivity: 47.8%; specificity: 87.5%; YI: 0.353).

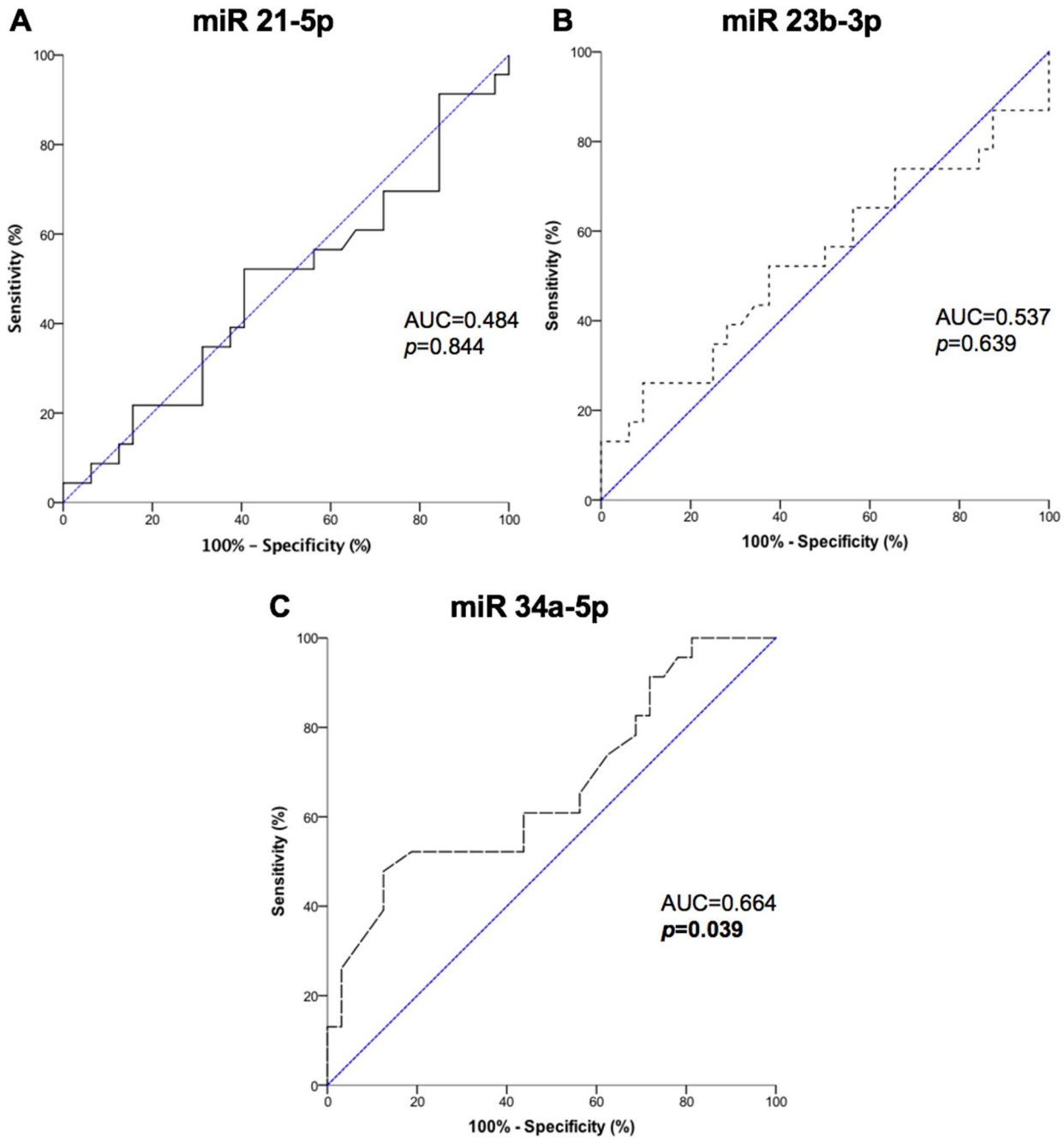

Figure 27 – ROC curves of miR 21-5p (**A**), miR 23b-3p (**B**) and miR 34a-5p (**C**) between healthy volunteers and patients at diagnosis.

Mean plasmatic concentrations of miR 21-5p (356.16 ± 303.89 vs. 114.28 ± 125.41 copies/μL; *p*=0.001) and miR 23b-3p (22.26 ± 19.04 vs. 4.43 ± 5.40 copies/μL; *p*<0.001) in patients 3 months

after surgery reached significantly higher levels compared to healthy volunteers. However, mean circulating levels of miR 34a-5p remained significantly higher in patients at each timing point compared to healthy volunteers (**Figure 28**).

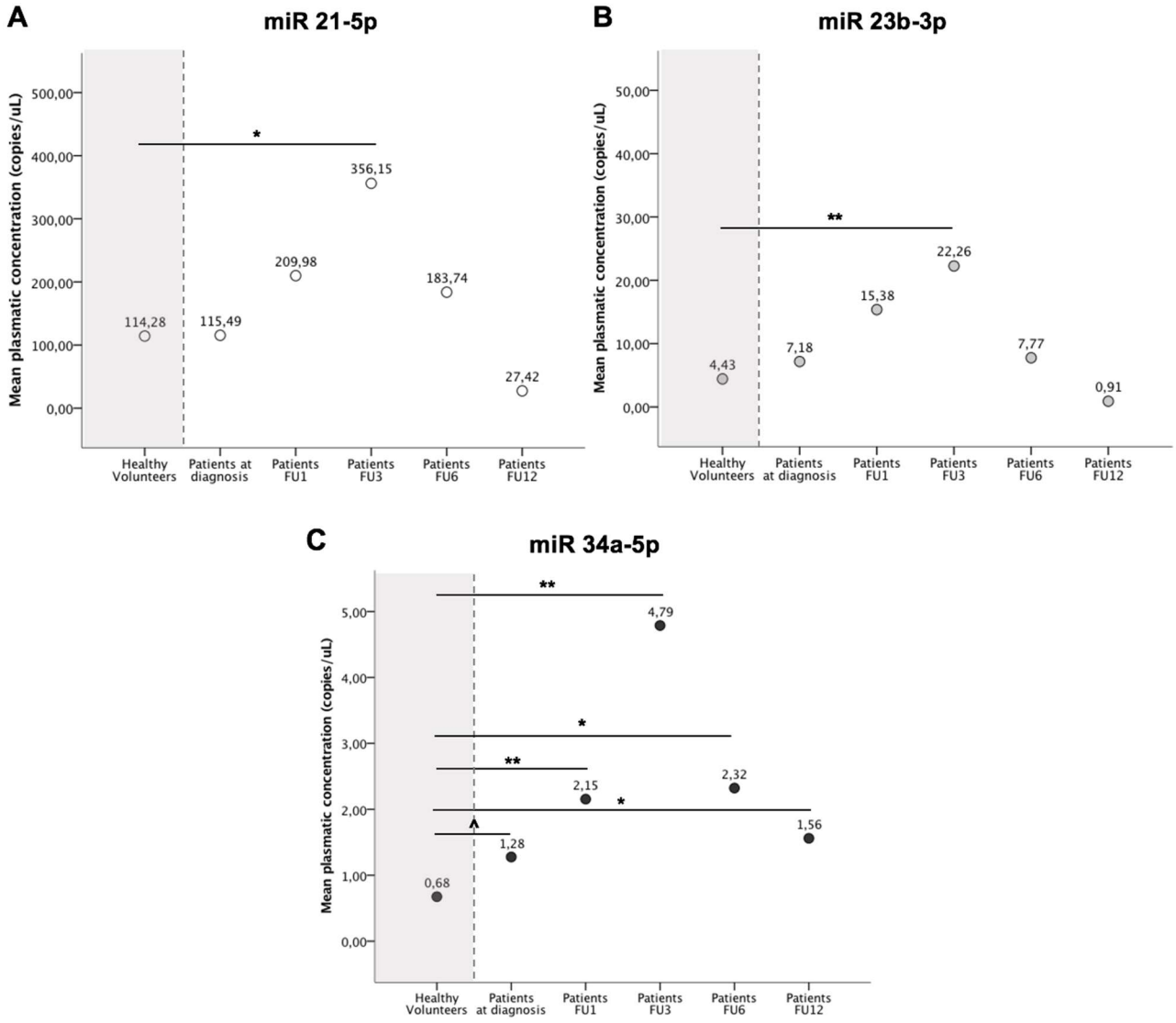

Figure 28 – Comparison of mean circulating levels of miR 21-5p (**A**), miR 23b-3p (**B**) and miR 34a-5p (**C**) between healthy volunteers and patients at different timing points (**: p<0.001; *: p=0.001; ^: p<0.05).

4.4 Patients' clustering according to miRNAs' plasmatic concentrations at diagnosis

Patients affected by GBM were clustered according to the similarity of their miRNAs' absolute circulating concentrations at the time of diagnosis (**Figure 29**). Specifically, two main groups of patients were identified: group 1 presented low absolute levels of all miRNAs; group 2 showed high levels of miRNAs. miR 21-5p (mean: 331.60 vs. 55.46 copies/μL, p<0.001) and miR 23b-3p (22.66 vs. 2.88 copies/μL, p<0.001), but not miR 34a-5p (1.90 vs. 1.10 copies/μL, p=0.155), were significantly higher in group 2.

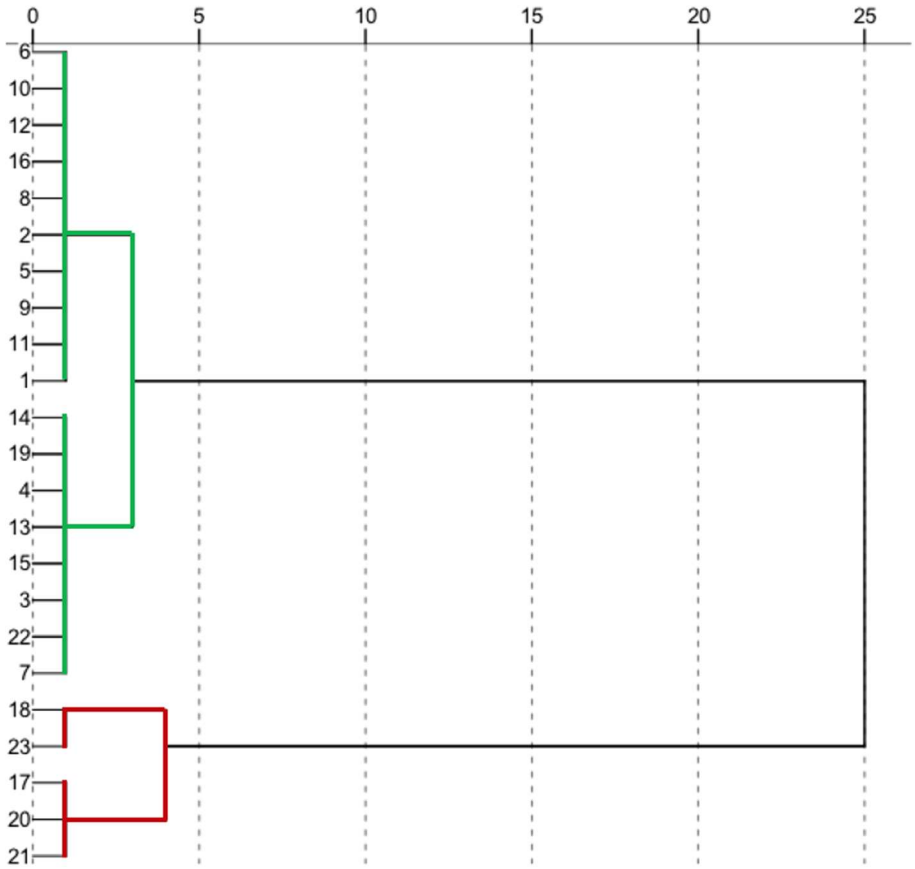

Figure 29 – Dendogram showing the hierarchical clustering of GBM patients according to their absolute circulating miRNAs' concentrations (miR 21-5p, miR 23b-3p and miR 34a-5p) at the time of diagnosis. Group 1 (green line); group 2 (maroon line).

Furthermore, we performed a hierarchical clustering to group GBM patients according to the similarity of their miRNAs' circulating profile at the time of diagnosis relative to the mean plasmatic levels in healthy volunteers (**Figure 30**). Patients were clustered into four distinct groups: group 1 presented high expression levels for all miRNAs; group 2 showed low levels of miR 21-5p and high levels of miR 23b-3p; group 3 presented low circulating levels of all miRNAs; group 4 mainly low levels of miR 21-5p and miR 23b-3p and high levels of miR 34a-5p.

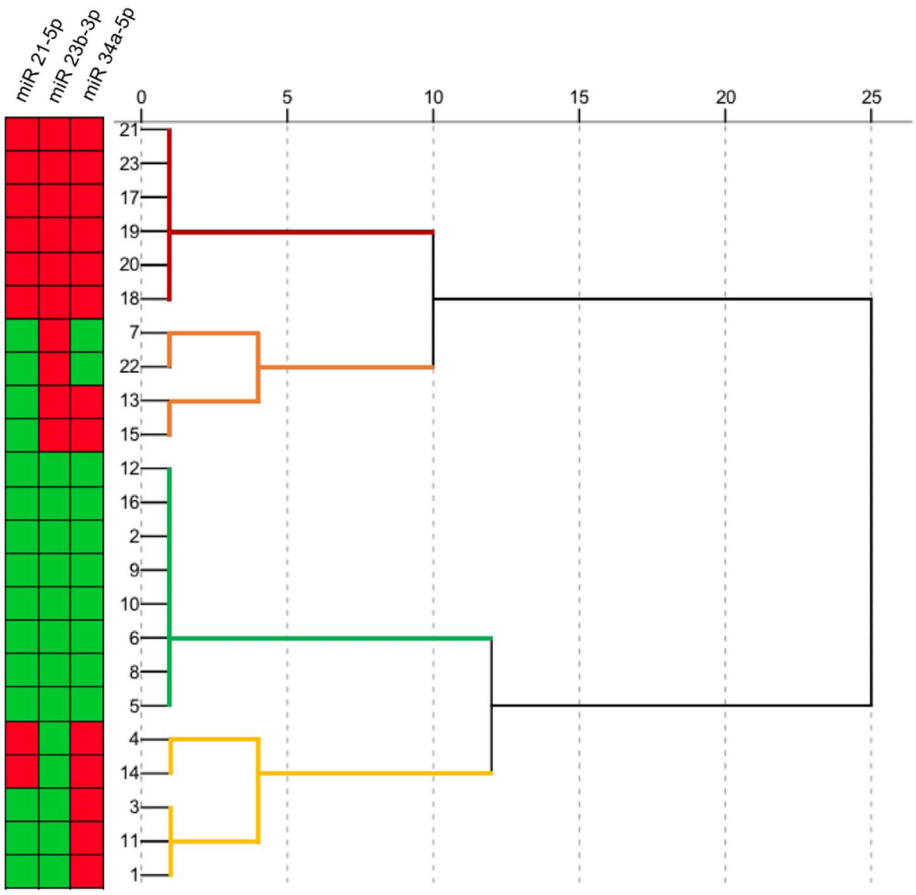

Figure 30 – Hierarchical clustering classifies GBM patients according to their circulating miRNAs' concentrations at the time of diagnosis (miR 21-5p, miR 23b-3p and miR 34a-5p) relative to the plasmatic levels in healthy volunteers. Group 1 (maroon line); group 2 (orange line); group 3 (green line); group 4 (yellow line). Matrix coding: a) red: above the mean miRNAs' circulating levels in healthy volunteers; b) green: below the mean miRNAs' circulating levels in healthy volunteers.

4.5 Longitudinal course of miRNAs' plasmatic concentrations

4.5.1 Variations of miRNAs' plasmatic concentrations

Patients experienced increase, decrease or stability of miRNAs plasmatic concentrations over time. Specifically, miR 21-5p: decreased and increased in 8 cases (50%), respectively, between the diagnosis and 1 month after surgery; decreased in 4 cases (66.7%) and increased in 2 cases (33.3%) between 1 and 3 months after surgery; decreased in 4 cases (80%) and increased in 1 case (20%) between 3 and 6 months after surgery; eventually, decreased in 4 cases (100%) between 6 and 12 months after surgery (**Figure 31**).

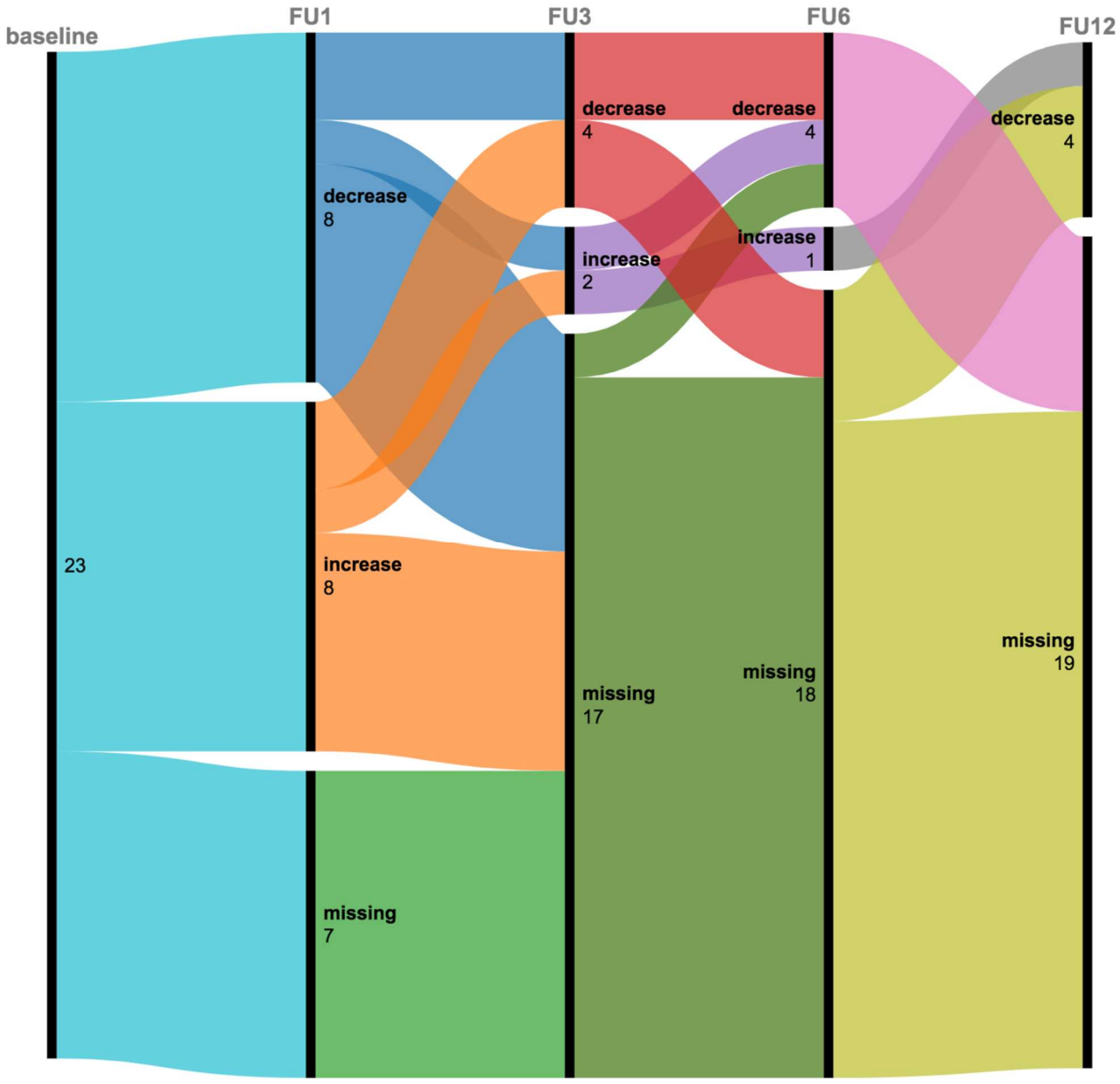

Figure 31 – Alluvial diagram for miR 21-5p plasmatic concentrations stratified by variations (increase, decrease and stability) over time (1, 3, 6 and 12 months after surgery).

miR 23b-3p plasmatic concentrations showed: stability in 2 cases (12.5%), increase in 8 cases (50%) and decrease in 6 cases (37.5%) between the diagnosis and 1 month after surgery; decrease in 4 cases (66.7%) and increase in 2 cases (33.7%) between 1 and 3 months after surgery; decrease in 5 cases (100%) between 3 and 6 months after surgery; decrease in 4 cases (100%) between 6 and 12 months after surgery (**Figure 32**).

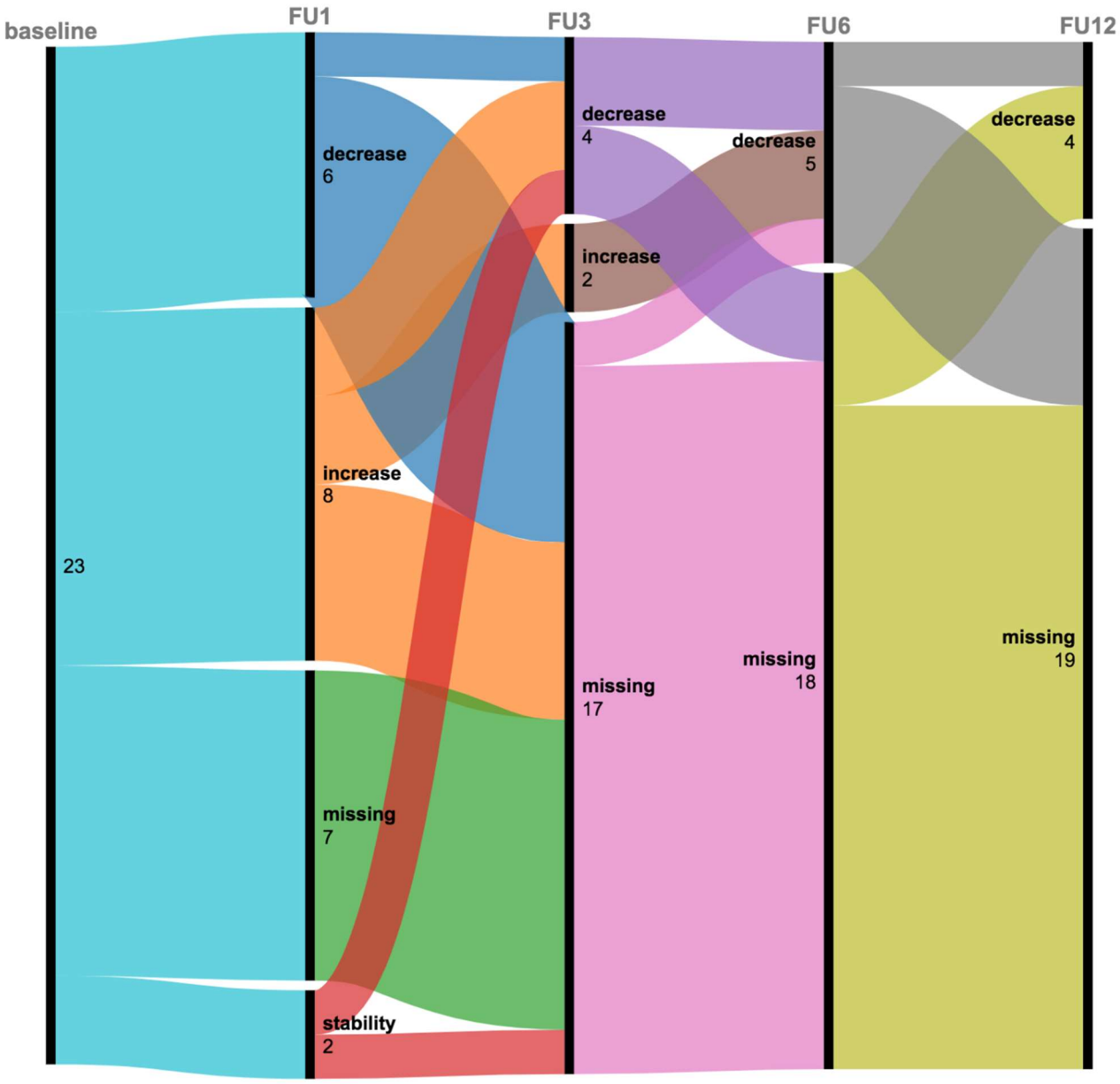

Figure 32 – Alluvial diagram for miR 23b-3p plasmatic concentrations stratified by variations (increase, decrease and stability) over time (1, 3, 6 and 12 months after surgery).

The longitudinal course of miR 34a-5p circulating levels registered: increase in 12 cases (75%) and decrease in 4 cases (25%) between the diagnosis and 1 month after surgery; decrease in 3 cases (50%), increase in 2 cases (33.7%) and stability in 1 case (16.7%) between 1 and 3 months after surgery; decrease in 3 cases (60%) and stability in 2 cases (40%) between 3 and 6 months after surgery; decrease and stability in 2 cases (50%), respectively, between 6 and 12 months after surgery (**Figure 33**).

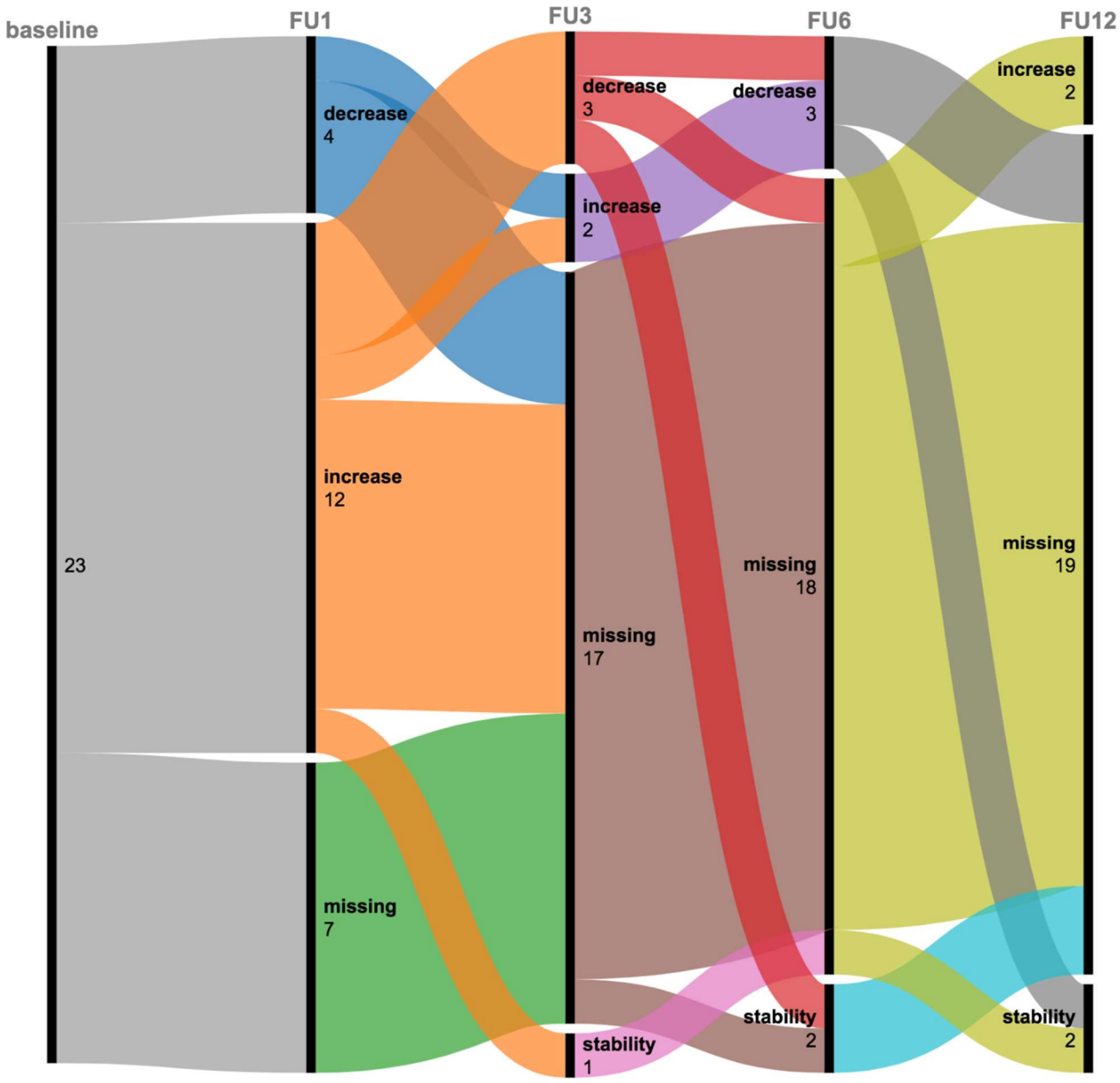

Figure 33 – Alluvial diagram for miR 34a-5p plasmatic concentrations stratified by variations (increase, decrease and stability) over time (1, 3, 6 and 12 months after surgery).

Between the diagnosis and 1 month after surgery the mean rates of increase were 55.5%, 74.7%, 53.7% and the mean rates of decrease were 42.2%, 58.4%, 55.7% for miR 21-5p, miR 23b-3p and miR 34a-5p, respectively (**Figure 34**).

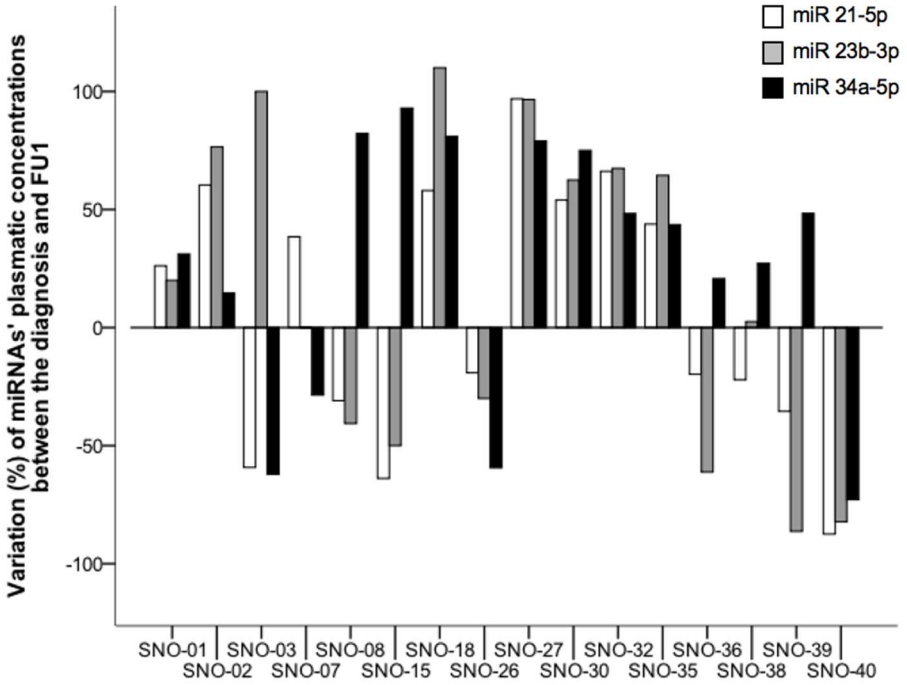

Figure 34 – Variations (%) of miR 21-5p, miR 23b-3p and miR 34a-5p plasmatic concentrations between the diagnosis and 1 month after surgery.

Between 1 and 3 months after surgery the mean rates of increase were 1621.9%, 15755.68%, 793.3% and the mean rates of decrease were 65.9%, 67.5%, 51.8% for miR 21-5p, miR 23b-3p and miR 34a-5p, respectively (**Figure 35**).

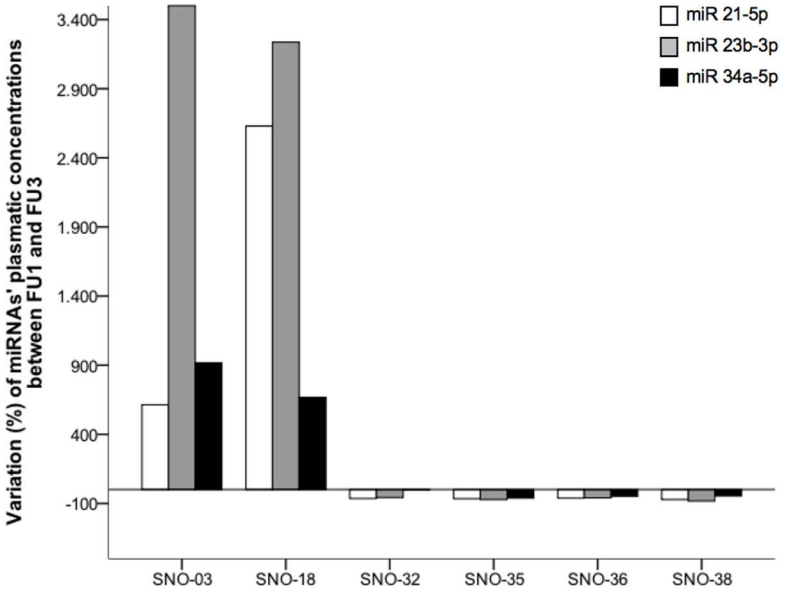

Figure 35 – Variations (%) of miR 21-5p, miR 23b-3p and miR 34a-5p plasmatic concentrations between 1 and 3 months after surgery.

Between 3 and 6 months after surgery the mean rates of increase were 37.5%, 0%, 0% and the mean rates of decrease were 74.2%, 76.7%, 78.5% for miR 21-5p, miR 23b-3p and miR 34a-5p, respectively (**Figure 36**).

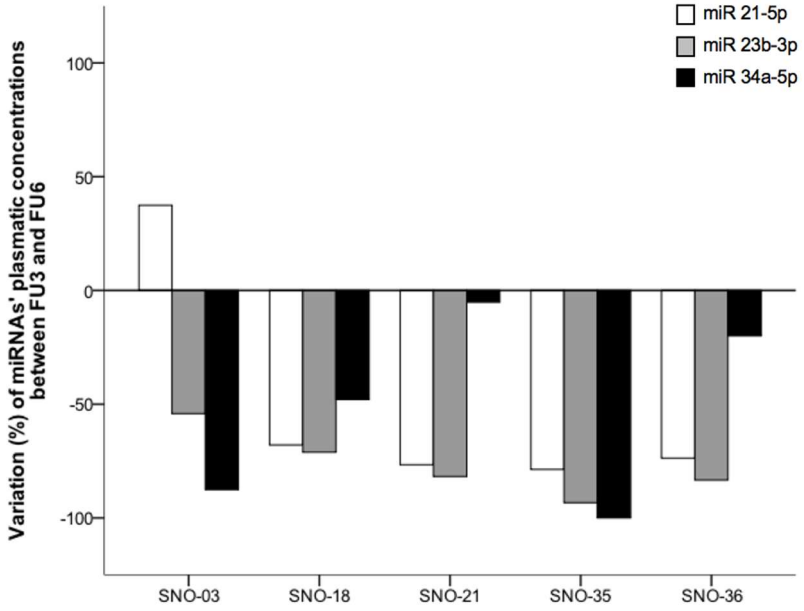

Figure 36 – Variations (%) of miR 21-5p, miR 23b-3p and miR 34a-5p plasmatic concentrations between 3 and 6 months after surgery.

Eventually, between 6 and 12 months after surgery miR 21-5p, miR 23b-3p and miR 34a-5p increased in mean of 0%, 0%, 125.0% and decreased in mean of 85.9%, 85.8%, 66.7%, respectively (**Figure 37**).

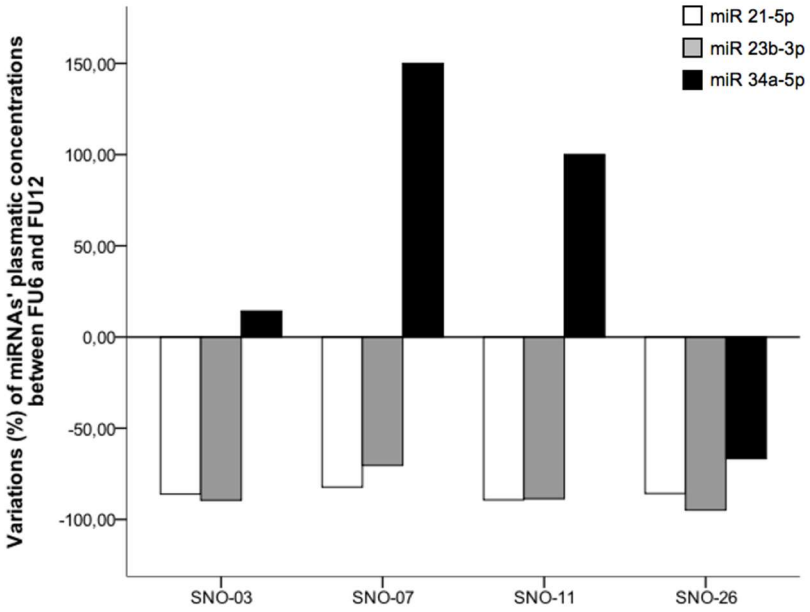

Figure 37 – Variations (%) of miR 21-5p, miR 23b-3p and miR 34a-5p plasmatic concentrations between 6 and 12 months after surgery.

4.5.2 Mean miRNAs' plasmatic concentrations course

The mean plasmatic concentrations of each miRNA showed the same longitudinal course in patients affected by GBM. The circulating levels progressively increased 1 and 3 months after surgery, then decreased 6 and 12 months after surgery (**Figure 38**).

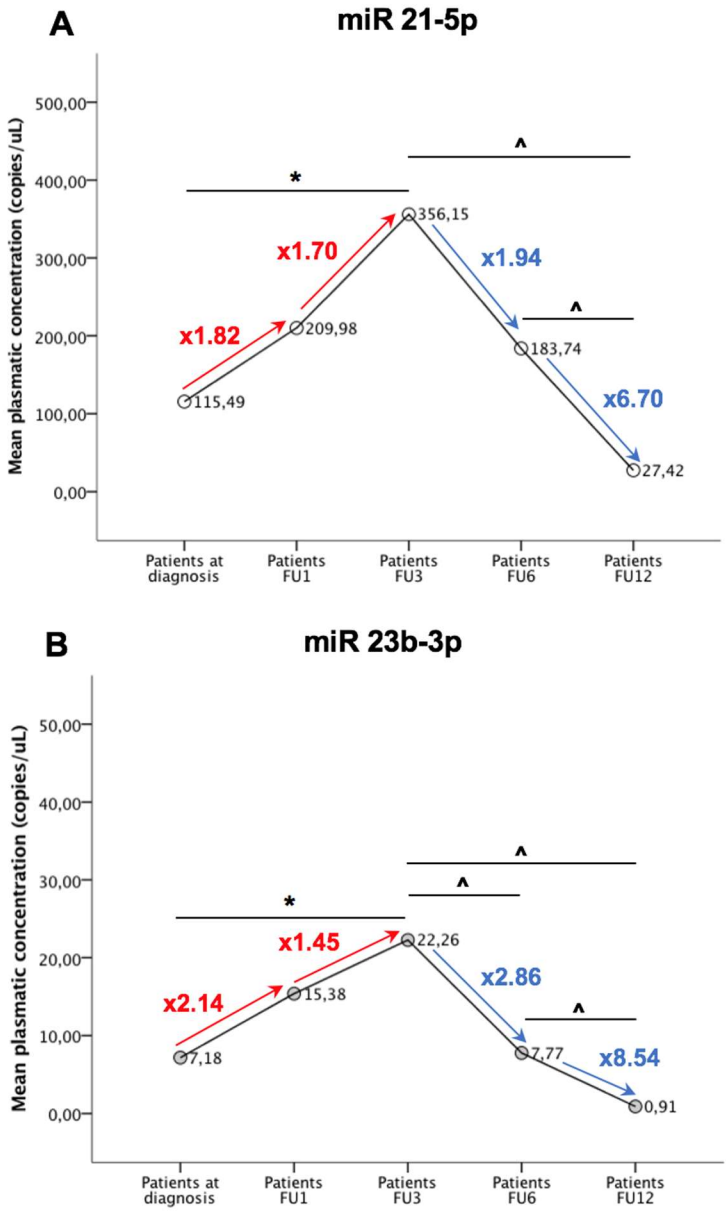

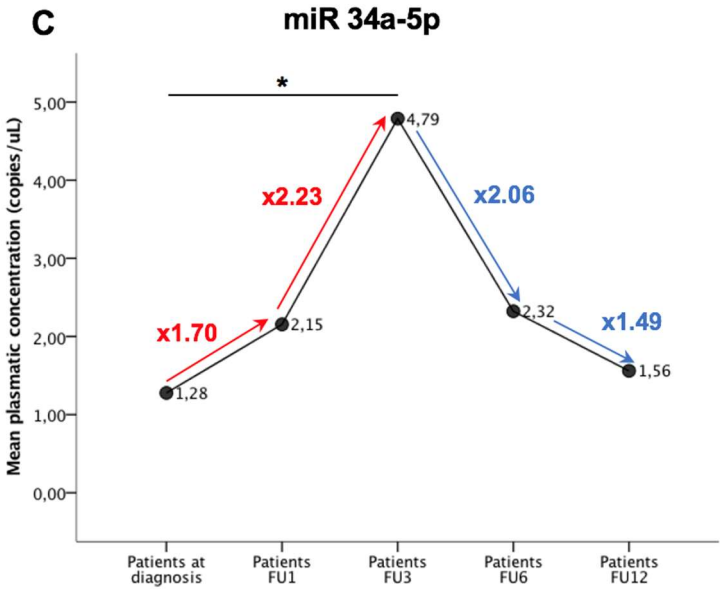

Figure 38 – Longitudinal course of mean plasmatic concentrations of miR 21-5p (**A**), miR 23b-3p (**B**) and miR 34a-5p (**C**) (*: p<0.01; ^: p<0.05).

In particular, the mean plasmatic concentration of miR 21-5p increased by 1.82 folds between the diagnosis and 1 month after surgery (115.49 ± 132.57 vs. 209.98 ± 356.28 copies/μL; p=0.251) and by 1.70 folds between the first and the third month after surgery (209.98 ± 356.28 vs. 356.15 ± 303.89 copies/μL; p=0.310). Then it decreased by 1.94 folds between 3 and 6 months (356.15 ± 303.89 vs. 183.74 ± 141.87 copies/μL; p=0.174) and by 6.70 folds between 6 and 12 months after surgery (183.74 ± 141.87 vs. 27.42 ± 17.27 copies/μL; p=0.033).

Similarly, the mean miR 23b-3p levels showed a 2.14 fold increase between the diagnosis and 1 month after surgery (7.18 ± 10.15 vs. 15.38 ± 32.73 copies/μL; p=0.345) and a 1.45 fold increase between 1 and 3 months after surgery (15.38 ± 32.73 vs. 22.26 ± 19.04 copies/μL; p=0.523), followed by a 2.86 fold decrease between 3 and 6 months (22.26 ± 19.04 vs. 7.77 ± 6.16 copies/μL; p=0.047) and a 8.54 fold decrease between 6 and 12 months after surgery (7.77 ± 6.16 vs. 0.91 ± 0.42 copies/μL; p=0.031).

Eventually, the mean miR 34a-5p plasmatic concentrations were 1.70 folds higher 1 month after surgery than at the time of diagnosis (2.15 ± 1.71 vs. 1.28 ± 1.10 copies/μL; p=0.083), and 2.23 folds higher 3 months than 1 month after surgery (4.79 ± 5.17 vs. 2.15 ± 1.71 copies/μL; p=0.074), then 2.06 and 1.49 folds lower 6 months than 3 months after surgery (2.32 ± 2.43 vs. 4.79 ± 5.17 copies/μL; p=0.246) and 12 months than 6 months after surgery (1.56 ± 0.34 vs. 2.32 ± 2.43copies/μL; p=0.505), respectively.

All the investigated miRNAs displayed significantly higher plasmatic concentrations 3 months after surgery compared to the time of diagnosis (miR 21-5p: 356.15 ± 303.89 vs. 115.49 ± 132.57 copies/μL, p=0.004; miR 23b-3p: 22.26 ± 19.04 vs. 7.18 ± 10.15 copies/μL, p=0.008; miR 34a-5p:

4.79 ± 5.17 vs. 1.28 ± 1.10 copies/μL, *p*=0.004). Furthermore, miR 21-5p and miR 23b-3p showed significantly lower circulating levels 12 months after surgery (miR 21-5p: 27.42 ± 17.27 copies/μL; miR 23b-3p: 0.91 ± 0.42 copies/μL) compared to 3 months (miR 21-5p: 356.15 ± 303.89 copies/μL, *p*=0.037; miR 23b-3p: 22.26 ± 19.04 copies/μL, *p*=0.031) and 6 months after surgery (miR 21-5p: 183.74 ± 141.87 copies/μL, *p*=0.033; miR 23b-3p: 7.77 ± 6.16 copies/μL, *p*=0.031).

4.6 Correlation analyses between miRNAs' plasmatic concentrations at diagnosis and clinical, neuroradiological and pathological features

There were no significant differences in plasmatic concentration of miRNAs and clinical, neuroradiological and histological features apart from preoperative corticosteroid therapy and ATRX status.

The mean circulating levels of miR 23b-3p (6.14 ± 10.01 vs. 18.10 ± 1.56 copies/μL, *p*<0.001) and miR 34a-5p (1.16 ± 1.07 vs. 2.56 ± 0.35 copies/μL, *p*=0.021) at diagnosis resulted significantly higher in patients who were not administered preoperative corticosteroids (**Table 1**).

	miR 21-5p at diagnosis (mean, SD)	*p* value	**miR 23b-3p at diagnosis** (mean, SD)	*p* value	**miR 34a-5p at diagnosis** (mean, SD)	*p* value
Gender (n, %)						
Males (14, 60.9)	86.62 (92.39)	0.200	4.38 (6.22)	0.170	1.36 (1.25)	0.638
Females (9, 39.1)	160.39 (175.30)		11.53 (13.62)		1.15 (0.86)	
mRS (n, %)						
≤ 2 (21,91.3)	109.67 (122.45)	0.668	7.16 (10.40)	0.682	1.29 (1.08)	0.737
> 2 (2, 8.7)	218.45 (268.06)		10.40 (12.45)		1.75 (1.48)	
KPS (n, %)						
70-80 (5, 21.7)	156.04 (163.53)	0.576	8.58 (8.10)	0.754	2.12 (1.39)	0.182
90-100 (18, 78.3)	108.82 (128.13)		7.12 (11.06)		1.10 (0.91)	
Steroids (n, %)						
Yes (21, 91.3)	95.72 (117.87)	0.204	**6.14 (10.01)**	**< 0.001**	**1.16 (1.07)**	**0.021**
No (2, 8.7)	323.00 (120.21)		**18.10 (1.56)**		**2.56 (0.35)**	
AEDs (n, %)						
Yes (10, 43.5)	70.18 (69.93)	0.155	3.56 (4.56)	0.137	1.29 (1.33)	0.969
No (13, 56.5)	150.34 (159.76)		9.96 (12.41)		1.27 (0.94)	

Table 1 – Comparison of miR 21-5p, miR 23b-3p and miR 34a-5p plasmatic concentrations at diagnosis with patients' clinical features (23 patients).
AEDs: anti-epileptic drugs; KPS: Karnofsky Performance Status; mRS: modified Ranking Score.

Furthermore, the plasmatic concentrations of all miRNAs were significantly higher at the time of diagnosis in tumours showing retained ATRX expression on IHC (miR 21-5p: 136.05 ± 137.44 vs.

8.15 ± 5.87 copies/μL, *p*=0.001; miR 23b-3p: 8.51 ± 10.73 vs. 0.36 ± 0.40 copies/μL, *p*=0.004; miR 34a-5p: 1.47 ± 1.11 vs. 0.37 ± 0.03 copies/μL, *p*<0.001) (**Table 2**).

	miR 21-5p at diagnosis (mean, SD)	*p* value	**miR 23b-3p at diagnosis** (mean, SD)	*p* value	**miR 34a-5p at diagnosis** (mean, SD)	*p* value
Preoperative MRI						
Location (n, %)						
Right (9, 39.1)	105.18 (121.57)	0.602	5.53 (6.65)	0.443	1.19 (1.04)	0.807
Left (11, 47.8)	140.62 (154.59)		9.87 (13.12)		1.43 (1.22)	
Midline (3, 13.1)	54.27 (71.65)		2.24 (2.73)		1.00 (1.04)	
Necrosis (n, %)						
Yes (20, 86.7)	122.78 (143.06)	0.271	8.06 (10.97)	0.075	1.14 (0.92)	0.486
No (3, 13.3)	62.43 (64.58)		2.57 (2.45)		2.16 (2.07)	
Tumour volume						
≤ 30 cc (10, 43.5)	105.85 (128.68)	0.765	5.22 (7.27)	0.403	1.71 (1.41)	0.096
> 30 cc (13, 56.5)	122.90 (140.22)		8.68 (11.99)		0.94 (0.65)	
Primary vs recurrent GBM						
Primary (19, 82.6)	119.38 (140.51)	0.718	7.25 (10.81)	0.932	1.29 (1.14)	0.863
Recurrent (4, 17.4)	96.98 (99.27)		6.85 (7.40)		1.19 (0.99)	
MGMT methylation status (n, %)						
Un-methylated (12, 52.2)	134.44 (141.68)	0.484	9.83 (12.23)	0.190	1.14 (0.86)	0.565
Methylated (11, 47.8)	94.81 (125.22)		4.28 (6.67)		1.42 (1.39)	
ATRX expression (n, %)						
Lost (3, 13.0)	**8.15 (5.87)**	**0.001**	**0.36 (0.40)**	**0.004**	**0.37 (0.03)**	**< 0.001**
Retained (20, 87.0)	**136.05 (137.44)**		**8.51 (10.73)**		**1.47 (1.11)**	
p53 expression (n, %)						
Absent (2, 8.7)	165.00 (196.58)	0.574	10.30 (13.01)	0.782	0.84 (1.08)	0.817
Intermediate (13, 56.5)	82.20 (80.05)		5.55 (6.35)		1.35 (1.26)	
Diffuse (8, 34.8)	128.99 (165.81)		8.16 (15.39)		1.15 (0.86)	

Table 2 – Comparison of miR 21-5p, miR 23b-3p and miR 34a-5p plasmatic concentrations at diagnosis with histological and radiological tumour' features (23 patients).
ATRX: alpha thalassemia/mental retardation syndrome X-linked; MGMT: O-6-methylguanine-DNA-methyltransferase.

However, the correlation and multivariate analyses showed no significant results (see **Appendix** – **Tables 3-6**).

4.7 Correlation analyses between miRNAs' plasmatic concentrations over the follow up, extent of tumour resection and adjuvant therapies

Analysing the miRNAs' levels over the follow up, the only significant difference was found in miR 34a-5p plasmatic concentration 1 month after surgery that was significantly higher in patients who underwent near-total compared to subtotal resection (2.70 ± 1.93 vs. 1.13 ± 0.61 copies/μL, p = 0.040). The correlation and multivariate analyses did not show any significant results (see **Appendix – Tables 7-17**).

4.8 Mutual correlation analyses between miRNAs' plasmatic concentrations at different timing points

Correlation analyses of miRNA plasmatic concentrations at different timing points were detailed in **Tables 3-7**.

	miR 21-5p at diagnosis			**miR 23b-3p at diagnosis**			**miR 34a-5p at diagnosis**		
	R	R^2	*p*	R	R^2	*p*	R	R^2	*p*
At diagnosis									
miR 21-5p				**0.931**	**0.867**	**<0.001**	**0.420**	**0.176**	**0.046**
miR 23b-3p	**0.931**	**0.867**	**<0.001**				0.253	0.064	0.244
miR 34a-5p	**0.420**	**0.176**	**0.046**	0.253	0.064	0.244			
FU1									
miR 21-5p	**0.651**	**0.424**	**0.006**	**0.796**	**0.634**	**<0.001**	0.013	0.000	0.961
miR 23b-3p	**0.672**	**0.452**	**0.004**	**0.819**	**0.671**	**<0.001**	0.018	0.000	0.947
miR 34a-5p	0.160	0.026	0.554	0.182	0.033	0.501	**0.522**	**0.272**	**0.038**
FU3									
miR 21-5p	-0.325	0.106	0.432	-0.141	0.020	0.738	**-0.750**	**0.563**	**0.032**
miR 23b-3p	0.227	0.052	0.589	0.386	0.149	0.345	-0.424	0.180	0.295
miR 34a-5p	-0.572	0.327	0.139	-0.480	0.230	0.228	-0.242	0.059	0.564
FU6									
miR 21-5p	-0.226	0.051	0.559	-0.289	0.084	0.451	-0.130	0.017	0.738
miR 23b-3p	0.029	0.001	0.940	0.041	0.002	0.917	-0.282	0.080	0.462
miR 34a-5p	-0.227	0.052	0.556	-0.145	0.021	0.710	-0.242	0.059	0.530
FU12									
miR 21-5p	0.839	0.704	0.075	0.137	0.019	0.826	0.220	0.048	0.722
miR 23b-3p	-0.007	0.000	0.991	-0.001	0.000	0.999	-0.354	0.125	0.559
miR 34a-5p	-0.479	0.229	0.415	-0.607	0.368	0.277	0.757	0.573	0.138

Table 3 – Correlation analysis between miR 21-5p, miR 23b-3p and miR 34a-5p plasmatic concentrations (copies/μL) at diagnosis and miR 21-5p, miR 23b-3p and miR 34a-5p plasmatic concentrations (copies/μL) at diagnosis, 1 (FU1), 3 (FU3), 6 (FU6) and 12 (FU12) months after surgery.

	miR 21-5p FU1			miR 23b-3p FU1			miR 34a-5p FU1		
	R	R^2	*p*	R	R^2	*p*	R	R^2	*p*
FU1									
miR 21-5p				**0.987**	**0.974**	**<0.001**	0.310	0.096	0.242
miR 23b-3p	**0.987**	**0.974**	**<0.001**				0.283	0.080	0.289
miR 34a-5p	0.310	0.096	0.242	0.283	0.080	0.289			
FU3									
miR 21-5p	0.115	0.013	0.829	0.154	0.024	0.770	-0.343	0.118	0.505
miR 23b-3p	0.675	0.456	0.141	0.707	0.500	0.116	-0.214	0.046	0.683
miR 34a-5p	-0.387	0.150	0.449	-0.343	0.118	0.505	-0.717	0.514	0.109
FU6									
miR 21-5p	-0.032	0.001	0.946	0.063	0.004	0.894	-0.039	0.002	0.934
miR 23b-3p	0.420	0.176	0.349	0.540	0.292	0.211	0.298	0.089	0.517
miR 34a-5p	-0.146	0.021	0.754	-0.085	0.007	0.856	-0.048	0.002	0.919
FU12									
miR 21-5p	0.431	0.186	0.569	-0.063	0.004	0.937	-0.108	0.012	0.892
miR 23b-3p	-0.659	0.434	0.341	-0.940	0.884	0.060	-0.113	0.013	0.887
miR 34a-5p	-0.456	0.208	0.544	-0.443	0.196	0.557	0.895	0.801	0.105

Table 4 – Correlation analysis between miR 21-5p, miR 23b-3p and miR 34a-5p plasmatic concentrations (copies/μL) 1 month (FU1) after surgery and miR 21-5p, miR 23b-3p and miR 34a-5p plasmatic concentrations (copies/μL) 1 (FU1), 3 (FU3), 6 (FU6) and 12 (FU12) months after surgery.

	miR 21-5p FU3			miR 23b-3p FU3			miR 34a-5p FU3		
	R	R^2	*p*	R	R^2	*p*	R	R^2	*p*
FU3									
miR 21-5p				**0.760**	**0.578**	**0.028**	0.689	0.475	0.059
miR 23b-3p	**0.760**	**0.578**	**0.028**				0.385	0.148	0.346
miR 34a-5p	0.689	0.475	0.059	0.385	0.148	0.346			
FU6									
miR 21-5p	0.585	0.342	0.300	0.717	0.134	0.849	**0.940**	**0.884**	**0.018**
miR 23b-3p	0.737	0.543	0.156	0.860	0.009	0.062	**0.945**	**0.893**	**0.015**
miR 34a-5p	**0.983**	**0.966**	**0.003**	0.849	0.924	0.069	0.448	0.201	0.171
FU12									
miR 21-5p	-	-	-	-	-	-	-	-	-
miR 23b-3p	-	-	-	-	-	-	-	-	-
miR 34a-5p	-	-	-	-	-	-	-	-	-

Table 5 – Correlation analysis between miR 21-5p, miR 23b-3p and miR 34a-5p plasmatic concentrations (copies/μL) 3 months (FU3) after surgery and miR 21-5p, miR 23b-3p and miR 34a-5p plasmatic concentrations (copies/μL) 3 (FU3), 6 (FU6) and 12 (FU12) months after surgery.

	miR 21-5p FU6			miR 23b-3p FU6			miR 34a-5p FU6		
	R	R^2	*p*	R	R^2	*p*	R	R^2	*p*
FU6									
miR 21-5p				**0.847**	**0.717**	**0.004**	0.400	0.160	0.287
miR 23b-3p	**0.847**	**0.717**	**0.004**				0.349	0.122	0.358
miR 34a-5p	0.400	0.160	0.287	0.349	0.122	0.358			
FU12									
miR 21-5p	**0.968**	**0.937**	**0.032**	0.830	0.689	0.170	0.259	0.067	0.741
miR 23b-3p	0.559	0.312	0.441	0.634	0.402	0.366	-0.688	0.473	0.312
miR 34a-5p	0.200	0.040	0.800	-0.001	0.000	0.999	-0.729	0.531	0.271

Table 6 – Correlation analysis between miR 21-5p, miR 23b-3p and miR 34a-5p plasmatic concentrations (copies/μL) 6 months (FU6) after surgery and miR 21-5p, miR 23b-3p and miR 34a-5p plasmatic concentrations (copies/μL) 6 (FU6) and 12 (FU12) months after surgery.

	miR 21-5p FU12			miR 23b-3p FU12			miR 34a-5p FU12		
	R	R^2	*p*	R	R^2	*p*	R	R^2	*p*
FU12									
miR 21-5p				0.447	0.200	0.451	-0.164	0.027	0.792
miR 23b-3p	0.447	0.200	0.451				-0.027	0.001	0.965
miR 34a-5p	-0.164	0.027	0.792	-0.027	0.001	0.965			

Table 7 – Correlation analysis between miR 21-5p, miR 23b-3p and miR 34a-5p plasmatic concentrations (copies/μL) 12 months (FU12) after surgery.

miR 21-5p levels at diagnosis were significantly correlated to miR 23b-3p (r=0.931, R^2=0.867; *p*<0.001) and miR 34a-5p levels at diagnosis (r = 0.420, R^2 = 0.176; *p*=0.046), but also to miR 21-5p levels 1 month after surgery (r=0.651, R^2=0.424; *p*=0.006) and miR 23b-3p levels 1 month after surgery (r=0.672, R^2=0.452; *p*=0.004). Similarly, miR 21-5p levels 1 month after surgery were significantly correlated to miR 23b-3p levels 1 month after surgery (r=0.987, R^2=0.974; *p*<0.001) (**Figure 39**).

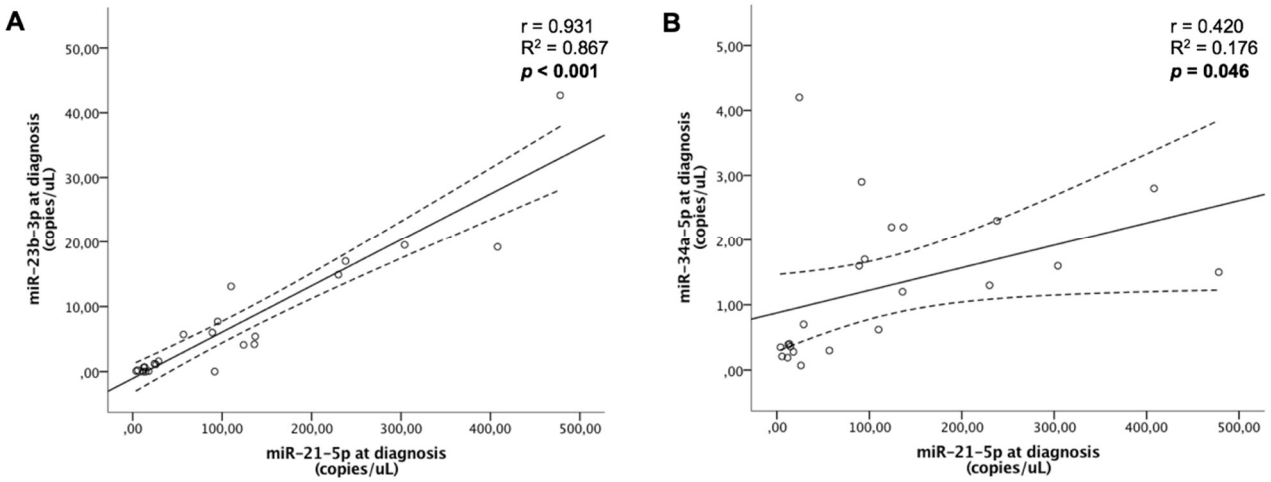

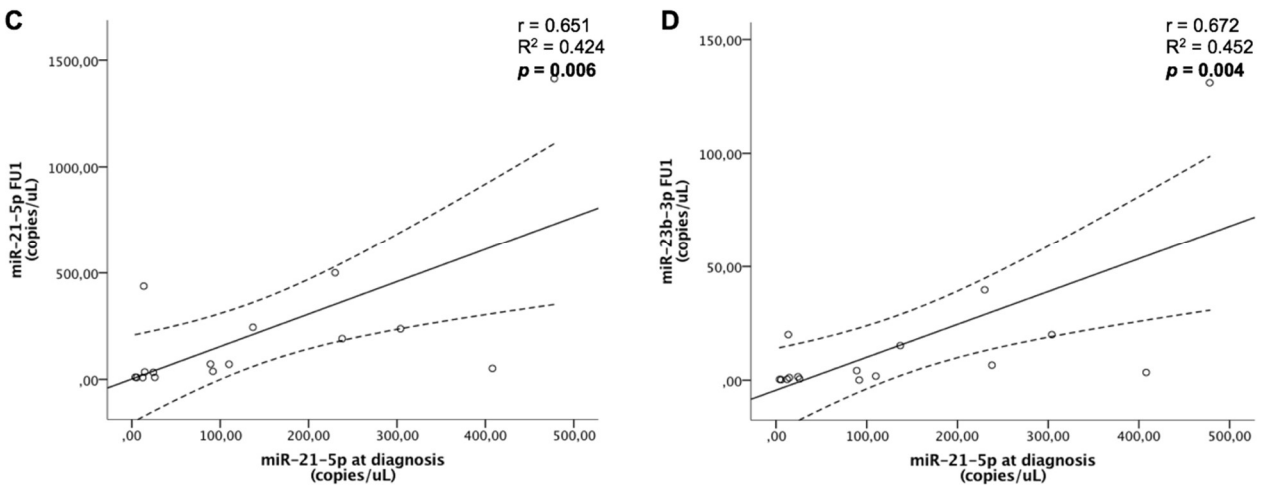

Figure 39 – Scatter plots correlating miR 21-5p plasmatic concentrations at diagnosis with miR 23b-3p plasmatic concentrations at diagnosis (**A**), miR 34a-5p plasmatic concentrations at diagnosis (**B**), miR 21-5p plasmatic concentrations 1 month after surgery (**C**) and miR 23b-3p plasmatic concentrations at 1 month after surgery (**D**).

miR 21-5p levels 3 months after surgery were significantly correlated to miR 23b-3p levels 3 months after surgery (r=0.760, R^2=0.578; *p*=0.028) and miR 34a-5p 6 months after surgery (r=0.983, R^2=0.966; *p*=0.003). miR 21-5p levels 6 months after surgery were related to miR 23b-3p levels 6 months after surgery (r=0.847, R^2=0.717; *p*=0.004) and to miR 21-5p levels 12 months after surgery (r=0.968, R^2=0.937; *p*=0.032) (**Figure 40**).

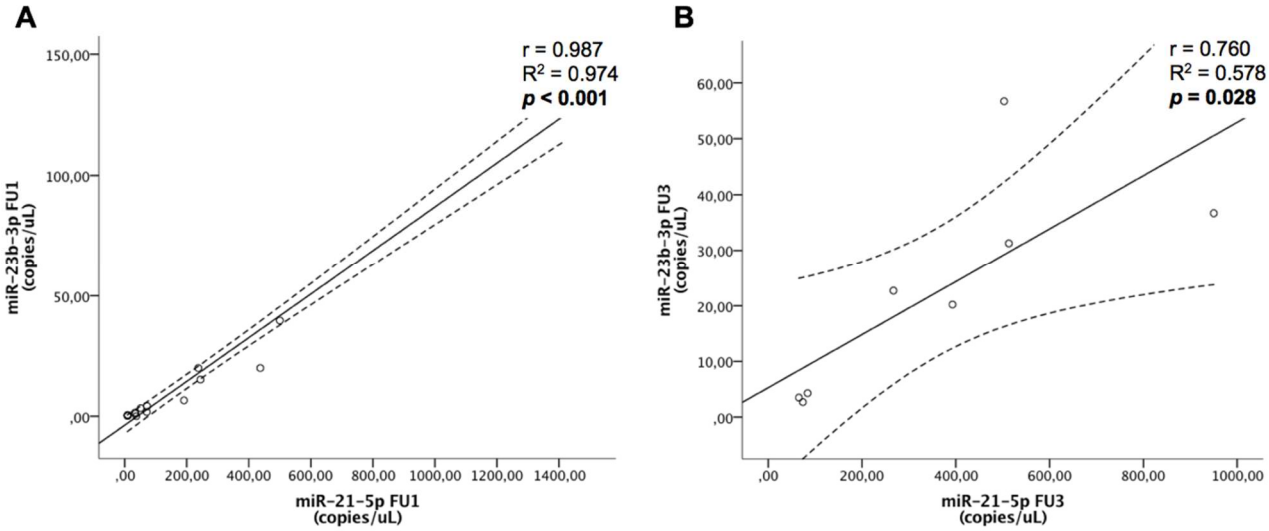

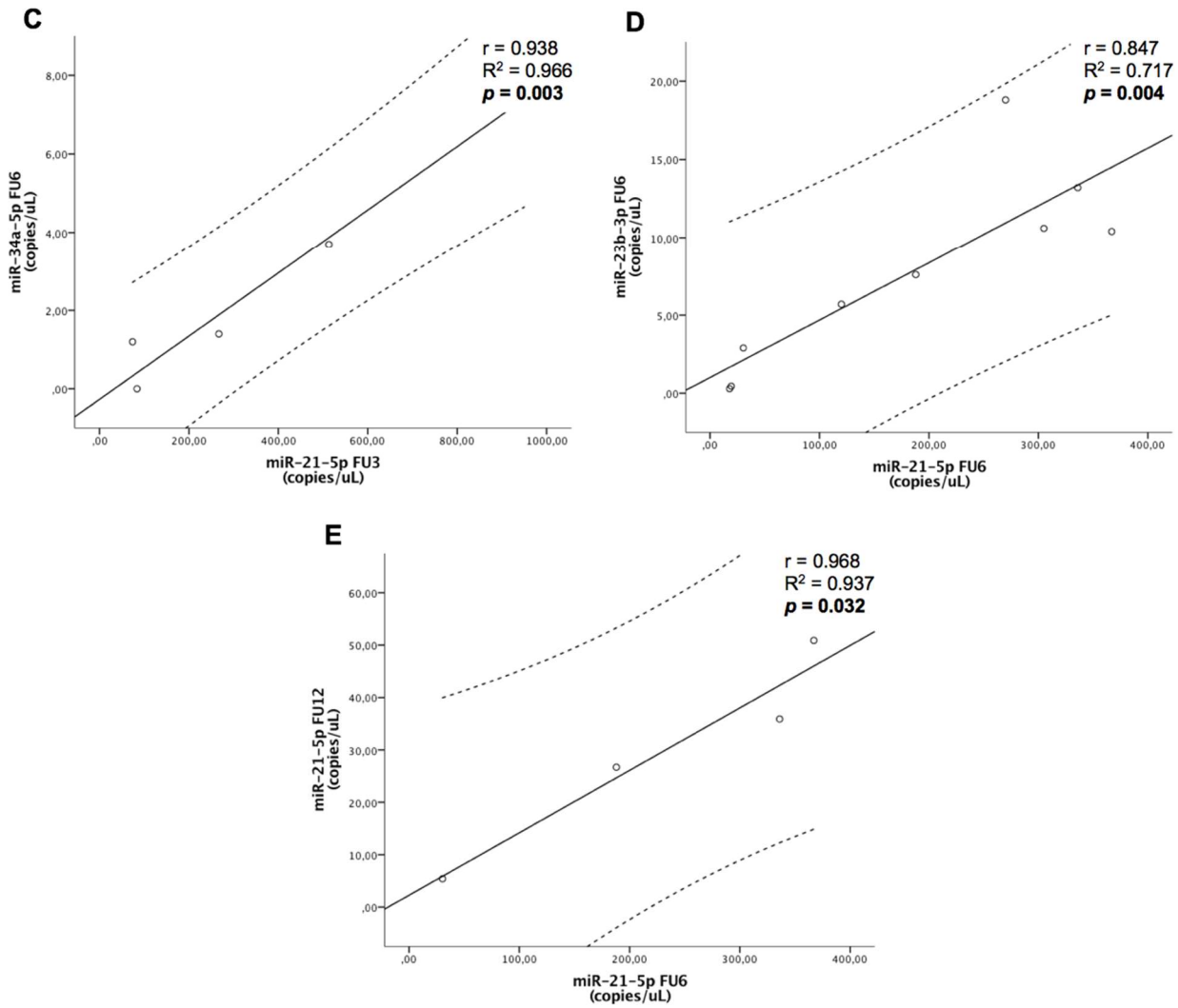

Figure 40 – Scatter plots showing mutual correlation of miR 21-5p plasmatic concentrations at different timing points.

miR 23b-3p levels at diagnosis were significantly correlated to miR 21-5p levels at diagnosis (r=0.931, R^2=0.867; *p*<0.001), miR 21-5p levels 1 month after surgery (r=0.796, R^2=0.634; *p*<0.001) and miR 23b-3p 1 month after surgery (r=0.819, R^2=0.671; *p*<0.001). Similarly, miR 23b-3p levels 1 month after surgery were significantly correlated to miR 21-5p levels 1 month after surgery (r=0.987, R^2=0.974; *p*<0.001) (**Figure 41**).

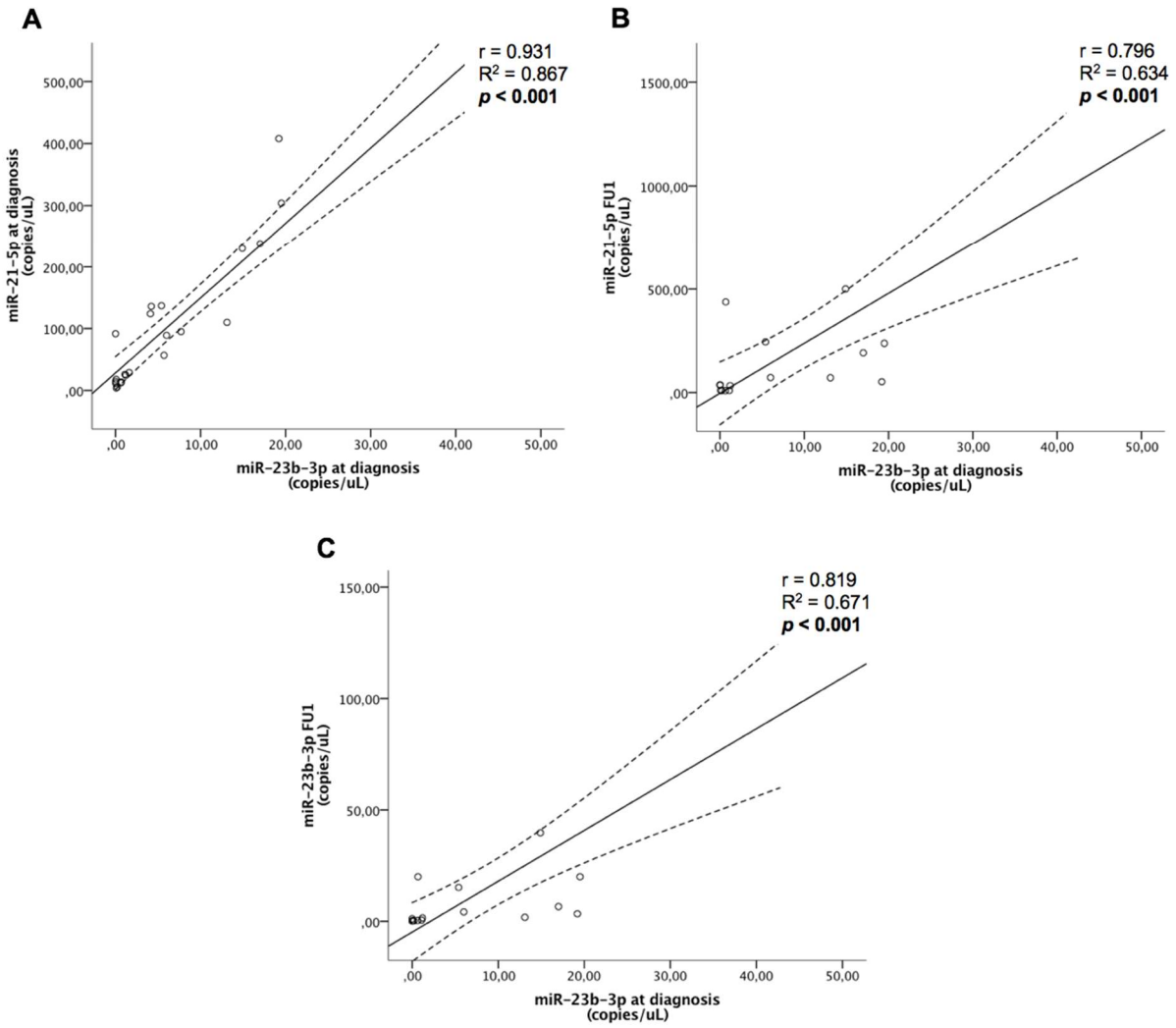

Figure 41 – Scatter plots displaying mutual correlation of miR 23b-3p plasmatic concentrations at different timing points.

miR 34a-5p levels at diagnosis were significantly correlated to miR 21-5p levels at diagnosis (r=0.420, R^2=0.176; *p*=0.046), miR 34a-5p levels 1 month after surgery (r=0.522, R^2=0.272; *p*=0.038) and miR 21-5p levels 3 months after surgery (r=-0.750, R^2=0.563; *p*=0.032). Furthermore, miR 34a-5p levels 3 months after surgery were significantly related to miR 21-5p (r=0.940, R^2=0.884; *p*=0.018) and miR 23b-3p (r=0.945, R^2=0.893; *p*=0.015) levels 6 months after surgery (**Figure 42**).

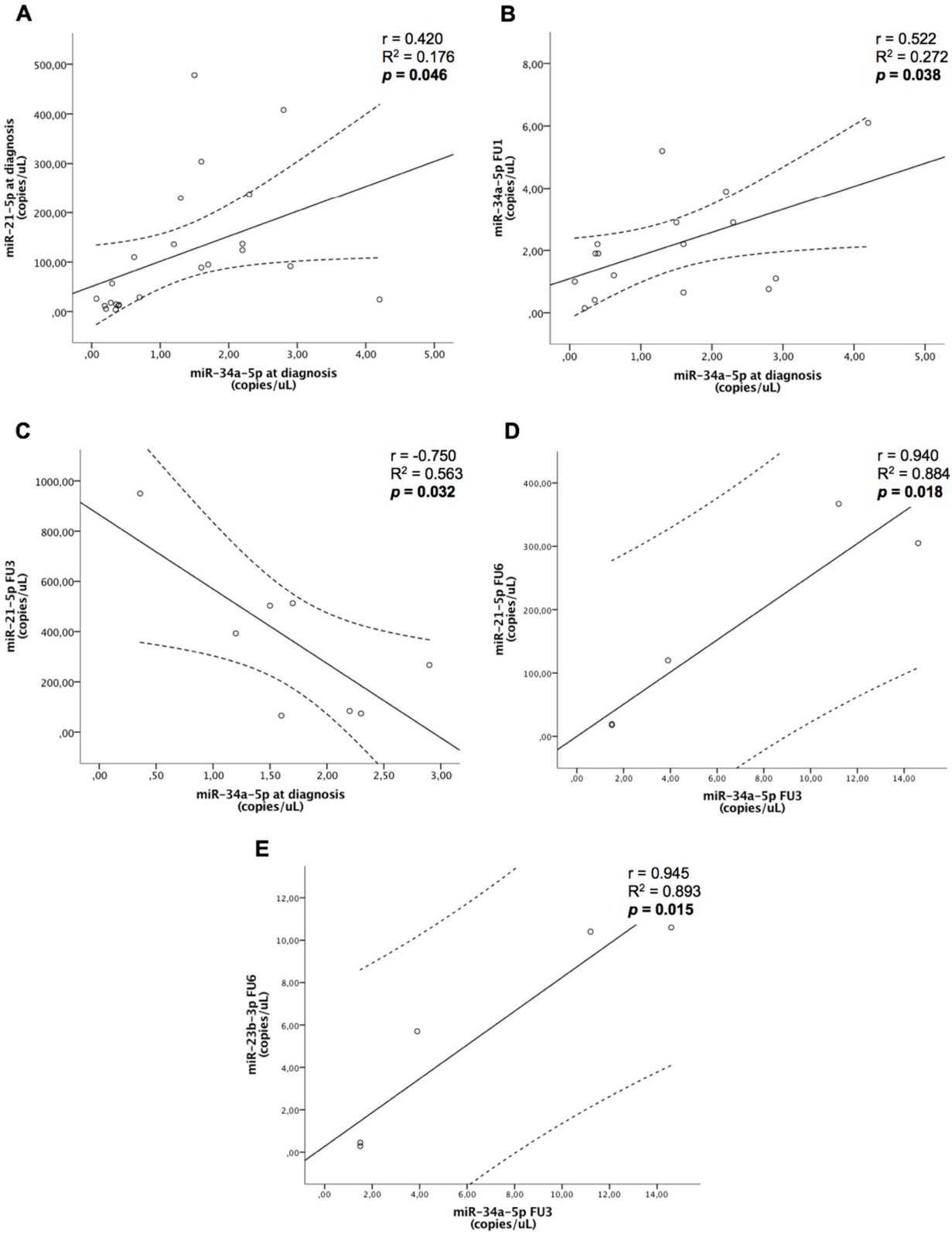

Figure 42 – Scatter plots showing mutual correlation of miR 34a-5p plasmatic concentrations at different timing points.

The multivariate linear regression analyses (see **Appendix** – **Tables 18-22**) showed that miR 23b-3p (OR 11.50, 95% C.I. 9.53 – 13.47, *p*<0.001) and miR 34a-5p (OR 23.80, 95% C.I. 5.57 – 42.02, *p*=0.013) levels at diagnosis were predictors of miR 21-5p levels at diagnosis such as miR 21-5p levels at diagnosis independently predicted miR 23b-3p (OR 0.08, 95% C.I. 0.06 – 0.09, *p*<0.001) and miR 34a-5p (OR 0.01, 95% C.I. 0.00 – 0.02, *p*=0.013) levels at diagnosis. Furthermore, miR 23b-3p plasmatic concentrations 1 month after surgery predicted miR 21-5p levels 1 month after surgery (OR 10.83, 95% C.I. 8.34 – 13.32, *p*<0.001) and vice versa (OR 0.08, 95% C.I. 0.06 – 0.10, *p*<0.001). miR 21-5p levels 6 months after surgery predicted miR 23b-3p levels 6 months after surgery (OR 0.02, 95% C.I. 0.01 – 0.03, *p*=0.022) (**Table 8**).

	OR	95% CI	*p* value
miR 21-5p at diagnosis			
miR 23b-3p at diagnosis	**11.50**	**9.53 – 13.47**	**<0.001**
miR 34a-5p at diagnosis	**23.80**	**5.57 – 42.02**	**0.013**
miR 23b-3p at diagnosis			
miR 21-5p at diagnosis	**0.08**	**0.06 – 0.09**	**<0.001**
miR 34a-5p at diagnosis			
miR 21-5p at diagnosis	**0.01**	**0.00 – 0.02**	**0.013**
miR 21-5p at FU1			
miR 23b-3p at FU1	**10.83**	**8.34 – 13.32**	**<0.001**
miR 23b-3p at FU1			
miR 21-5p at FU1	**0.08**	**0.06 – 0.10**	**<0.001**
miR 23b-3p at FU6			
miR 21-5p at FU6	**0.02**	**0.01 – 0.03**	**0.022**

Table 8 – Multivariate linear regression analysis between miR 21-5p, miR 23b-3p and miR 34a-5p plasmatic concentrations.

4.9 miRNA network analysis

According to the miRNet analysis (see **Appendix** – **Table 23**), we identified 5 genes (*E2F1*, *TNPO1*, *MTAP*, *CPEB3*, *NUFIP2*) regulated by miR 21-5p, miR-23b-3p and miR 34a-5p. Among them, *E2F1* was deregulated in gliomas (**Figure 43**).

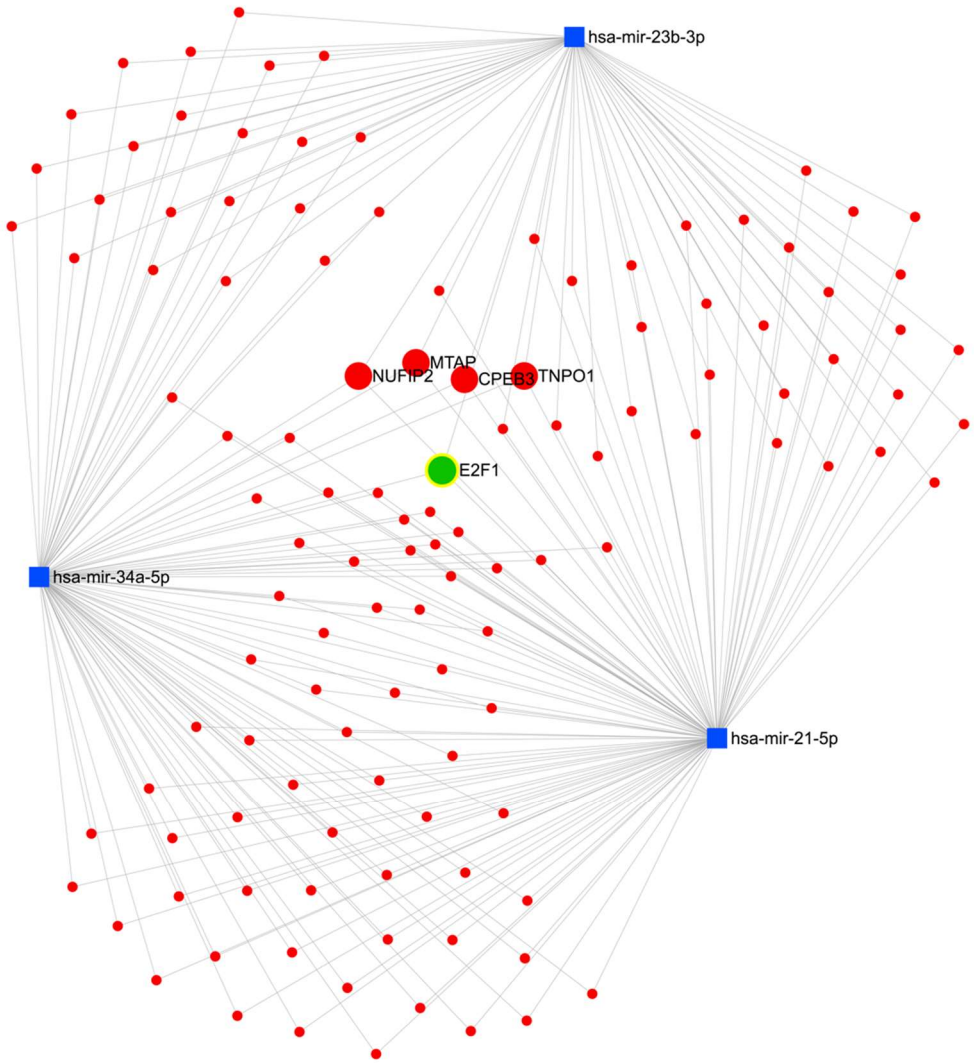

Figure 43 – Network visualization of miR 21-5p, miR-23b-3p and miR 34a-5p (blue squares) and related genes (red dots), highlighting genes deregulated in gliomas (green dots; miRNet version 2.0).

Focusing on miR 21-5p and miR 23b-3p, the network analysis (see **Appendix** – **Table 24**) identified 36 genes 4 of which (*E2F1*, *PTEN*, *PIK3R1*, *RB1*) were related to gliomas (**Figure 44**).

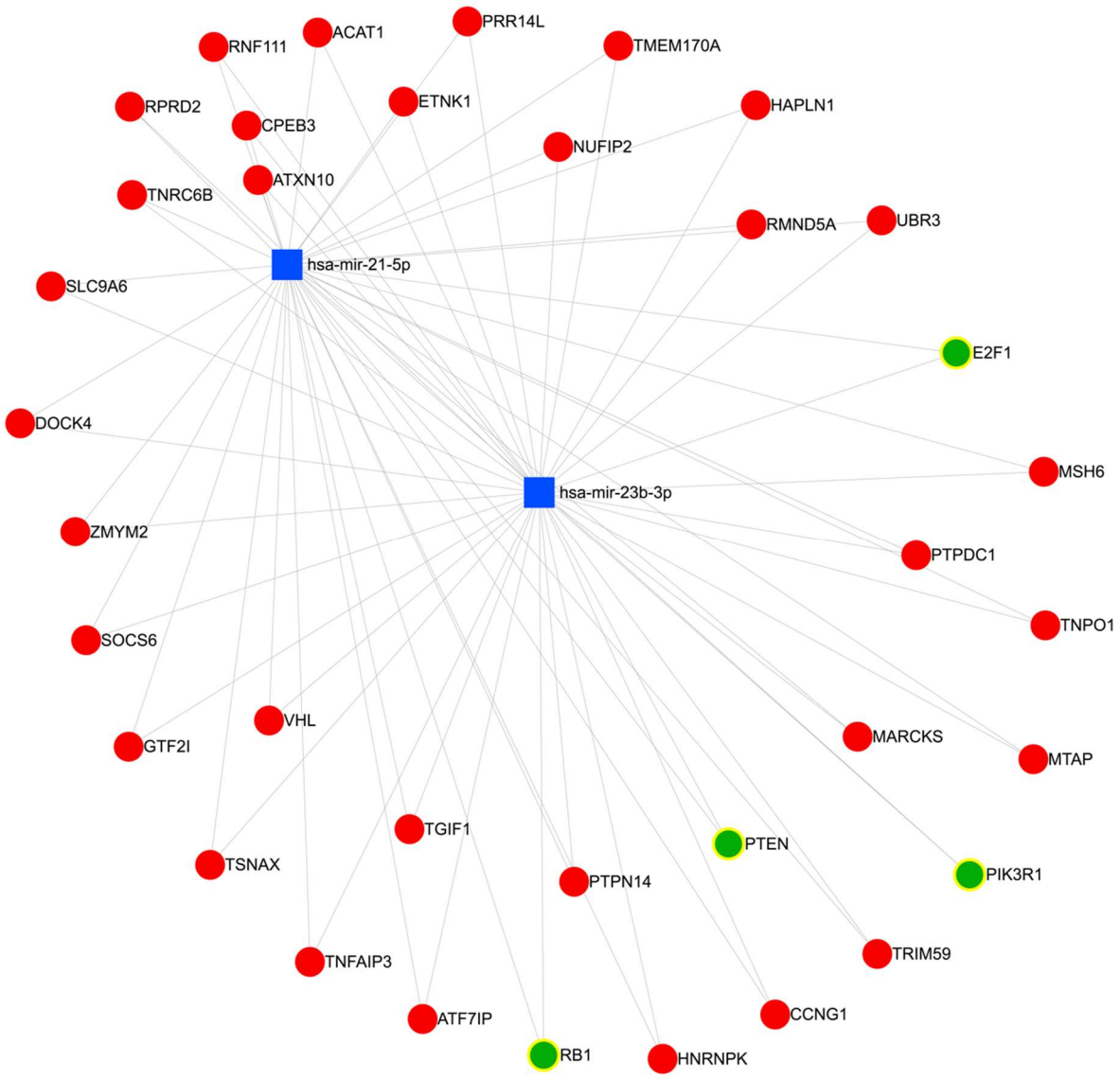

Figure 44 – Network visualization of miR 21-5p and miR 23b-3p (blue squares) and related genes (red dots), highlighting genes deregulated in gliomas (green dots; miRNet version 2.0).

Analysing miR 21-5p and miR 34a-5p, the network analysis (see **Appendix** – **Table 25**) identified 67 genes 4 of which (*E2F1*, *E2F3*, *CDK6*, *IGF1R*) were involved in the pathogenesis of gliomas (**Figure 45**).

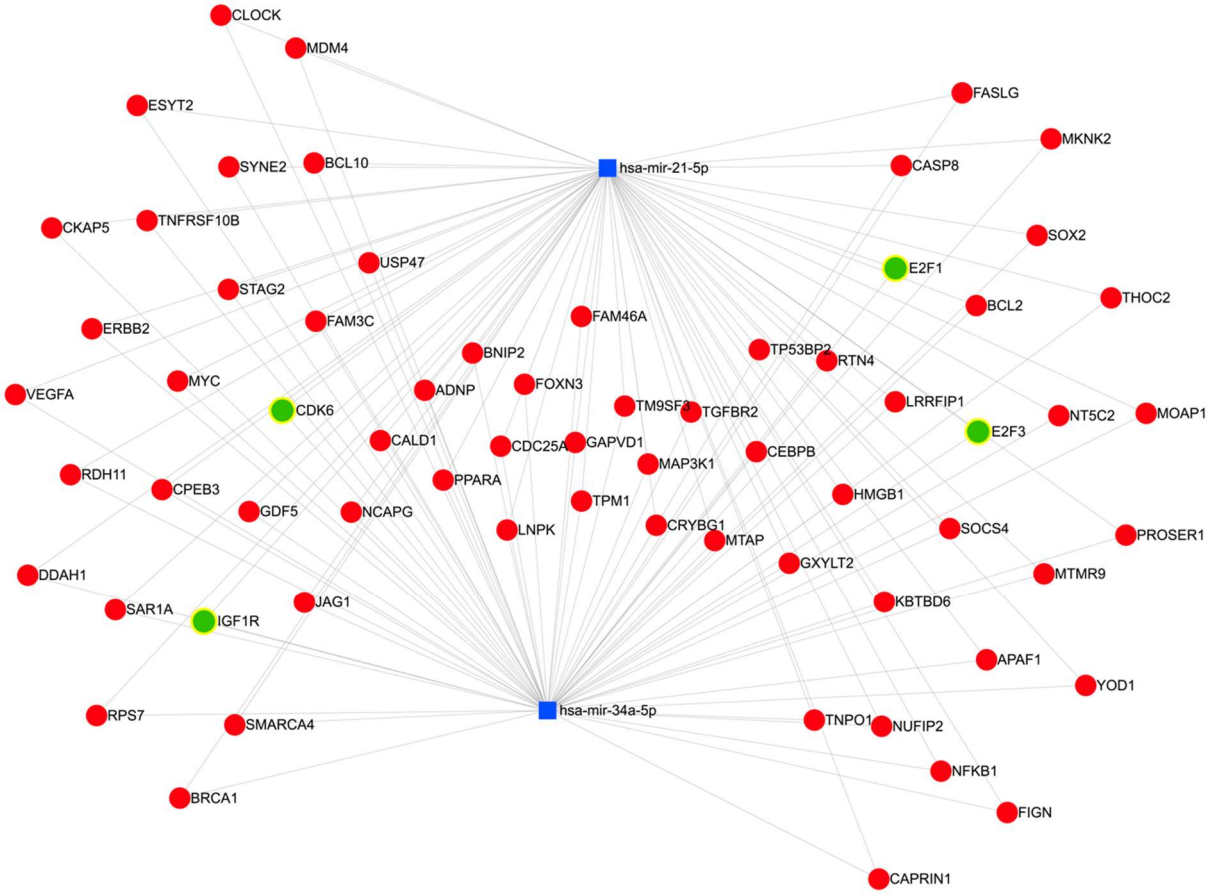

Figure 45 – Network visualization of miR 21-5p and miR 34a-5p (blue squares) and related genes (red dots), highlighting genes deregulated in gliomas (green dots; miRNet version 2.0).

4.10 Overall survival analysis

The mean length of follow-up was 11.9 months (± 9.4; median 8.0, IQR: 3.0-17.0). The mean OS was 12.4 months (95% C.I. 8.4 – 16.4) with 39.1% and 21.7% of predicted OS at 1 and 2 years, respectively (**Figure 46**).

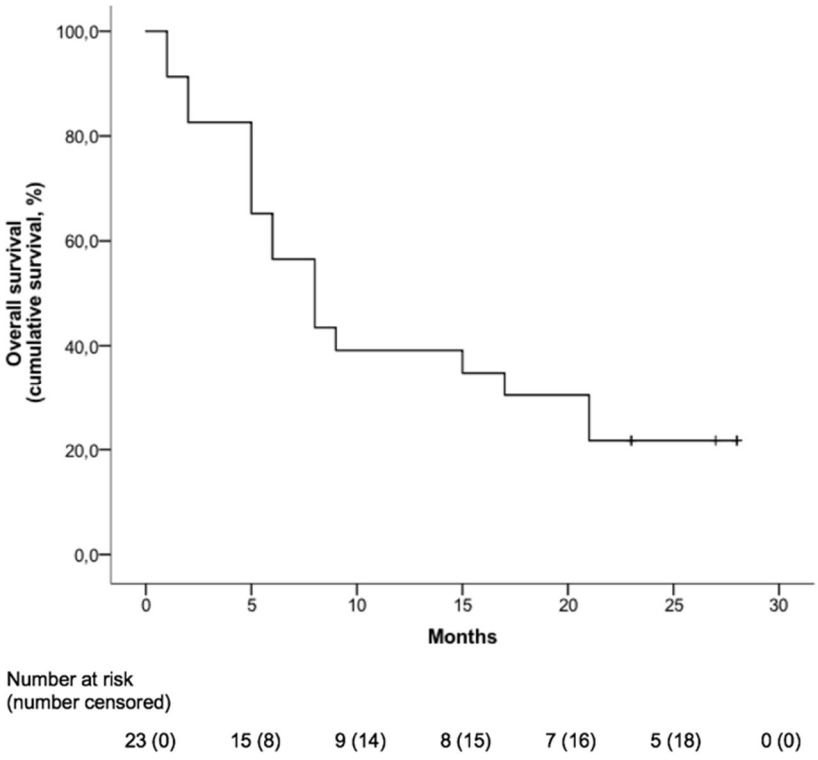

Figure 46 – Overall survival; **B**) Recurrence free survival.

The Cox regression analysis showed no relationships between miR 21-5p, miR 23b-3p and miR 34a-5p plasmatic concentrations at different timing points and OS or RFS (see **Appendix** – **Tables 26-27**).

4.10.1 Overall survival according to miRNAs' variations at different timing points

After splitting the population in two groups of patients experiencing increase or stability/decrease of miRNAs circulating levels over the follow up, the mean OS were compared (**Table 9**).

		Mean OS (95% C.I.)	pOS at 1 year (%)	pOS at 2 years (%)	*p* value
miR 21-5p diagnosis-FU1	Increase	14.6 (7.5 – 21.8)	50.0	25.0	0.763
	Stability/Decrease	12.1 (5.3 – 18.9)	37.5	25.0	
miR 23b-3p diagnosis-FU1	Increase	15.5 (7.8 – 23.2)	50.0	37.5	0.353
	Stability/Decrease	10.6 (5.5 – 15.8)	25.0	12.5	
miR 34a-5p diagnosis-FU1	Increase	11.0 (5.8 – 16.2)	25.0	16.7	0.171
	Stability/Decrease	20.5 (11.3 – 29.7)	75.0	50.0	
miR 21-5p FU1-FU3	Increase	**24.5 (19.7 – 29.4)**	**50.0**	**50.0**	**0.049**
	Stability/Decrease	**8.5 (4.1 – 12.9)**	**25.0**	**0.0**	
miR 23b-3p FU1-FU3	Increase	**24.5 (19.7 – 29.4)**	**50.0**	**50.0**	**0.049**
	Stability/Decrease	**8.5 (4.1 – 12.9)**	**25.0**	**0.0**	
miR 34a-5p FU1-FU3	Increase	**24.5 (19.7 – 29.4)**	**50.0**	**50.0**	**0.049**
	Stability/Decrease	**8.5 (4.1 – 12.9)**	**25.0**	**0.0**	
miR 21-5p FU3-FU6	Increase	-	-	-	0.156
	Stability/Decrease	-	-	-	
miR 23b-3p FU3-FU6	Increase	-	-	-	-
	Stability/Decrease	16.2 (9.6 – 22.8)	60.0	20.0	
miR 34a-5p FU3-FU6	Increase	-	-	-	-
	Stability/Decrease	16.2 (9.6 – 22.8)	60.0	20.0	
miR 21-5p FU6-FU12	Increase	-	-	-	-
	Stability/Decrease	23.5 (18.9 – 28.1)	100.0	50.0	
miR 23b-3p FU6-FU12	Increase	-	-	-	-
	Stability/Decrease	23.5 (18.9 – 28.1)	100.0	50.0	
miR 34a-5p FU6-FU12	Increase	-	-	-	0.090
	Stability/Decrease	-	-	-	

Table 9 – Mean and predicted OS according to variations (increase or stability/decrease) of circulating levels of miR 21-5p, miR 23b-3p and miR 34a-5p at different timing points.
pOS: predicted overall survival.

The mean OS was significantly longer in patients presenting increased levels of miR 21-5p, miR 23b-3p and miR 34a-5p (24.5 months, 95% C.I. 19.7 – 29.4 vs. 8.5 months, 95% C.I. 4.1 – 12.9; *p*=0.049) between 1 and 3 months after surgery (**Figures 47-50**).

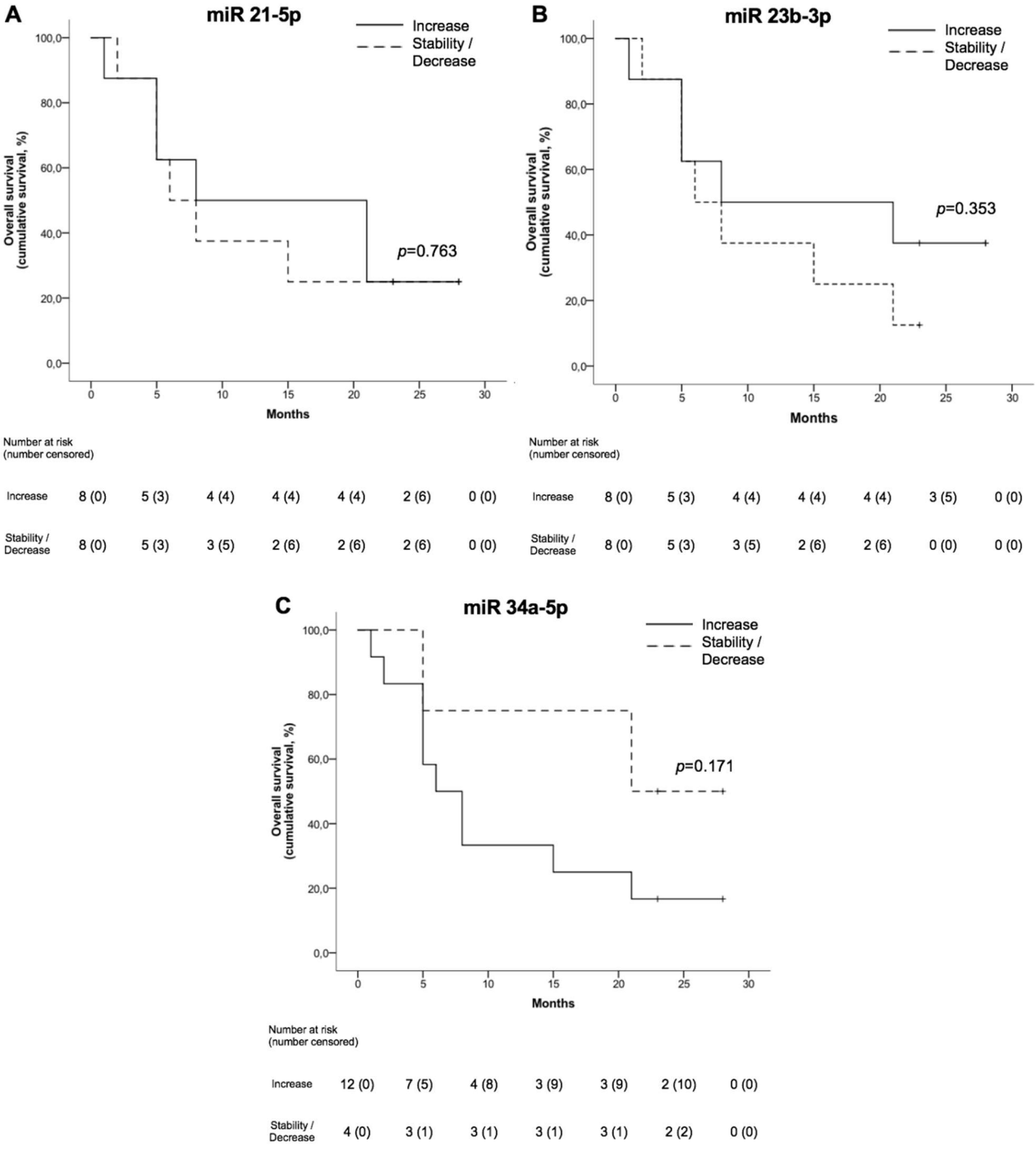

Figure 47 – Overall survival Kaplan–Meier curves comparing patients with increased (solid line) and stable or decreased (dashed line) circulating levels of miR 21-5p (**A**), miR 23b-3p (**B**) and miR 34a-5p (**C**) between the diagnosis and 1 month after surgery.

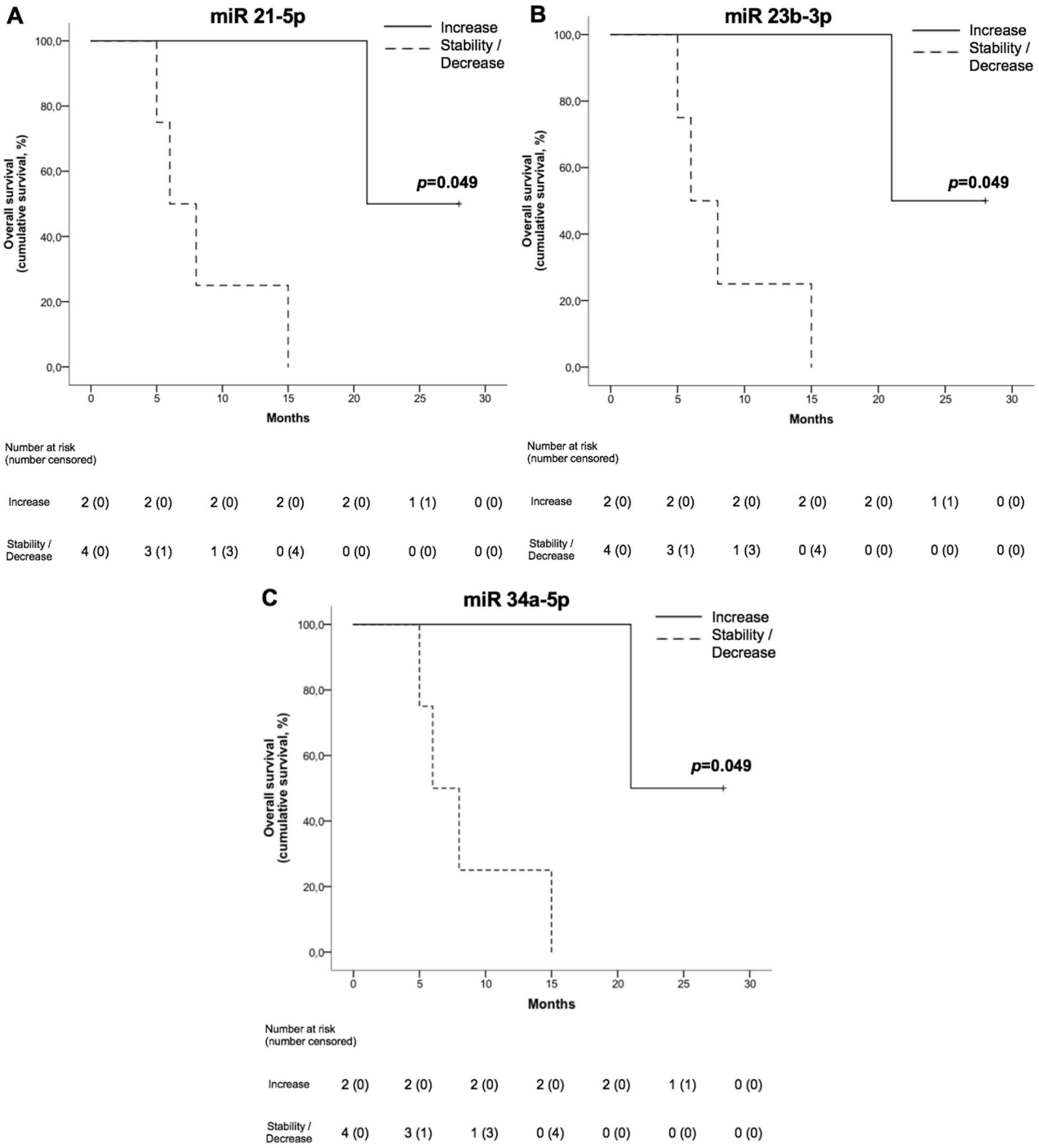

Figure 48 – Overall survival Kaplan–Meier curves comparing patients with increased (solid line) and stable or decreased (dashed line) circulating levels of miR 21-5p (**A**), miR 23b-3p (**B**) and miR 34a-5p (**C**) between 1 and 3 months after surgery.

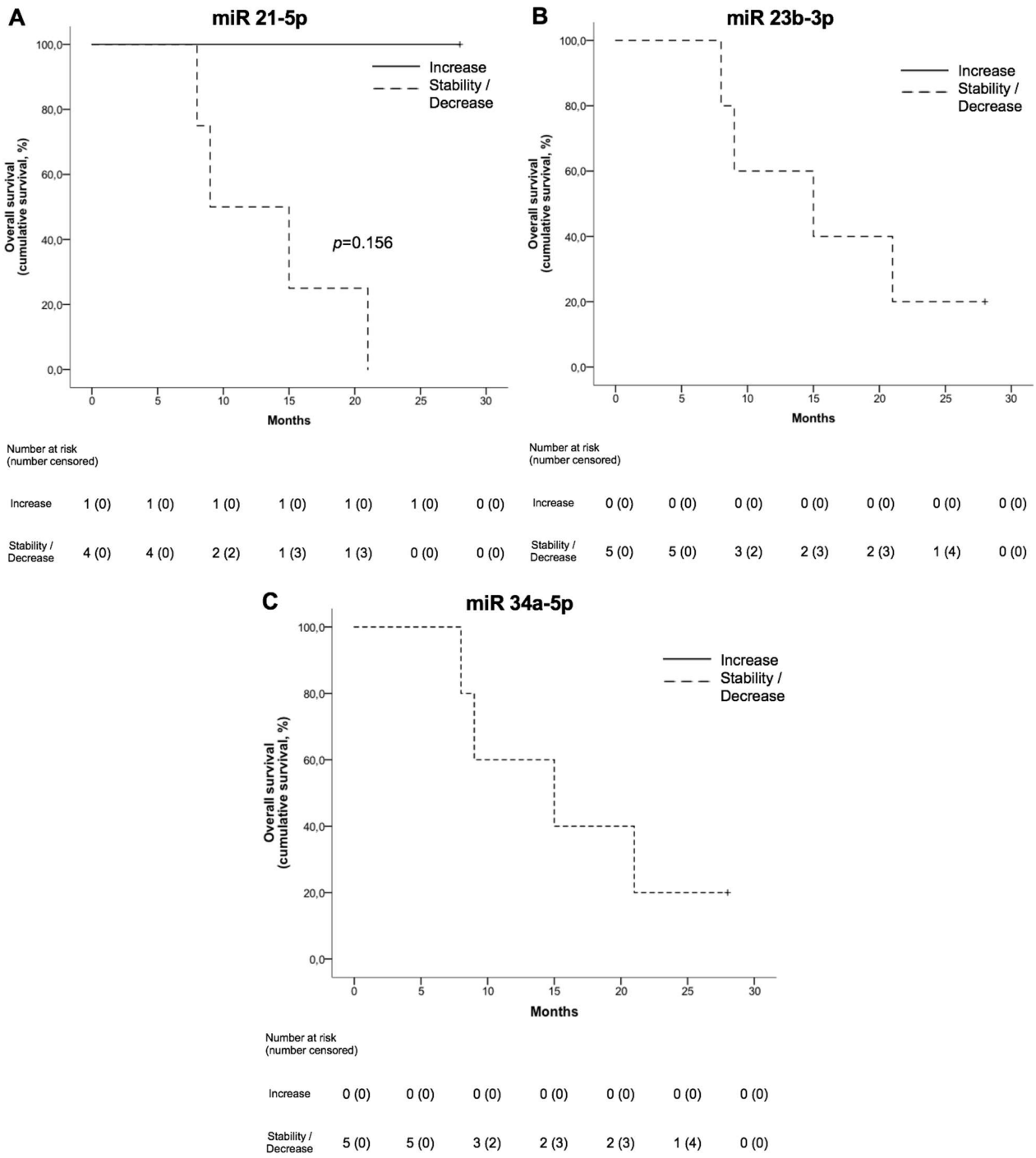

Figure 49 – Overall survival Kaplan–Meier curves comparing patients with increased (solid line) and stable or decreased (dashed line) circulating levels of miR 21-5p (**A**), miR 23b-3p (**B**) and miR 34a-5p (**C**) between 3 and 6 months after surgery.

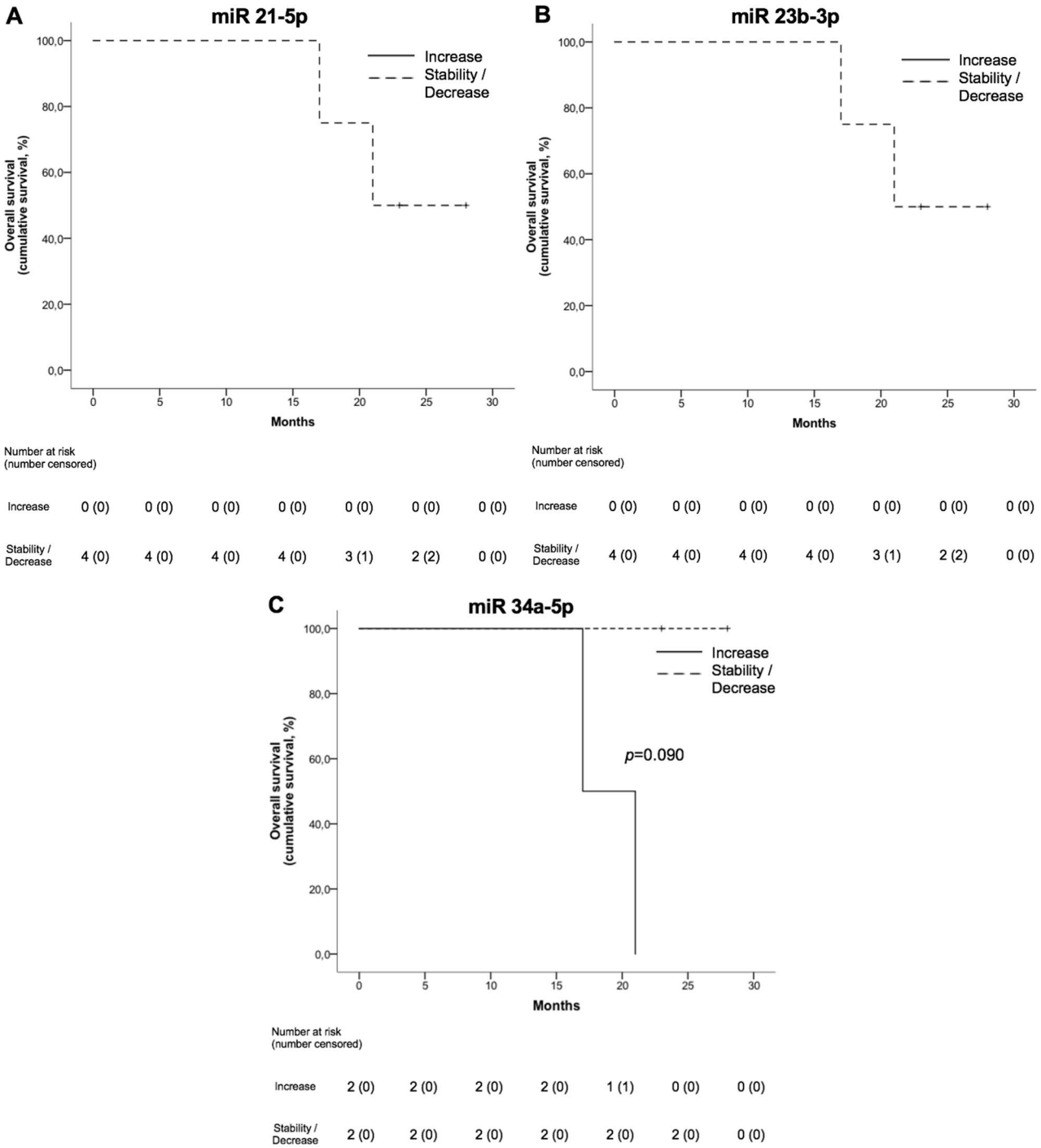

Figure 50 – Overall survival Kaplan–Meier curves comparing patients with increased (solid line) and stable or decreased (dashed line) circulating levels of miR 21-5p (**A**), miR 23b-3p (**B**) and miR 34a-5p (**C**) between 6 and 12 months after surgery.

4.10.2 Overall survival according to mean miRNAs' plasmatic concentrations

After splitting the population above and below the mean values of circulating miRNAs at different timing points (**Table 10**). The mean OS was significantly shorter in patients with miR 34a-5p levels below the mean 3 months after surgery (8.2 months, 95% C.I. 5.2 – 11.1 vs 24.5 months, 95% C.I. 19.6 – 29.4; *p*=0.032) and in those with miR 21-5p levels below the mean 6 months after surgery (13.3 months, 95% C.I. 7.4 – 19.2 vs 24.4 months, 95% C.I. 20.4 – 28.4; *p*=0.024) (**Figures 51-55**).

		Mean OS (95% C.I.)	**pOS at 1 year (%)**	**pOS at 2 years (%)**	***p* value**
miR 21-5p at diagnosis	Below the mean	14.1 (8.8 – 19.3)	46.7	26.7	0.265
	Above the mean	8.6 (4.1 – 13.2)	25.0	12.5	
miR 23b-3p at diagnosis	Below the mean	13.4 (4.3 – 14.3)	43.8	25.0	0.456
	Above the mean	9.3 (8.4 – 16.4)	28.6	14.3	
miR 34a-5p at diagnosis	Below the mean	10.3 (5.5 – 15.1)	33.3	8.3	0.213
	Above the mean	14.6 (8.4 – 20.9)	45.5	36.4	
miR 21-5p at FU1	Below the mean	14.7 (8.6 – 20.9)	54.5	27.3	0.618
	Above the mean	9.4 (3.4 – 15.4)	20.0	20.0	
miR 23b-3p at FU1	Below the mean	14.2 (8.4 – 19.9)	50.0	25.0	0.734
	Above the mean	9.8 (2.2 – 17.3)	25.0	25.0	
miR 34a-5p at FU1	Below the mean	13.2 (6.4 – 20.1)	44.4	22.2	0.808
	Above the mean	13.6 (6.4 – 20.7)	42.9	28.6	
miR 21-5p at FU3	Below the mean	14.3 (5.8 – 22.7)	50.0	25.0	0.475
	Above the mean	10.3 (3.0 – 17.5)	25.0	0	
miR 23b-3p at FU3	Below the mean	8.8 (4.6 – 12.9)	25.0	0	0.230
	Above the mean	15.8 (6.7 – 24.8)	50.0	25.0	
miR 34a-5p at FU3	Below the mean	**8.2 (5.2 – 11.1)**	**16.7**	**0**	**0.032**
	Above the mean	**24.5 (19.6 – 29.4)**	**100.0**	**50.0**	
miR 21-5p at FU6	Below the mean	**13.3 (7.4 – 19.2)**	**50.0**	**0**	**0.024**
	Above the mean	**24.4 (20.4 – 28.4)**	**100.0**	**60.0**	
miR 23b-3p at FU6	Below the mean	15.2 (9.9 – 20.5)	60.0	20.0	0.230
	Above the mean	23.5 (18.9 – 28.1)	100.0	50.0	
miR 34a-5p at FU6	Below the mean	17.8 (12.0 – 23.6)	80.0	20.0	0.356
	Above the mean	19.0 (13.3 – 24.7)	75.0	50.0	
miR 21-5p at FU12	Below the mean	25.7 (21.9 – 29.4)	100.0	66.7	0.592
	Above the mean	22.5 (14.9 – 30.1)	100.0	50.0	
miR 23b-3p at FU12	Below the mean	25.7 (21.9 – 29.4)	100.0	66.7	0.592
	Above the mean	22.5 (14.9 – 30.1)	100.0	50.0	
miR 34a-5p at FU12	Below the mean	-	100.0	33.3	0.199
	Above the mean	-	100.0	100.0	

Table 10 – Mean and predicted OS according to mean miR 21-5p, miR 23b-3p and miR 34a-5p plasmatic concentrations at diagnosis, 1 (FU1), 3 (FU3), 6 (FU6) and 12 months (FU12) after surgery.

pOS: predicted overall survival.

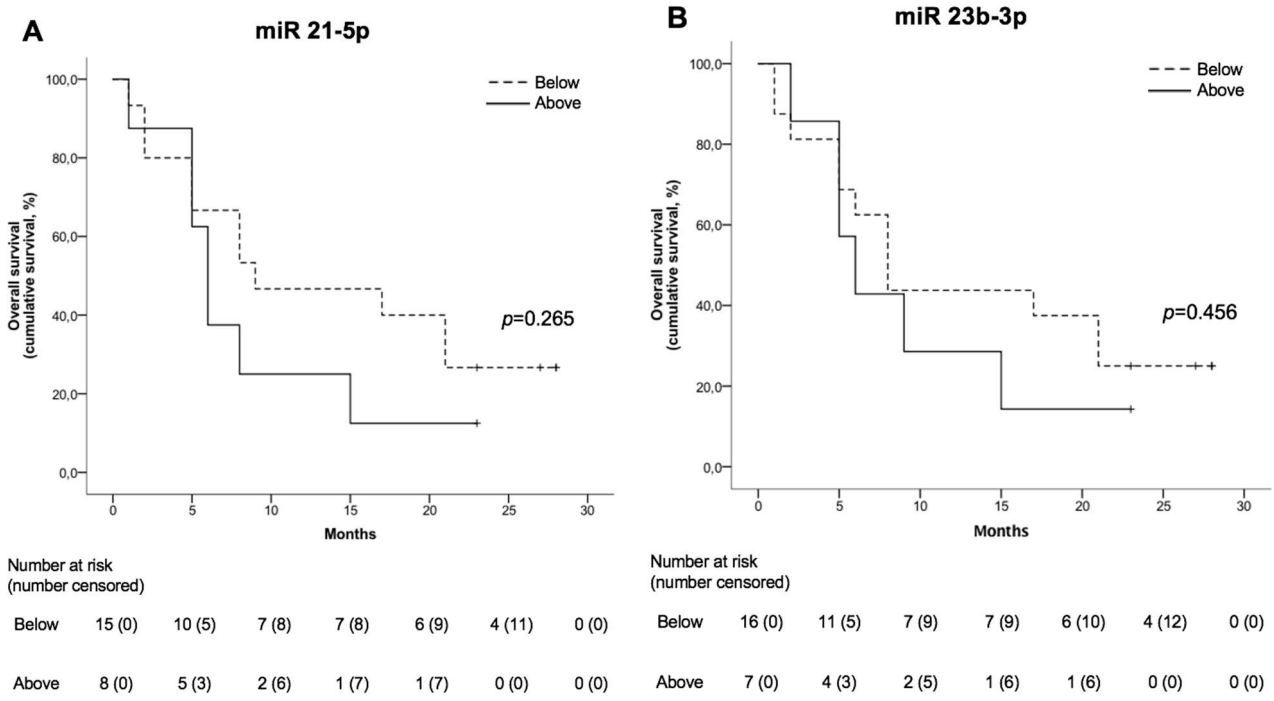

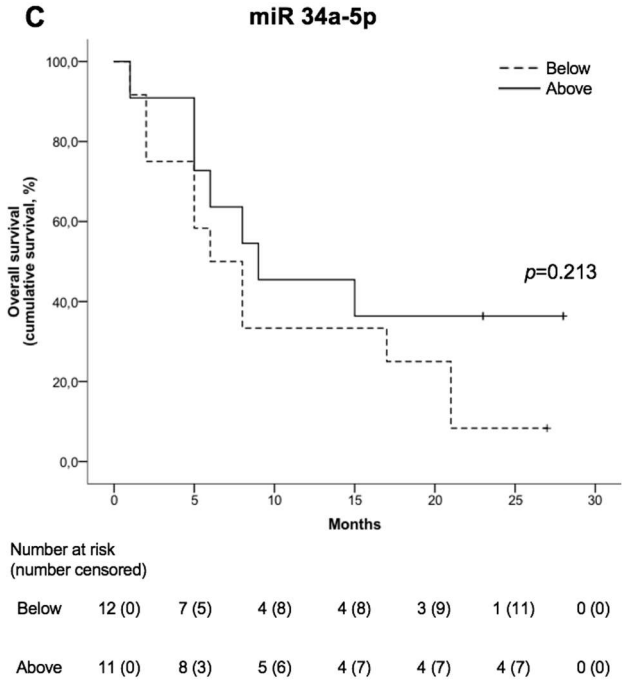

Figure 51 – Overall survival Kaplan–Meier curves comparing patients with circulating levels of miR 21-5p (**A**), miR 23b-3p (**B**) and miR 34a-5p (**C**) below (dashed line) and above (solid line) the mean at diagnosis.

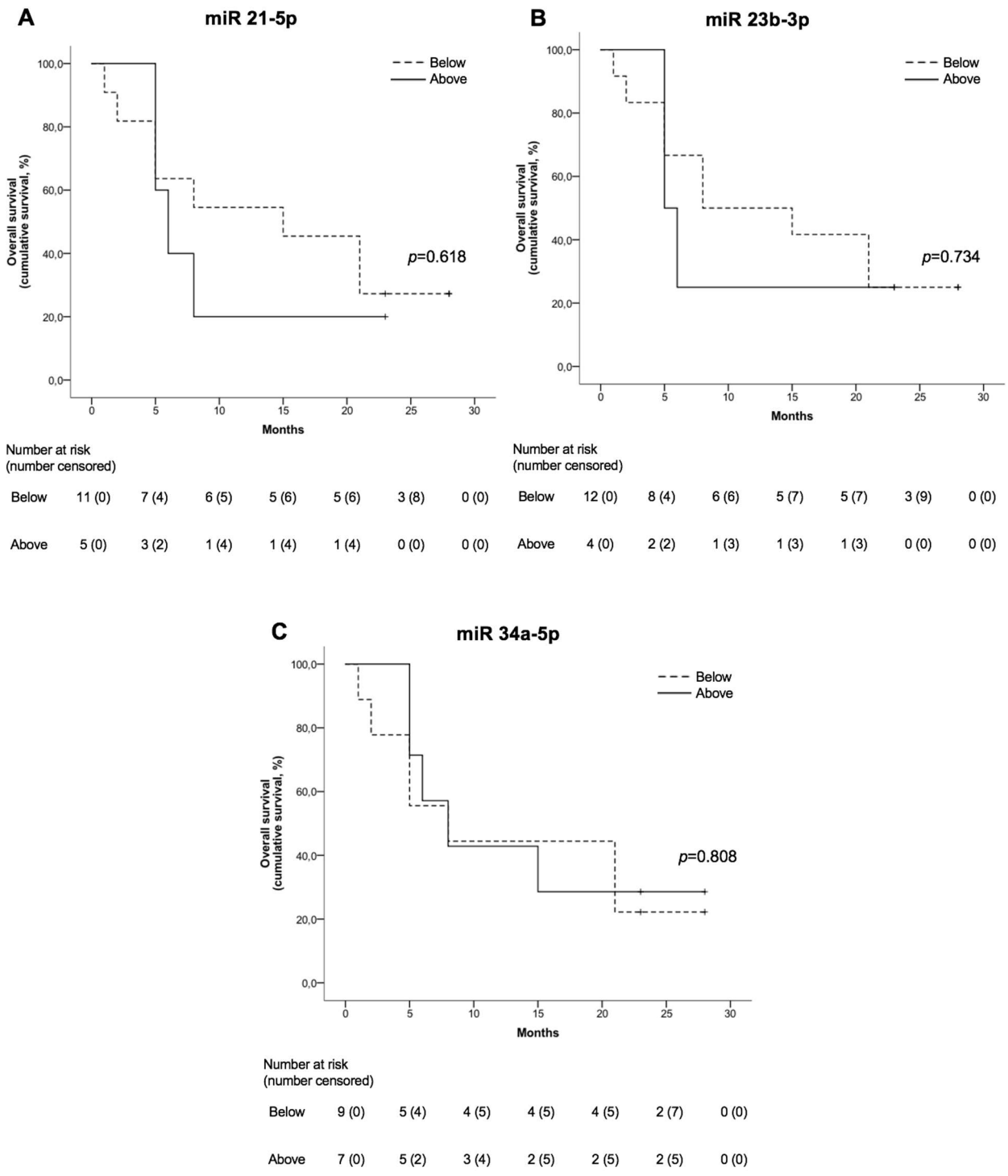

Figure 52 – Overall survival Kaplan–Meier curves comparing patients with circulating levels of miR 21-5p (**A**), miR 23b-3p (**B**) and miR 34a-5p (**C**) below (dashed line) and above (solid line) the mean 1 month after surgery.

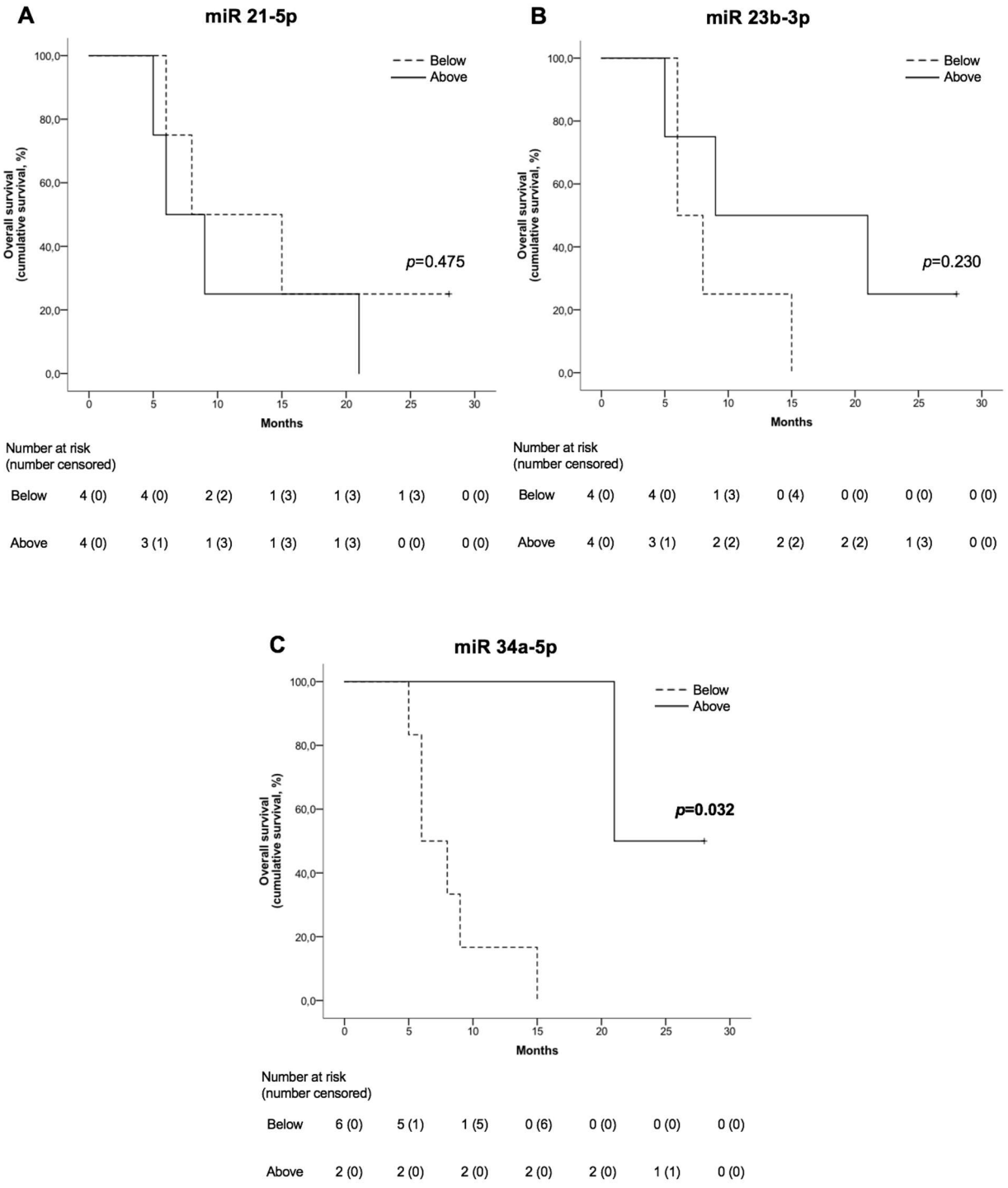

Figure 53 – Overall survival Kaplan–Meier curves comparing patients with circulating levels of miR 21-5p (**A**), miR 23b-3p (**B**) and miR 34a-5p (**C**) below (dashed line) and above (solid line) the mean 3 months after surgery.

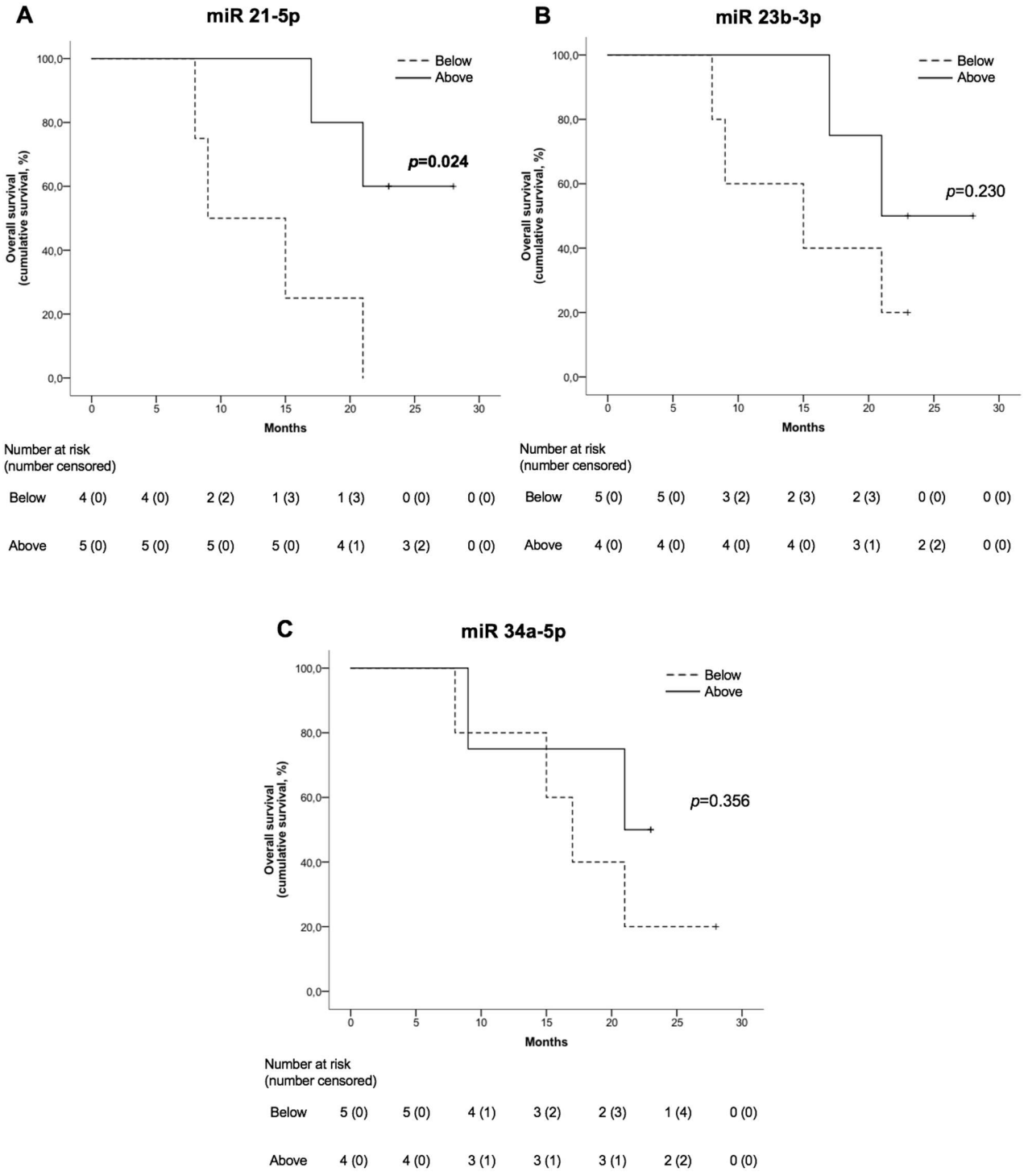

Figure 54 – Overall survival Kaplan–Meier curves comparing patients with circulating levels of miR 21-5p (**A**), miR 23b-3p (**B**) and miR 34a-5p (**C**) below (dashed line) and above (solid line) the mean 6 months after surgery.

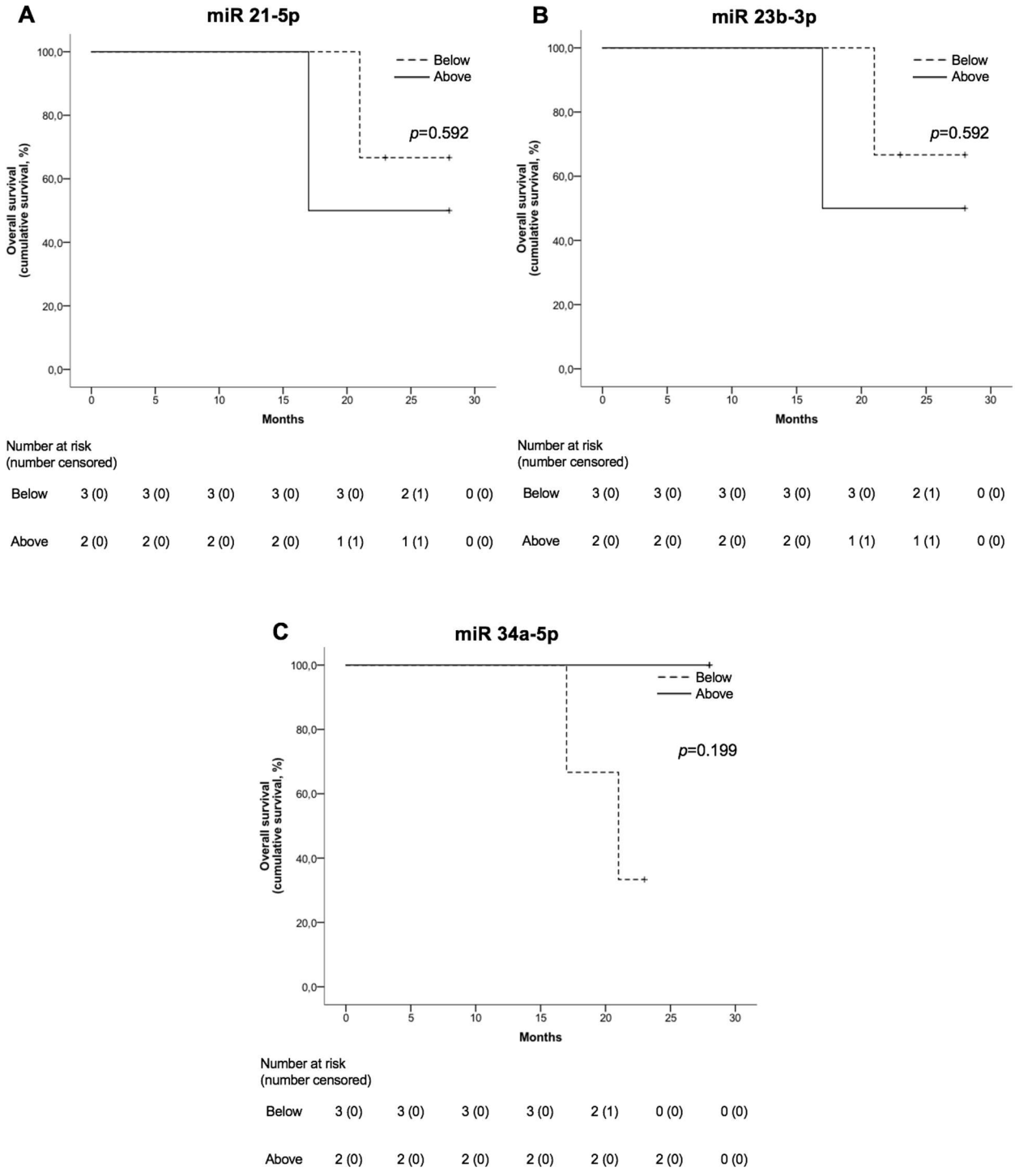

Figure 55 – Overall survival Kaplan–Meier curves comparing patients with circulating levels of miR 21-5p (**A**), miR 23b-3p (**B**) and miR 34a-5p (**C**) below (dashed line) and above (solid line) the mean 12 months after surgery.

4.11 Recurrence free survival analysis

The mean RFS was 11.4 months (95% C.I. 6.8 – 16.0) with 31.9% and 26.6% of predicted RFS at 1 and 2 years, respectively (**Figure 56**).

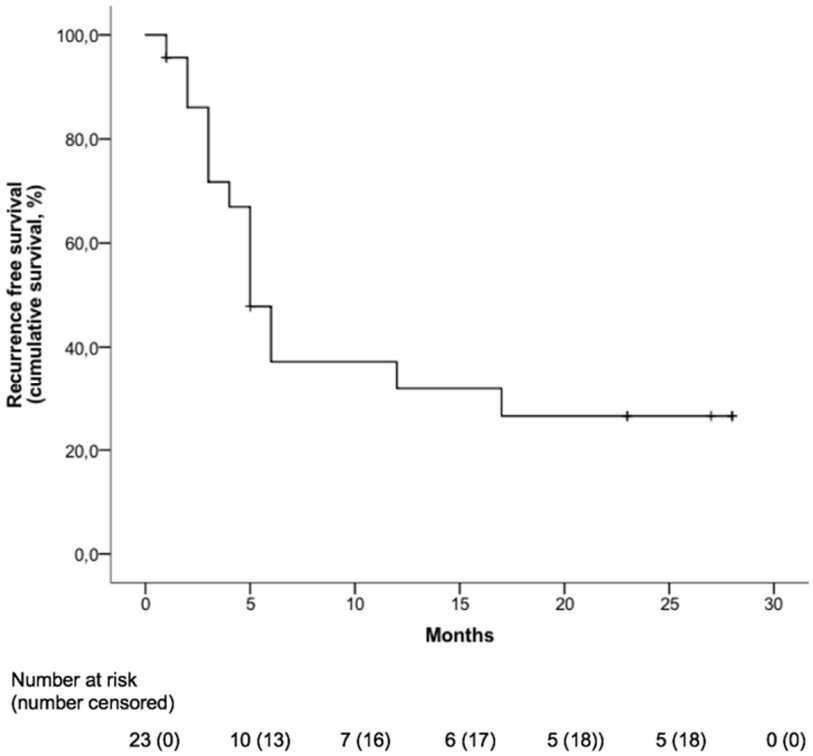

Figure 56 – Recurrence free survival.

4.11.1 Recurrence free survival according to miRNAs' variations at different timing points

After splitting the population in two groups of patients experiencing increase or stability/decrease of miRNAs circulating levels over the follow up, the RFS were compared (**Table 11**) and no significant differences surfaced (**Figures 57-60**).

		Mean RFS (95% C.I.)	pRFS at 1 year (%)	pRFS at 2 years (%)	*p* value
miR 21-5p diagnosis-FU1	Increase	15.5 (7.2 – 23.8)	57.1	38.1	0.412
	Stability/Decrease	9.8 (2.4 – 17.1)	25.0	25.0	
miR 23b-3p diagnosis-FU1	Increase	17.6 (8.6 – 26.5)	57.1	57.1	0.135
	Stability/Decrease	7.8 (2.6 – 12.9)	25.0	12.5	
miR 34a-5p diagnosis-FU1	Increase	9.6 (3.0 – 16.2)	24.4	24.4	0.211
	Stability/Decrease	19.5 (10.2 – 28.8)	75.0	50.0	
miR 21-5p FU1-FU3	Increase	15.5 (0.0 – 32.8)	50.0	50.0	0.535
	Stability/Decrease	4.5 (2.7 – 6.3)	0.0	0.0	
miR 23b-3p FU1-FU3	Increase	15.5 (0.0 – 32.8)	50.0	50.0	0.535
	Stability/Decrease	4.5 (2.7 – 6.3)	0.0	0.0	
miR 34a-5p FU1-FU3	Increase	15.5 (0.0 – 32.8)	50.0	50.0	0.535
	Stability/Decrease	4.5 (2.7 – 6.3)	0.0	0.0	
miR 21-5p FU3-FU6	Increase	-	-	-	0.116
	Stability/Decrease	-	-	-	
miR 23b-3p FU3-FU6	Increase	-	-	-	-
	Stability/Decrease	8.6 (0.0 – 17.2)	20.0	20.0	
miR 34a-5p FU3-FU6	Increase	-	-	-	-
	Stability/Decrease	8.6 (0.0 – 17.2)	20.0	20.0	
miR 21-5p FU6-FU12	Increase	-	-	-	-
	Stability/Decrease	21.3 (14.4 – 28.1)	75.0	50.0	
miR 23b-3p FU6-FU12	Increase	-	-	-	-
	Stability/Decrease	21.3 (14.4 – 28.1)	75.0	50.0	
miR 34a-5p FU6-FU12	Increase	-	-	-	0.090
	Stability/Decrease	-	-	-	

Table 11 – Mean and predicted RFS according to variations (increase or stability/decrease) of circulating levels of miR 21-5p, miR 23b-3p and miR 34a-5p at different timing points.
pRFS: predicted recurrence free survival.

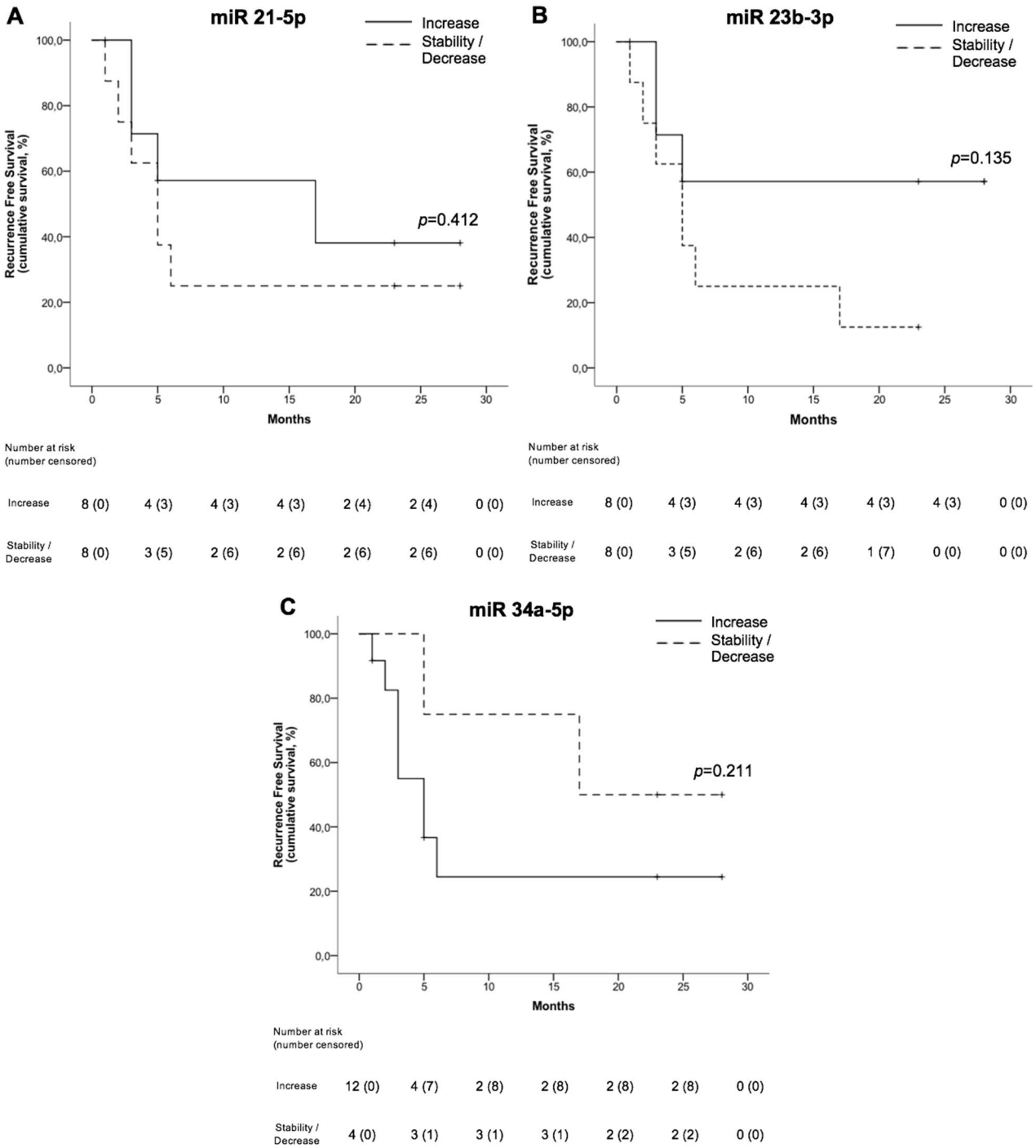

Figure 57 – Recurrence free survival Kaplan–Meier curves comparing patients with increased (solid line) and stable or decreased (dashed line) circulating levels of miR 21-5p (**A**), miR 23b-3p (**B**) and miR 34a-5p (**C**) between the diagnosis and 1 month after surgery.

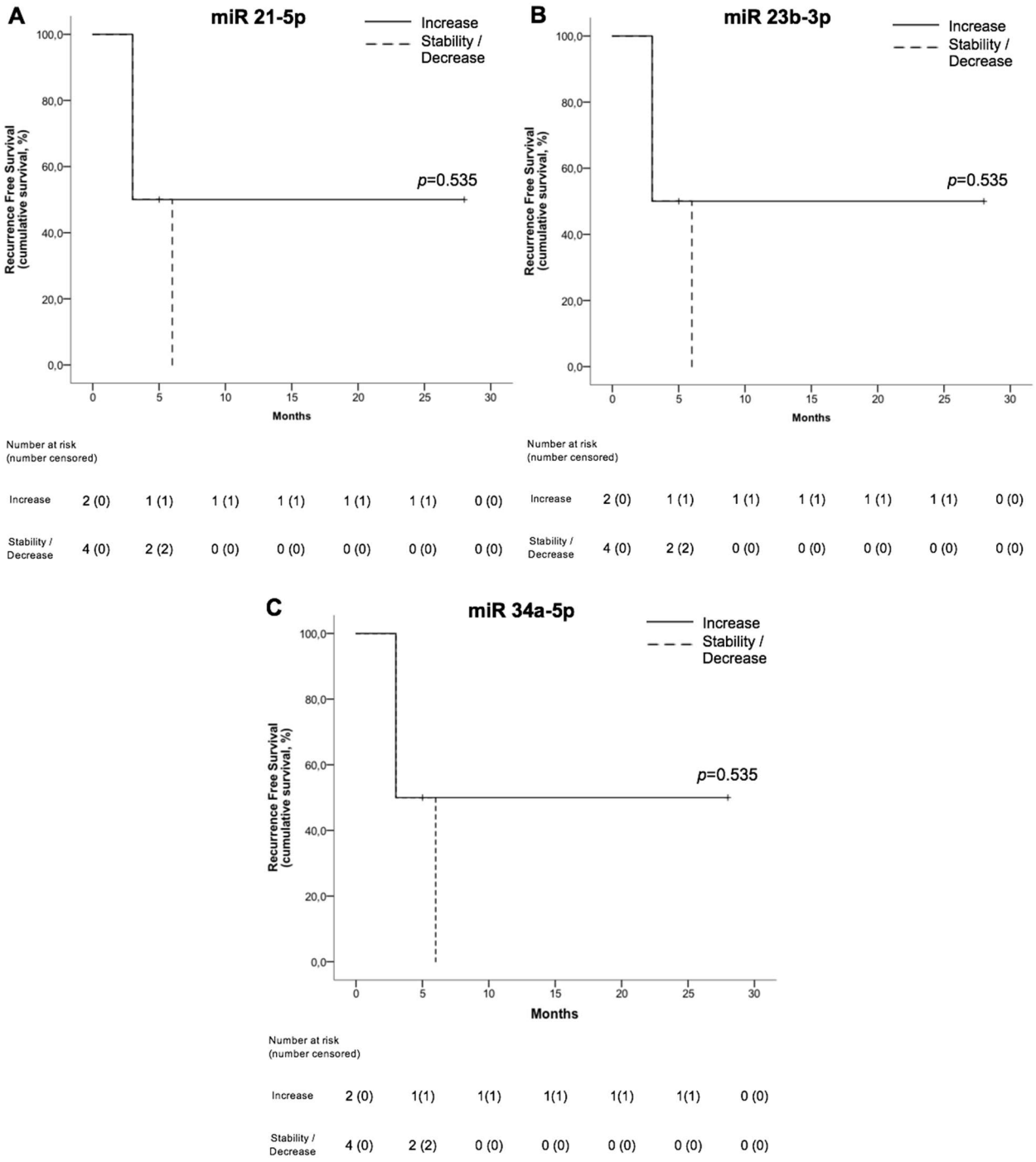

Figure 58 – Recurrence free survival Kaplan–Meier curves comparing patients with increased (solid line) and stable or decreased (dashed line) circulating levels of miR 21-5p (**A**), miR 23b-3p (**B**) and miR 34a-5p (**C**) between 1 and 3 months after surgery.

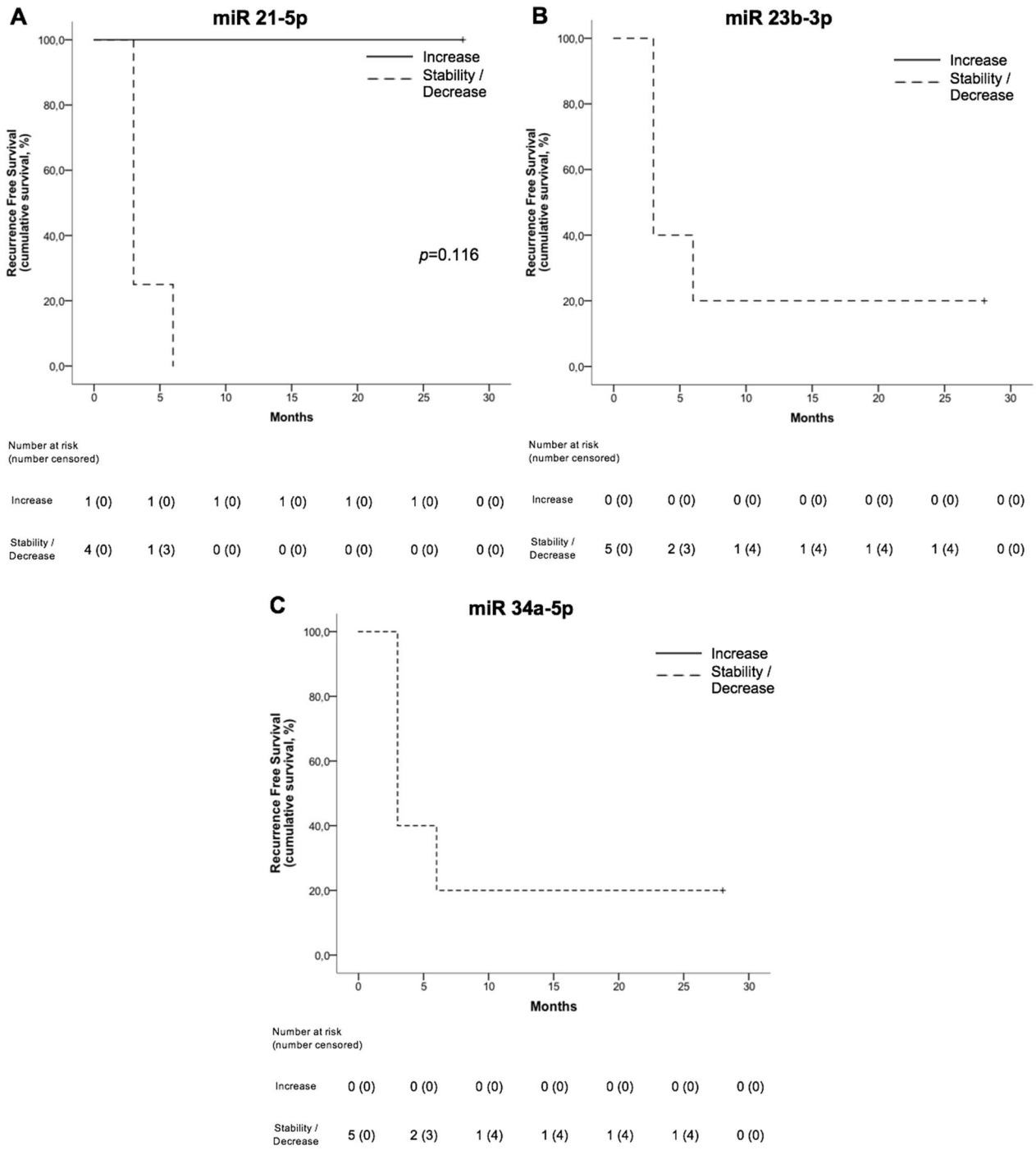

Figure 59 – Recurrence free survival Kaplan–Meier curves comparing patients with increased (solid line) and stable or decreased (dashed line) circulating levels of miR 21-5p (**A**), miR 23b-3p (**B**) and miR 34a-5p (**C**) between 3 and 6 months after surgery.

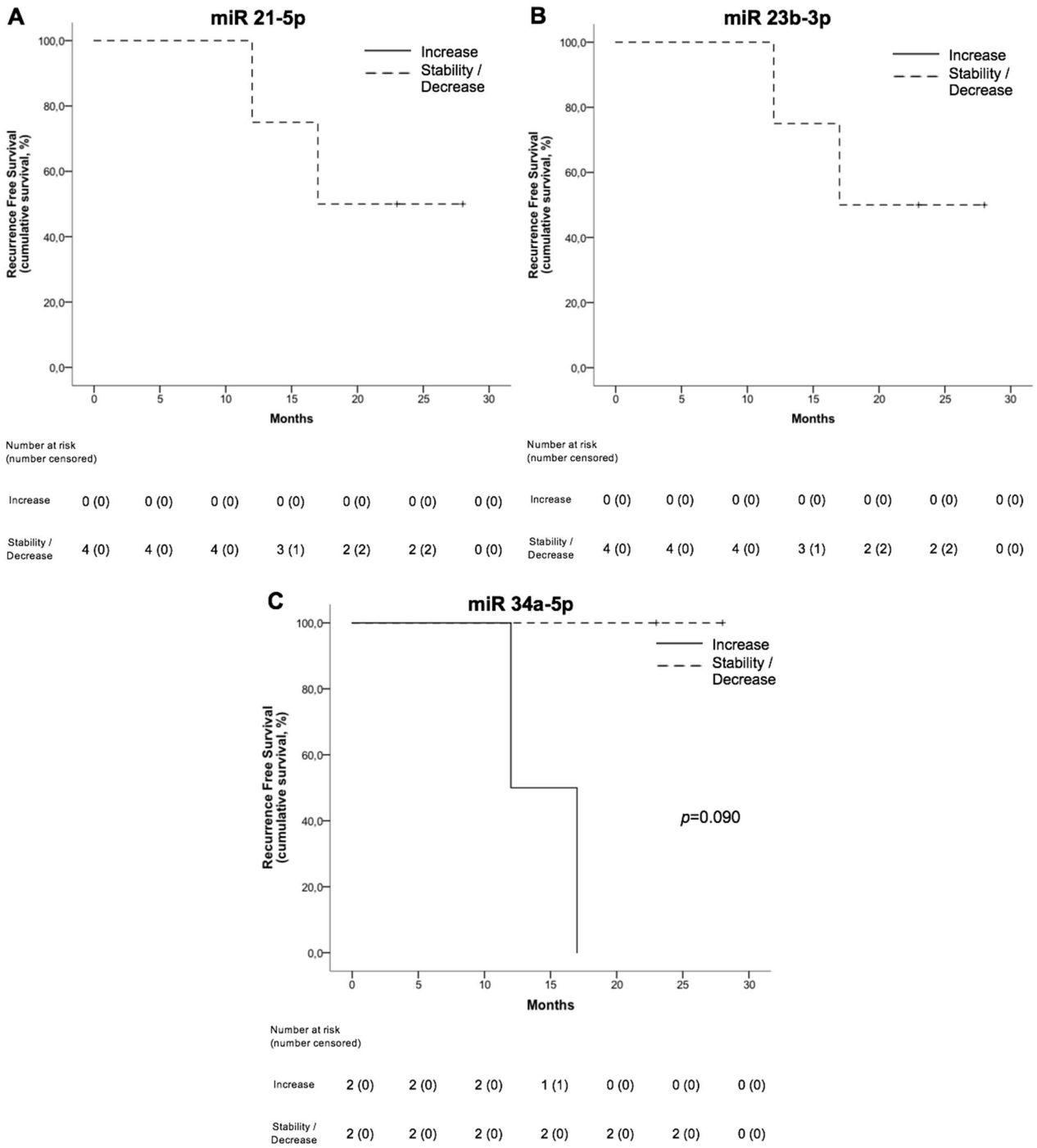

Figure 60 – Recurrence free survival Kaplan–Meier curves comparing patients with increased (solid line) and stable or decreased (dashed line) circulating levels of miR 21-5p (**A**), miR 23b-3p (**B**) and miR 34a-5p (**C**) between 6 and 12 months after surgery.

4.11.2 Recurrence free survival according to mean miRNAs' plasmatic concentrations

After splitting the population above and below the mean values of circulating miRNAs at different timing points (**Table 12**), the mean RFS was significantly shorter in patients with miR 34a-5p levels below the mean at diagnosis (7.6 months, 95% C.I. 3.1 – 12.1 vs 15.6 months, 95% C.I. 8.0 – 23.1, *p*=0.049) (**Figures 61-65**).

		Mean RFS (95% C.I.)	**pRFS at 1 year (%)**	**pRFS at 2 years (%)**	***p* value**
miR 21-5p at diagnosis	Below the mean	12.1 (6.4 – 17.8)	35.9	28.7	0.872
	Above the mean	8.5 (2.1 – 14.9)	21.4	21.4	
miR 23b-3p at diagnosis	Below the mean	12.2 (6.5 – 17.9)	36.1	28.8	0.878
	Above the mean	8.1 (2.0 – 14.1)	19.0	19.0	
miR 34a-5p at diagnosis	Below the mean	**7.6 (3.1 – 12.1)**	**18.3**	**9.2**	**0.049**
	Above the mean	**15.6 (8.0 – 23.1)**	**46.7**	**46.7**	
miR 21-5p at FU1	Below the mean	12.1 (5.1 – 19.1)	40.4	30.3	0.692
	Above the mean	10.3 (1.9 – 18.7)	30.0	30.0	
miR 23b-3p at FU1	Below the mean	11.3 (4.7 – 17.8)	36.7	27.5	0.383
	Above the mean	12.1 (2.4 – 21.8)	37.5	37.5	
miR 34a-5p at FU1	Below the mean	11.6 (4.4 – 18.8)	37.5	25.0	0.812
	Above the mean	12.8 (3.3 – 22.3)	38.1	38.1	
miR 21-5p at FU3	Below the mean	10.0 (0 – 20.3)	25.0	25.0	0.815
	Above the mean	5.0 (3.5 – 6.5)	0	0	
miR 23b-3p at FU3	Below the mean	4.3 (2.8 – 5.7)	0	0	0.151
	Above the mean	13.5 (0.6 – 26.4)	37.5	37.5	
miR 34a-5p at FU3	Below the mean	4.8 (3.6 – 6.0)	0	0	0.486
	Above the mean	15.5 (0 – 32.8)	50.0	50.0	
miR 21-5p at FU6	Below the mean	7.3 (0.7 – 13.8)	25.0	0	0.076
	Above the mean	19.8 (10.7 – 29.0)	60.0	60.0	
miR 23b-3p at FU6	Below the mean	10.4 (3.3 – 17.5)	40.0	20.0	0.412
	Above the mean	17.8 (7.2 – 21.2)	50.0	50.0	
miR 34a-5p at FU6	Below the mean	12.6 (4.4 – 20.8)	40.0	20.0	0.519
	Above the mean	13.8 (4.6 – 22.9)	50.0	50.0	
miR 21-5p at FU12	Below the mean	24.3 (18.5 – 30.2)	100.0	66.7	0.592
	Above the mean	20.0 (8.9 – 31.1)	50.0	50.0	
miR 23b-3p at FU12	Below the mean	24.3 (18.5 – 30.2)	100.0	66.7	0.592
	Above the mean	20.0 (8.9 – 31.1)	50.0	50.0	
miR 34a-5p at FU12	Below the mean	-	66.7	33.3	0.199
	Above the mean	-	100.0	100.0	

Table 12 – Mean and predicted RFS according to mean miR 21-5p, miR 23b-3p and miR 34a-5p plasmatic concentrations at diagnosis, 1 (FU1), 3 (FU3), 6 (FU6) and 12 months (FU12) of follow up. pRFS: predicted recurrence free survival.

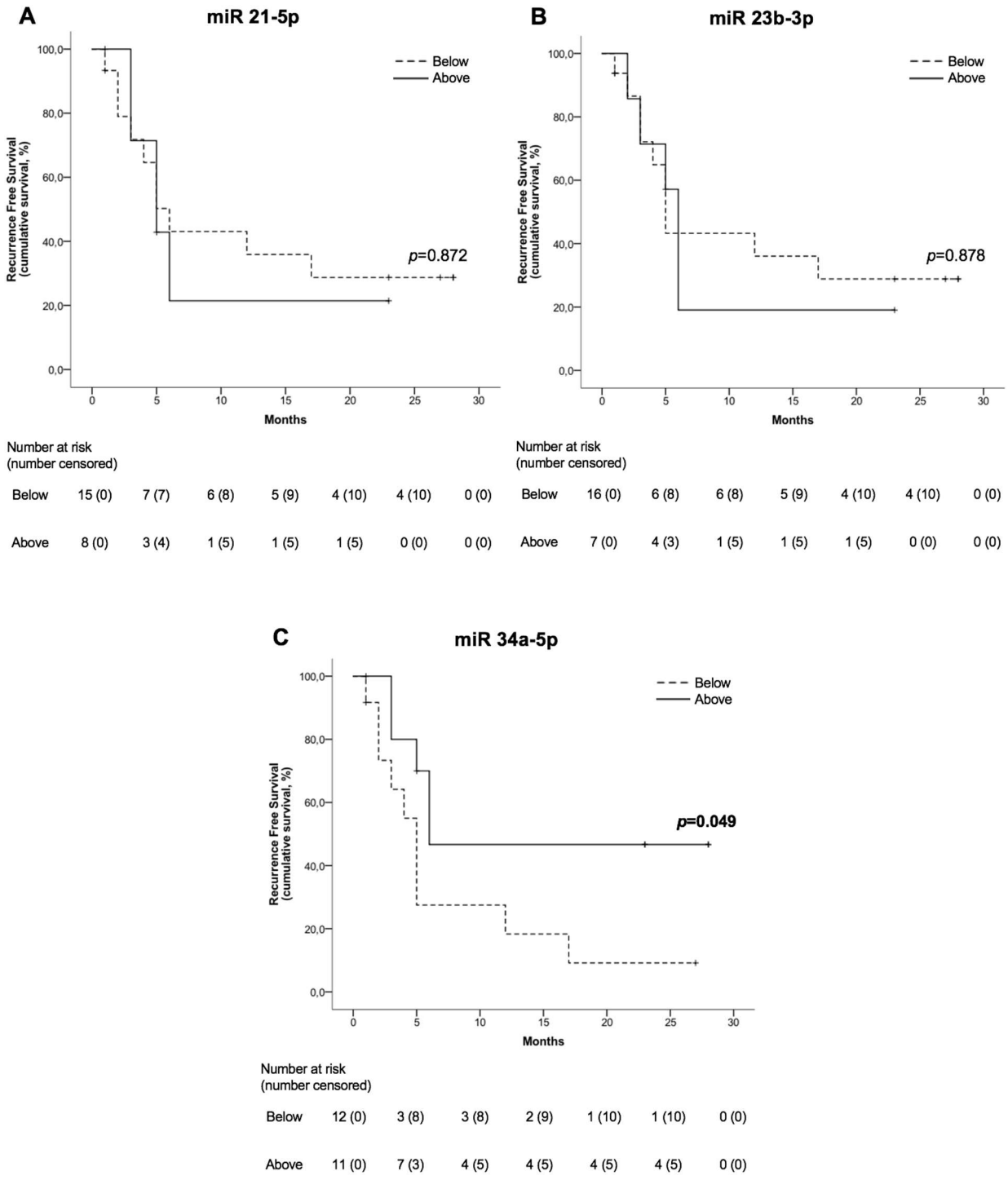

Figure 61 – Recurrence free survival Kaplan–Meier curves comparing patients with circulating levels of miR 21-5p (**A**), miR 23b-3p (**B**) and miR 34a-5p (**C**) below (dashed line) and above (solid line) the mean at diagnosis.

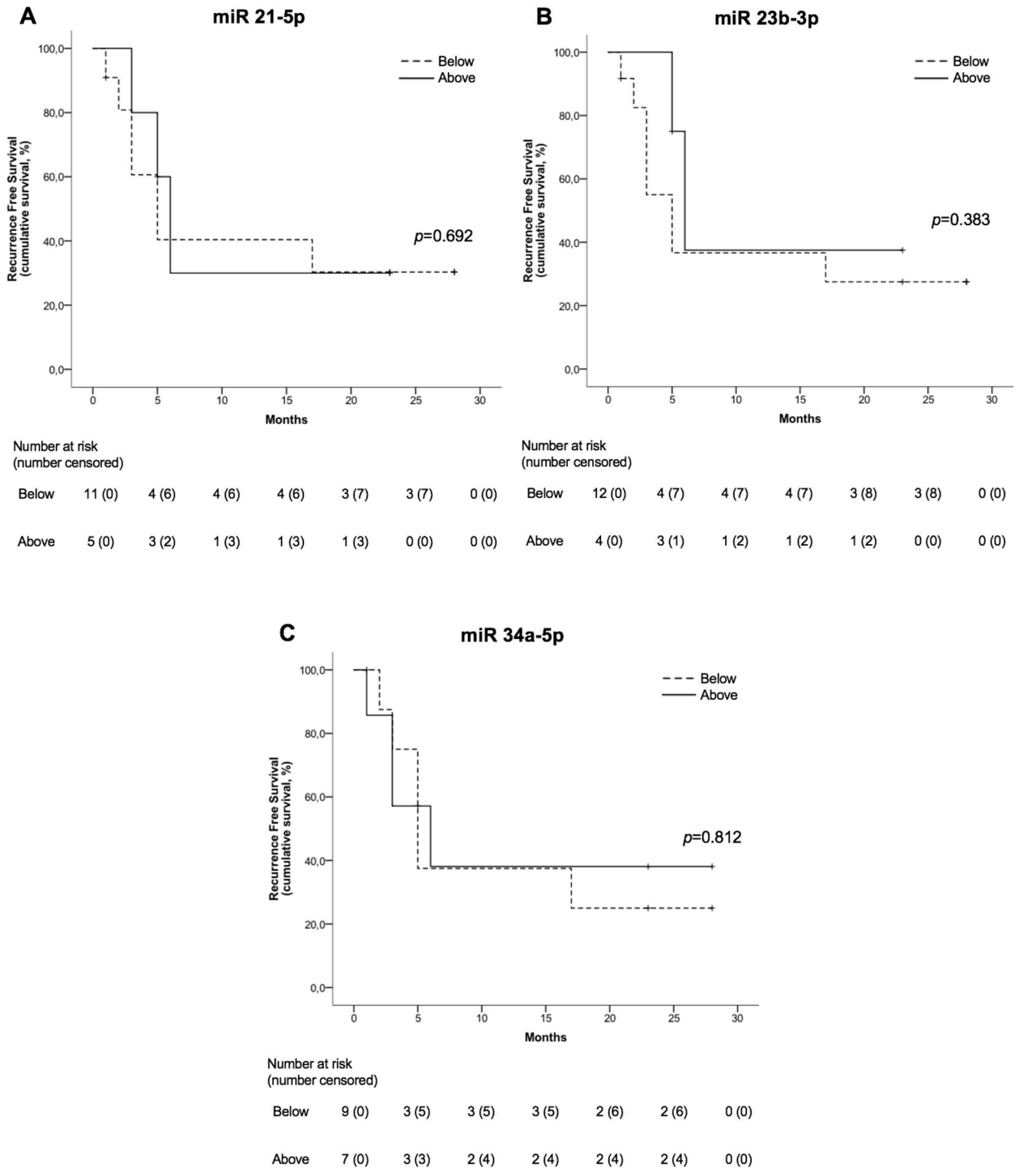

Figure 62 – Recurrence free survival Kaplan–Meier curves comparing patients with circulating levels of miR 21-5p (**A**), miR 23b-3p (**B**) and miR 34a-5p (**C**) below (dashed line) and above (solid line) the mean 1 month after surgery.

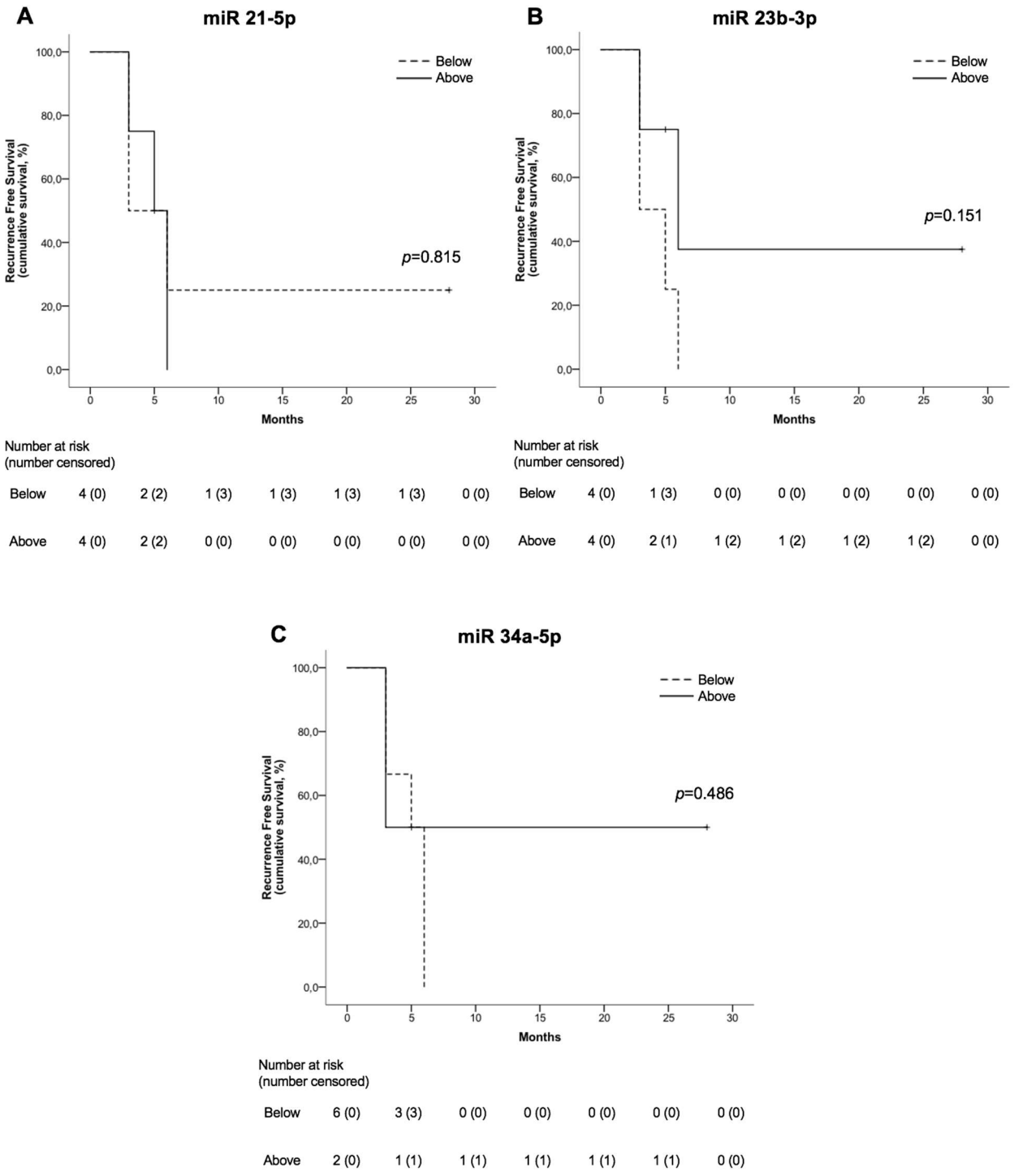

Figure 63 – Recurrence free survival Kaplan–Meier curves comparing patients with circulating levels of miR 21-5p (**A**), miR 23b-3p (**B**) and miR 34a-5p (**C**) below (dashed line) and above (solid line) the mean 3 months after surgery.

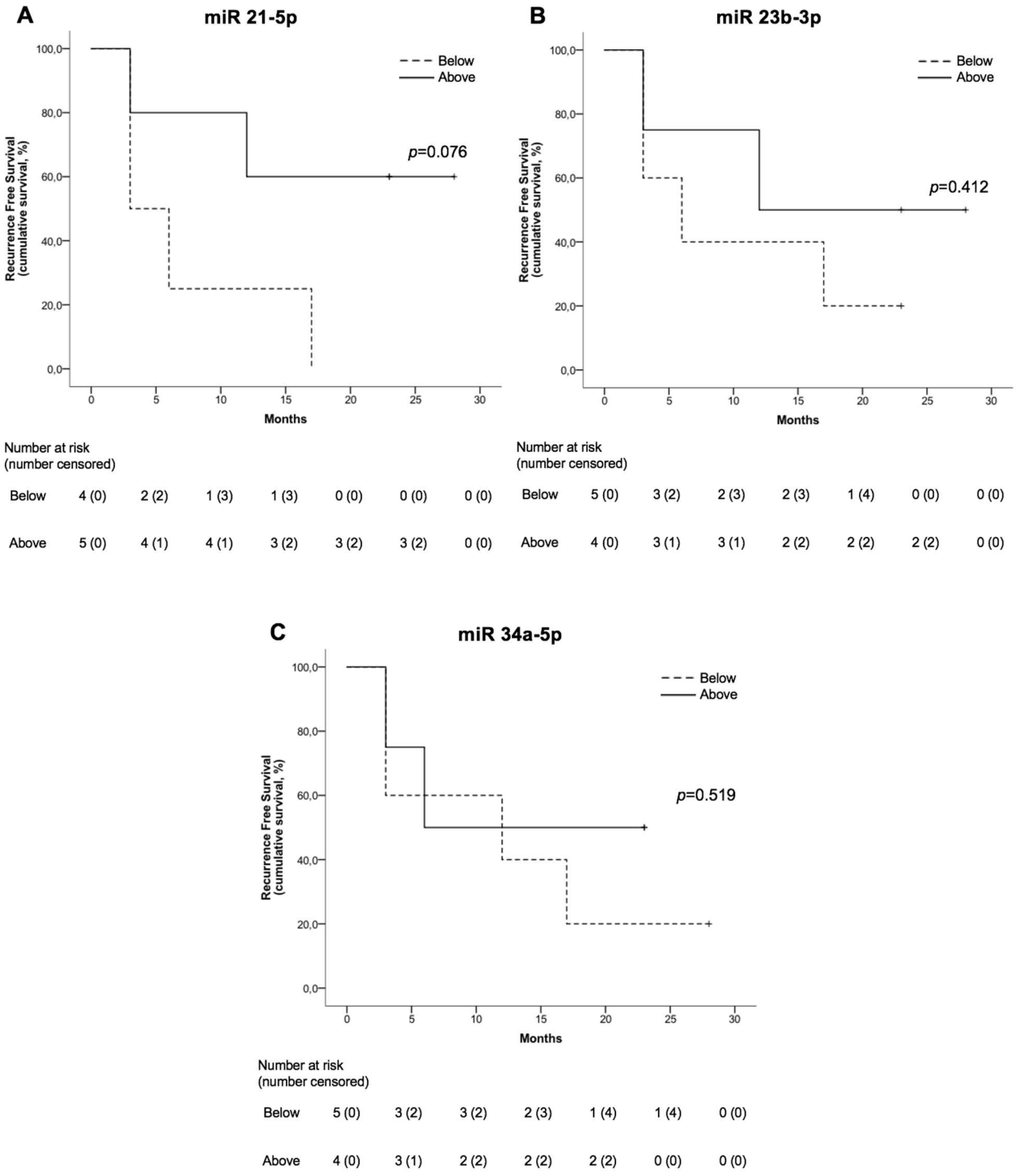

Figure 64 – Recurrence free survival Kaplan–Meier curves comparing patients with circulating levels of miR 21-5p (**A**), miR 23b-3p (**B**) and miR 34a-5p (**C**) below (dashed line) and above (solid line) the mean 6 months after surgery.

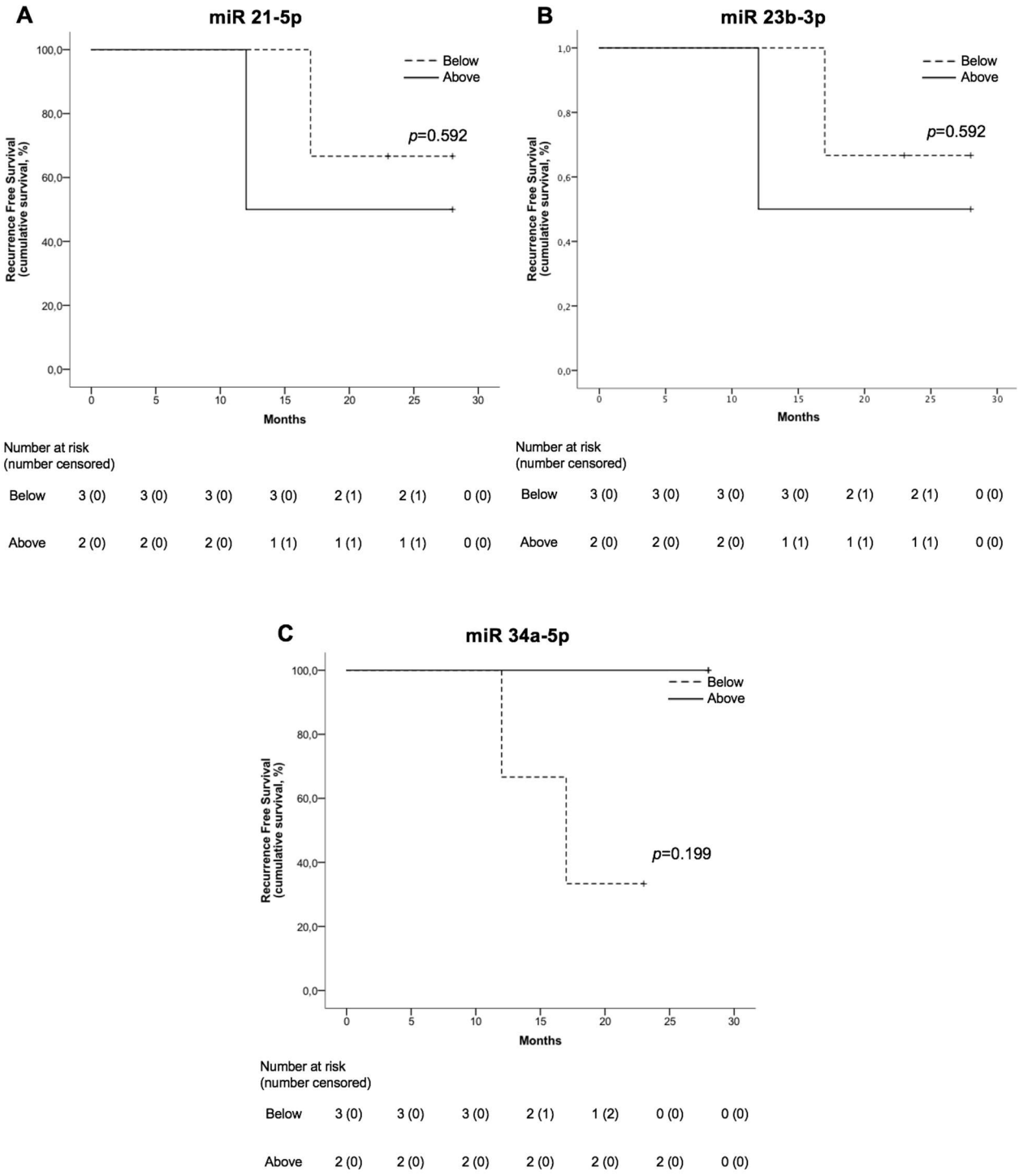

Figure 65 – Recurrence free survival Kaplan–Meier curves comparing patients with circulating levels of miR 21-5p (**A**), miR 23b-3p (**B**) and miR 34a-5p (**C**) below (dashed line) and above (solid line) the mean 12 months after surgery.

5. DISCUSSION

5.1 Liquid biopsy in GBM

In the neuro-oncology field, liquid biopsy has recently surged in popularity as a potential tool for diagnosis, prognosis and treatment monitoring[3-7]. GBM is characterized by molecular and genetic heterogeneity, presenting distinct genetic features in different tumour regions[71]. Liquid biopsy provides a comprehensive picture of the cancer's landscape more than tumour tissue analysis, capturing genetic materials reversed in the bloodstream by all the tumour components.

In the era of precision medicine, liquid biopsy may offer the potential for early GBM detection, serial monitoring over time for disease progression and response to treatments, allowing the identification of molecular targets for personalized therapies.

However, the identification of GBM-specific circulating biomarkers presents some challenges and limitations. Sensitivity and specificity of the detection techniques might be influenced by the low concentrations of circulating analytes in part due to the presence of the blood brain barrier[5,6,14-16,44]. Moreover, standardization of methodologies and further validation studies are needed to establish clinical reliability of these biomarkers for GBM.

5.2 Plasmatic miRNAs' assessment by ddPCR

This study was aimed to explore the role of circulating non-coding RNAs as potential GBM-specific longitudinal peripheral biomarkers using ddPCR. In particular, the detection and quantification of selected miRNAs was accomplished by ddPCR on plasma samples, collected at specific timing points.

miRNAs are involved in the tumorigenesis of different types of cancers. Specific miRNA expression profiles are often associated with different tissues and pathological conditions. Changes of their expression can reflect tissue alterations, such as cancerous changes[15,17,23-25,28,33]. For this reason, circulating miRNAs have been explored as potential tumour-specific biomarkers[4,17,18,21,23-25,27,28,30]. Using circulating miRNAs for liquid biopsy brings several advantages and we focused our attention on their assessment.

miRNAs are relatively stable in comparison with other circulating nucleic acids[1,2,17,18,72]. Furthermore, they are protected from degradation thanks to their encapsulation in extracellular vesicles and apoptotic bodies or protein binding, but show also resistence to endogenous RNase activity[18,31].

However, clinical application of miRNA as tumour biomarkers has been mainly limited by the lack of standard methods for blood collection, RNA extraction, RNA sequencing and normalization methods based on endogenous controls[73-75].

Although both plasma and serum are suitable for miRNAs' analysis, some studies have reported that the identification of extracellular ("cell-free") miRNAs may be more reliable in plasma samples for different reasons: i) anticoagulation prevents the degranulation of platelets (specifically tumour-educated platelets), a crucial step in the clotting process, that can cause the release of intracellular miRNAs; ii) plasma is not affected by haemolysis that can influence miRNA profiles by leaking intracellular miRNAs; iii) plasma contains higher concentrations of extracellular vesicles (particularly exosomes) that contribute to the global pool of extracellular miRNAs[7,35,72,76-78]. Accordingly, we decided to quantify miRNAs' plasmatic levels.

We then adopted ddPCR for an absolute quantification of our target molecules, differently from real time PCR that provides a relative quantification, without relying on standard curves based on endogenous controls. Despite different suggestions, there is no universal housekeeping control for miRNAs and the process of choosing a suitable reference is still controversial contributing to the final heterogeneity of data reported in literature for real time PCR[5,37,79-81].

The ddPCR partitions the process into thousands of independent reactions (droplets) enabling an highly sensitive detection of low-abundant targets, such as circulating nucleic acids[32,82]. Moreover, ddPCR is less affected by the presence of PCR inhibitors, an extraordinary advantage when working with complex samples such as blood, and by PCR amplification efficiency variability, that can limit the accuracy of relative quantification. Overall, ddPCR affords for consistent reaction conditions contributing to highly reproducible results[5,82].

Circulating miRNAs can also be analysed by microarrays and next generation sequencing. However, the quantitative accuracy of microarrays can be compromised by low concentrations of transcripts. On the other hand, next generation sequencing is significantly less affordable requiring substantial computational resources for data storage and processing compared to PCR[3].

5.3 miRNAs' selection: miR 21-5p, miR 23b-3p and miR 34a-5p

According to the literature review, we identified three miRNAs as potential peripheral biomarkers for GBM: miR 21-5p, miR 23b-3p and miR 34a-5p.

miR 21-5p is located on chromosome 17q23.2[83]. miR 21-5p has been extensively studied in various cancers, including GBM, for its oncogenic properties and implications in promoting cell proliferation, inhibiting apoptosis and contributing to tumour invasion and migration. miR 21-5p has been involved in three different tumour suppressor pathways, namely p53, TGF-beta and the mitochondrial apoptotic pathway[38,83-86]. It has been found as highly expressed in tissues and serum or plasma of patients affected by GBM compared to healthy controls and/or patients with low grade diffuse astrocytic gliomas, with all limitations of previous studies that did not follow the new WHO Classification of the Tumours of the CNS[14,15,35-43,87].

miR 23b-3p is located on chromosome 9p21.3. miR 23b-3p has been shown to influence tumour cell proliferation, invasion and migration and some studies reported its overexpression in cell cultures and tumour tissue derived from patients affected by GBM[45,47,48].

Eventually, *miR 34a-5p* sited on chromosome 1p36.22[49] is a direct transcriptional target of p53 and acts as a tumour suppressor miRNA. It promotes cell cycle arrest and apoptosis, suppresses cell invasion and extracellular matrix remodelling and targets key oncogenic signalling pathways. Downregulation of miR 34a-5p has been reported in tumour tissues and serum derived from patients affected by GBM[15,37,39,44,49,50,52,53].

5.4 Study population features

We analysed a homogenous population of patients presenting with GBM IDH-wildtype WHO grade 4 or astrocytoma IDH-mutant WHO grade 4, according to the fifth edition of the WHO Classification of the Tumours of the CNS[13,19].

All patients underwent standardized preoperative and postoperative clinical and neuroradiological evaluations, were treated following the international guidelines[10-12,59] and were followed at defined timing points: at diagnosis, 1 month after surgery, before starting RT and concomitant chemotherapy, 3 months after surgery, immediately after the end of RT and concomitant chemotherapy, 6 and 12 months after surgery.

5.5 miRNAs plasmatic concentrations in healthy volunteers and patients

miR 21-5p, miR 23b-3p and miR 34a-5p were all detectable in healthy volunteers. Only miR 34a-5p showed significantly higher levels in patients, with a diagnostic cut-off value of 1.25 copies/μL (sensitivity: 47.8%; specificity: 87.5%). In our cohort of patients, miR 21-5p showed similar plasmatic concentrations in healthy volunteers and patients, differently from data previously reported in literature. A high degree of inter-individual variability in the levels of circulating miRNAs has been reported, even when focusing only on healthy populations[88,89]. Furthermore, in contrast with literature reports of miR 21-5p and miR 23b-3p overexpression and miR 34a-5p downregulation in GBM tissues, our findings on their circulating levels may be due to the fact that aberrant expression of miRNAs in tissues may not be reflected in the circulation[40,87].

According to the absolute concentrations of miRNAs at diagnosis, patients were clustered in two groups presenting low and high levels of circulating miRNAs, respectively. Considering the miRNA expression levels relative to healthy volunteers, the population was grouped in patients with low levels of all miRNAs, patients with low levels of miR 21-5p and high levels of miR 23b-3p, patients with high levels of all miRNAs and patients with low levels of miR 21-5p and miR 23b-3p and high levels of miR 34a-5p. We can therefore identify at diagnosis different groups of patients.

miR 21-5p, miR 23b-3p and miR 34a-5p showed the same longitudinal course. Their plasmatic levels progressively increased 1 and 3 months after surgery, at the end of RT and concomitant chemotherapy, and then gradually decreased over time, at 6 and 12 months after surgery.
The blood brain barrier may affect the amount of miRNAs' released in the bloodstream of patients affected by GBM[85]. In our study population, miRNAs plasmatic concentrations resulted higher when the damage of the blood brain barrier might be potential maximal, particularly after the combined effect of surgery, RT and chemotherapy (3 months after surgery), to subsequently decrease probably as a consequence of the blood brain barrier healing processes[44].

5.6 miRNAs' correlations with clinical, neuroradiological and pathological features

Despite we registered higher levels of miR 23b-3p and miR 34a-5p at diagnosis in patients who were not administered steroids and lower levels of miR 21-5p, miR 23b-3p and miR 34a-5p in patients with tumours displaying loss of ATRX expression, these results were not confirmed by multivariate analysis. Furthermore, we did not identify significant correlations between the "tumour load", considered as preoperative tumour volume and postoperative tumour remnant volume, and miRNAs' circulating levels at diagnosis and over the follow up[14].

5.7 Mutual miRNAs' correlations

A direct correlation was recorded for each miRNA between their concentration at diagnosis and 1 month after surgery.
Furthermore, to the best of our knowledge, we firstly reported a significant direct correlation between miR 21-5p and miR 23b-3p circulating levels at each timing point of plasma collection, except for 12 months after surgery. The multivariate analysis confirmed this mutual correlation at diagnosis, 1 and 6 months after surgery. Similarly, miR 21-5p and miR 34a-5p levels at diagnosis were significantly directly correlated.
In keeping with our findings, we performed a network analysis to identify possible common molecular pathways for these miRNAs. Firstly, we identified four genes shared by miR 21-5p and miR 23b-3p in the context of gliomas: *E2F1*, *RB1*, *PTEN* and *PIK3R1*. Furthermore, we found four genes shared between miR 21-5p and miR 34a-5p in the same pathological scenario: *E2F1*, *E2F3*, *CDK6* and *IGF1R*. Eventually, the overall network analysis for miR 21-5p, miR 23b-3p and miR 34a-5p turned towards *E2F1*.

E2F1 and *E2F3* encode for two members of the E2F transcription factor family, key players in the regulation of the cell cycle, promoting the transition from the G1 to the S phase. *E2F1* and *E2F3* aberrant activation or dysregulation can contribute to tumorigenesis. There are growing evidences

of *E2F1* and *E2F3* overexpression in GBM tissue compared to normal brain, associated with tumour aggressiveness and therapy resistance[37,49,90,91].

RB1 is a tumour suppressor gene, that inhibits the activity of E2F transcription factors blocking the cell cycle progression. Loss of function of RB1 has been associated with a more aggressive tumour behaviour, increased cell proliferation and decreased apoptosis in GBM[92].

PTEN is another tumour suppressor gene that can be dysregulated in GBM, contributing to increased cell survival, proliferation, invasion and resistance to apoptosis. miR 21-5p and miR 23b-3p are known to negatively regulate *PTEN*, leading to the activation of the PI3K/AKT/mTOR signal pathway[37,38,83,85,86,93].

PIK3R1 encodes for the regulatory subunit of p85 alfa of PI3K, which increased activity promoting cell survival, proliferation and resistance to apoptosis. miR 21-5p and miR 23b-3p have been associated to this molecular pathway[37].

CDK6 encoding for a member of the cyclin-dependent kinase family involved in regulating the cell cycle promotes the transition from the G1 to the S phase. Downregulation of *CDK6* exerted by miR 34a-5p has been described in GBM[15,37,50,93].

Finally, *IGF1R* encodes for an insulin-like growth factor receptor, which activation favours cell proliferation and survival in the tumourigenesis including GBM[94,95].

5.8 Overall and recurrence free survival

According to previous studies, we documented significant impact of circulating miRNAs levels on OS[52,83,86,93,96]. Patients with increased levels of miR 21-5p, miR 23b-3p and miR 34a-5p between 1 and 3 months after surgery showed longer OS. Similarly, patients with miR 34a-5p circulating levels above the mean 3 months after surgery and miR 21-5p circulating levels above the mean 6 months after surgery showed longer OS.

By contrast, RFS resulted significantly longer in patients presenting miR 34a-5p circulating levels above the mean at diagnosis.

5.9 Study limitations and future perspectives

The generalization of our findings is limited by limited sizes of the study population. Nevertheless, these represent the preliminary results of an ongoing study, in which a larger number of patients with longer follow up is being enrolled.

This research has many future goals:

a) investigating possible correlations between plasmatic miRNAs and haematological parameters, such as blood cell counts, the neutrophil-to-lymphocyte ratio, the platelet-to-lymphocyte ratio, the lymphocyte-to-monocyte ratio, the systemic immune-inflammation index, the systemic

inflammation response index, and systemic inflammatory markers, such as fibrinogen, erythrocyte sedimentation rate and C-reactive protein;

b) early differentiating tumour 'pseudo-progression' from 'tumour progression' after adjuvant treatments during the neuroradiological follow-up according to different plasmatic miRNA expression;
c) quantifying miRNAs levels in tumour samples by ddPCR, as reported by some other groups[97-100];
d) identifying the correlations between circulating miRNAs and the GBM molecular features included in the fifth edition of the WHO Classification of the Tumours of the CNS (homozygous deletion of *CDKN2A*/*B*, *TERT* promoter mutation, *EGFR* amplification, +7/-10 cytogenetic signature, *BRAF* mutations);
e) following the longitudinal levels of plasmatic non-coding RNAs in patients who experienced tumour recurrence in order to assess the response to second-line therapies, such as VEGF (Vascular Endothelial Growth Factor) and tyrosine kinase inhibitors.

6. CONCLUSIONS

We reported a prospective case-control longitudinal study on plasmatic miR 21-5p, miR 23b-3p and miR 34a-5p detected by means of ddPCR as peripheral biomarkers of astrocytomas, IDH-mutant WHO grade 4 and GBM, IDH-wildtype WHO grade 4 according to the fifth edition of the WHO Classification of the Tumours of the CNS[13,19].

We detected all miRNAs both in healthy volunteers and patients and documented significantly higher levels of circulating miR 34a-5p in patients than healthy volunteers identifying a diagnostic absolute cut-off value of 1.25 copies/μL. Furthermore, two groups of patients were recognised showing high and low absolute plasmatic levels of miRNAs at diagnosis, respectively.

miR 21-5p, miR 23b-3p and miR 34a-5p showed the same longitudinal course with a progressive increase 1 and 3 months after surgery, when they all reached their zenith, followed by a gradual decrease 6 and 12 months after surgery.

We identified significant correlations of miRNAs' levels between the diagnosis and 1 month after surgery, and more interestingly we firstly reported a mutual correlation between miR 21-5p and miR 23b-3p at each timing point of plasma collection and between miR 21-5p and miR 34a-5p at diagnosis. A network analysis highlights some possible molecular pathways of interaction in the context of glioma such as cell cycle control (*E2F1*, *E2F3*, *RB1*, *CDK6*) and cell growth (*PTEN*, *PIK3R1*, *IGF1R*).

Eventually, high miRNA circulating levels seem to be good prognosticators in terms of OS and RFS. However, future studies with larger cohorts of patients are needed to support our findings.

7. APPENDIX

Table 1 – Patients' clinical features.

Variables		Chi square	*p* value
Gender			
Males (n, %)	14 (60.9)	1.087	0.297
Females (n, %)	9 (39.1)		
mRS			
0-2 (n, %)	**21 (91.3)**	**15.696**	**< 0.001**
3-5 (n, %)	**2 (8.7)**		
KPS			
70-80 – "Dependent" (n, %)	**5 (21.7)**	**7.348**	**0.007**
90-100 – "Independent" (n, %)	**18 (78.3)**		
Steroids			
Yes (n, %)	**21 (91.3)**	**15.696**	**< 0.001**
No (n, %)	**2 (8.7)**		
AEDs			
Yes (n, %)	10 (43.5)	0.391	0.532
No (n, %)	13 (56.5)		

AEDs: anti-epileptic drugs; KPS: Karnofsky Performance Status; mRS: modified Ranking Score.

Table 2 – Pathological, neuroradiological and surgical tumour's features.

Variables		Chi square	*p* value
Preoperative MRI			
Location			
Right	9 (39.1)	4.522	0.104
Left	11 (47.8)		
Midline	3 (13.1)		
Contrast enhancement			
Yes (n, %)	23 (100.0)	-	-
No (n, %)	0 (0.0)		
Necrosis			
Yes (n, %)	**20 (86.7)**	**11.636**	**0.001**
No (n, %)	**3 (13.3)**		
Primary vs recurrent GBM			
Primary (n, %)	**19 (82.6)**	**9.783**	**0.002**
Recurrent (n, %)	**4 (17.4)**		
Surgical procedure			
Craniotomy (n, %)	**21 (91.3)**	**15.696**	**< 0.001**
Frameless neuronavigated biopsy (n, %)	**2 (8.7)**		
Intraoperative tumour fluorescence			
Strong (n, %)	**22 (95.7)**	**19.174**	**< 0.001**
Weak (n, %)	**1 (4.3)**		
Absent (n, %)	**0**		
***IDH1*/*IDH2* status**			
Wild type (n, %)	**22 (95.7)**	**19.174**	**< 0.001**
Mutant (n, %)	**1 (4.3)**		
***MGMT* promoter methylation %** (mean, SD)	17.4 (17.3)		
***MGMT* promoter methylation status** (n, %)			
Un-methylated (< 9 %)	12 (52.2)	4.261	0.119
Methylated (9-29 %)	4 (17.4)		
Hyper-methylated (> 29%)	7 (30.4)		
ATRX expression			
Lost (n, %)	**3 (13.0)**	**13.762**	**< 0.001**
Retained (n, %)	**20 (87.0)**		
p53 expression			
Absent (n, %)	**2 (8.7)**	**7.143**	**0.028**
Intermediate (n, %)	**13 (56.5)**		
Strong (n, %)	**8 (34.8)**		
Ki67 % (mean, SD)	41.3 (19.8)		
Early postoperative MRI			
Extent of tumour resection^			
NTR (n, %)	15 (71.4)	3.857	0.050
STR (n, %)	6 (28.6)		
Contrast enhancement of the surgical cavity^			

Absent (n, %)	11 (52.4)	1.143	0.565
Linear (n, %)	6 (28.6)		
Nodular (n, %)	4 (19.0)		
RT + concomitant TMZ §			
Yes (n, %)	**17 (89.5)**	**11.842**	**0.001**
No (n, %)	**2 (10.5)**		
RT protocol			
Standard RT (n, %)	**15 (88.2)**	**9.941**	**0.002**
Hypo-fractionated RT (n, %)	**2 (11.8)**		
Adjuvant chemotherapy §			
Yes (n, %)	12 (52.2)	0.043	0.835
No (n, %)	11 (47.8)		

ATRX: alpha thalassemia/mental retardation syndrome X-linked; IDH: isocitrate dehydrogenase; MGMT: O-6-methylguanine-DNA-methyltransferase; NTR: near total resection; STR: subtotal resection; TMZ: temozolomide.

^ Extent of tumour resection assessed in 21 patients who underwent craniotomy for tumour resection.

§ In 19 patients with primary tumours.

Table 3 – Correlation analysis between miR 21-5p, miR 23b-3p and miR 34a-5p plasmatic concentrations at diagnosis and clinical, neuroradiological and pathological features.

	miR 21-5p at diagnosis			**miR 23b-3p at diagnosis**			**miR 34a-5p at diagnosis**		
	R	R^2	*p*	R	R^2	*p*	R	R^2	*p*
Gender (M vs F)	0.107	0.011	0.626	0.229	0.052	0.294	-0.074	0.005	0.738
Age (years)	0.402	0.162	0.057	0.389	0.151	0.067	0.176	0.031	0.421
mRS (≤ 2 vs > 2)	0.186	0.035	0.395	0.186	0.035	0.395	0.186	0.035	0.395
KPS (70-80 vs 90-100)	-0.175	0.031	0.425	-0.270	0.073	0.212	-0.374	0.140	0.079
Steroids (Yes vs No)	-0.419	0.176	0.054	-0.396	0.157	0.062	-0.396	0.157	0.062
AEDs (Yes vs No)	-0.185	0.034	0.398	-0.146	0.021	0.507	-0.073	0.005	0.741
MRI – Location (right, left, midline)	-0.079	0.006	0.720	0.034	0.001	0.879	0.023	0.001	0.916
MRI – Necrosis (Yes vs No)	0.010	0.000	0.963	0.052	0.003	0.817	-0.125	0.016	0.578
MRI – Tumour volume (cc)	0.019	0.000	0.932	0.076	0.006	0.729	-0.221	0.049	0.312
GBM type (primary vs recurrent)	0.086	0.007	0.695	0.156	0.024	0.478	0.017	0.000	0.938
MGMT promoter methylation (%)	-0.273	0.075	0.207	-0.362	0.131	0.089	0.107	0.011	0.628
MGMT promoter methylation (unmethylated vs methylated)	-0.223	0.050	0.306	-0.315	0.099	0.143	0.072	0.005	0.743
ATRX status (Lost vs Retained)	**0.0455**	**0.002**	**0.038**	0.268	0.072	0.240	0.268	0.072	0.240
p53 status (Lost vs Intermediate vs Diffuse)	-0.072	0.005	0.756	-0.156	0.024	0.499	0.039	0.002	0.867
Ki67 (%)	-0.331	0.110	0.123	-0.324	0.105	0.131	-0.180	0.032	0.412

AEDs: anti-epileptic drugs; ATRX: alpha thalassemia/mental retardation syndrome X-linked; KPS: Karnofsky Performance Status; mRS: modified Ranking Score; MGMT: O-6-methylguanine-DNA-methyltransferase.

Table 4 – Multivariate linear regression analysis between miR 21-5p plasmatic concentrations at diagnosis and clinical, pathological and neuroradiological features.

ANOVA: R 0.768; R^2 0.589; F 0.836; *p* value 0.626.

	OR	95% CI	*p* value
Gender (M vs F)	5.68	-182.70 – 194.08	0.948
Age (years)	4.19	-3.72 – 12.10	0.265
mRS (≤ 2 vs > 2)	-12.97	-384.60 – 358.65	0.940
KPS (70-80 vs 90-100)	-60.02	-331.99 – 211.94	0.634
Steroids (Yes vs No)	-207.32	-535.08 – 120.44	0.189
AEDs (Yes vs No)	2.24	-204.46 – 208.94	0.981
MRI Necrosis (Yes vs No)	52.26	-166.10 – 270.62	0.606
GBM type (Primary vs Recurrent)	-105.38	-326.77 – 116.00	0.314
MGMT promoter methylation (unmethylated vs methylated)	-125.80	-301.52 – 49.93	0.142
ATRX status (Lost vs Retained)	80.318	-262.23 – 422.85	0.597
Ki67 (%)	-1.24	-5.22 – 2.75	0.505

AEDs: anti-epileptic drugs; ATRX: alpha thalassemia/mental retardation syndrome X-linked; KPS: Karnofsky Performance Status; mRS: modified Ranking Score; MGMT: O-6-methylguanine-DNA-methyltransferase; OR: odd ratio.

Table 5 – Multivariate linear regression analysis between miR 23b-3p plasmatic concentrations at diagnosis and clinical, pathological and neuroradiological features.

ANOVA: R 0.724; R^2 0.525; adjusted R^2 -0.290; F 0.644; *p* value 0.760.

	OR	95% CI	*p* value
Gender (M vs F)	2.62	-17.50 – 22.74	0.767
Age (years)	0.48	-0.49 – 1.45	0.279
mRS (≤ 2 vs > 2)	-0.58	-64.44 – 64.33	0.998
KPS (70-80 vs 90-100)	-4.58	-38.25 – 29.09	0.757
Steroids (Yes vs No)	-8.27	-55.43 – 38.88	0.691
AEDs (Yes vs No)	3.17	-23.42 – 29.65	0.789
MRI Necrosis (Yes vs No)	6.75	-23.58 – 37.08	0.615
GBM type (Primary vs Recurrent)	0.83	-43.80 – 45.47	0.966
MGMT promoter methylation (unmethylated vs methylated)	-12.45	-33.09 – 8.20	0.197
ATRX status (Lost vs Retained)	2.88	-25.42 – 31.18	0.817
Ki67 (%)	-0.10	-0.56 – 0.54	0.966

AEDs: anti-epileptic drugs; ATRX: alpha thalassemia/mental retardation syndrome X-linked; KPS: Karnofsky Performance Status; mRS: modified Ranking Score; MGMT: O-6-methylguanine-DNA-methyltransferase; OR: odd ratio.

Table 6 – Multivariate linear regression analysis between miR 34a-5p plasmatic concentrations at diagnosis and clinical, pathological and neuroradiological features.

ANOVA: R 0.881; R^2 0.776; adjusted R^2 0.392; F 2.022; *p* value 0.179.

	OR	95% CI	*p* value
Gender (M vs F)	-0.80	-2.26 – 0.67	0.238
Age (years)	0.02	-0.05 – 0.09	0.506
mRS (≤ 2 vs > 2)	2.22	-2.46 – 6.90	0.299
KPS (70-80 vs 90-100)	-1.32	-3.77 – 1.13	0.244
Steroids (Yes vs No)	0.77	-2.66 – 4.20	0.614
AEDs (Yes vs No)	-0.09	-2.02 – 1.84	0.912
MRI Necrosis (Yes vs No)	-1.58	-3.79 – 0.62	0.134
GBM type (Primary vs Recurrent)	2.09	-1.16 – 5.33	0.173
MGMT promoter methylation (unmethylated vs methylated)	-0.21	-1.71 – 1.29	0.751
ATRX status (Lost vs Retained)	1.04	-1.02 – 3.10	0.271
Ki67 (%)	0.02	-0.02 – 0.06	0.274

AEDs: anti-epileptic drugs; ATRX: alpha thalassemia/mental retardation syndrome X-linked; KPS: Karnofsky Performance Status; mRS: modified Ranking Score; MGMT: O-6-methylguanine-DNA-methyltransferase; OR: odd ratio.

Table 7 – Comparison of miR 21-5p, miR 23b-3p and miR 34a-5p plasmatic concentrations 1 month after surgery (FU1) according to extent of tumour resection (16 patients).

	miR 21-5p FU1 (mean, SD)	*p* value	**miR 23b-3p FU1** (mean, SD)	*p* value	**miR 34a-5p FU1** (mean, SD)	*p* value
Surgical procedure (n, %)						
Craniotomy (14, 87.5)	235.69 (375.09)	0.065	17.31 (34.69)	0.124	2.25 (1.79)	0.465
Neuronavigated biopsy (2, 22.5)	30.00 (30.41)		1.89 (2.14)		1.48 (1.02)	
Extent of tumour resection (n, %)^						
NTR (10, 71.4)	277.22 (427.14)	0.410	21.96 (40.29)	0.256	**2.70 (1.93)**	**0.040**
STR (4, 28.6)	131.87 (205.46)		5.67 (9.57)		**1.13 (0.61)**	
Postoperative contrast enhancement (n, %)^						
Absent (6, 42.9)	179.55 (179.03)	0.362	11.21 (14.94)	0.388	3.31 (2.18)	0.143
Linear (3, 21.4)	38.30 (31.10)		1.04 (0.80)		1.08 (0.88)	
Nodular (5, 35.7)	421.50 (582.75)		34.38 (54.89)		1.68 (0.99)	

NTR: near total resection; STR: subtotal resection.

^ Extent of resection data analysed on 14 patients who underwent craniotomy.

Table 8 – Comparison of miR 21-5p, miR 23b-3p and miR 34a-5p plasmatic concentrations 3 months after surgery (FU3) according to extent of tumour resection and adjuvant therapies (8 patients).

	miR 21-5p FU3 (mean, SD)	*p* value	**miR 23b-3p FU3** (mean, SD)	*p* value	**miR 34a-5p FU3** (mean, SD)	*p* value
Surgical procedure (n, %)						
Craniotomy (8, 100.0)	356.15 (303.89)	-	22.26 (19.04)	-	4.79 (5.17)	-
Neuronavigated biopsy (0, 0)	-		-		-	
Extent of tumour resection (n, %)						
NTR (7, 87.5)	333.74 (321.02)	0.620	20.97 (20.18)	0.649	4.91 (5.57)	0.870
STR (1, 22.5)	513.00		31.30		3.90	
Postoperative contrast enhancement (n, %)						
Absent (4, 50.0)	204.45 (153.88)	0.105	12.48 (10.43)	0.398	3.95 (4.83)	0.393
Linear (2, 25.0)	731.50 (309.01)		34.00 (3.82)		9.25 (7.57)	
Nodular (2, 25.0)	284.20 (309.43)		30.10 (37.62)		2.00 (1.13)	
RT + concomitant TMZ (n, %)						
Yes (6, 75.0)	377.05 (328.50)	0.778	24.02 (20.27)	0.718	5.48 (5.87)	0.339
No (2, 25.0)	293.45 (310.49)		17.00 (20.22)		2.70 (1.70)	

NTR: near total resection; RT: radiotherapy; STR: subtotal resection; TMZ: temozolomide.

Table 9 – Comparison of miR 21-5p, miR 23b-3p and miR 34a-5p plasmatic concentrations 6 months after surgery (FU6) according to extent of tumour resection and adjuvant therapies (9 patients).

	miR 21-5p FU6 (mean, SD)	*p* value	**miR 23b-3p FU6** (mean, SD)	*p* value	**miR 34a-5p FU6** (mean, SD)	*p* value
Surgical procedure (n, %)						
Craniotomy (9, 100.0)	183.74 (141.87)	-	7.77 (6.16)	-	2.32 (2.43)	-
Neuronavigated biopsy (0, 0)	-		-		-	
Extent of tumour resection (n, %)						
NTR (8, 88.9)	191.71 (149.50)	0.665	8.03 (6.53)	0.747	2.15 (2.53)	0.582
STR (1, 11.1)	120.00		5.70		3.70	
Postoperative contrast enhancement (n, %)						
Absent (6, 66.7)	199.72 (153.10)	0.664	8.46 (7.28)	0.668	1.60 (1.33)	0.228
Linear (3, 33.3)	151.80 (140.03)		6.40 (3.90)		3.77 (3.80)	
Nodular (0, 0)	-		-		-	
RT + concomitant TMZ (n, %)						
Yes (7, 77.8)	216.33 (142.89)	0.122	9.11 (6.23)	0.187	2.29 (2.70)	0.926
No (2, 22.2)	69.70 (71.13)		3.08 (3.71)		2.45 (1.77)	
Adjuvant chemotherapy (n, %)						
Yes (8, 88.9)	164.71 (138.84)	0.283	7.09 (6.21)	0.385	2.53 (2.51)	0.515
No (1, 11.1)	336.00		13.20		0.70	

NTR: near total resection; RT: radiotherapy; STR: subtotal resection; TMZ: temozolomide.

Table 10 – Comparison of miR 21-5p, miR 23b-3p and miR 34a-5p plasmatic concentrations 12 months after surgery (FU12) according to extent of tumour resection and adjuvant therapies (5 patients).

	miR 21-5p FU12 (mean, SD)	*p* value	**miR 23b-3p FU12** (mean, SD)	*p* value	**miR 34a-5p FU12** (mean, SD)	*p* value
Surgical procedure (n, %)						
Craniotomy (5, 100.0)	27.42 (17.27)	-	0.91 (0.42)	-	1.56 (0.34)	-
Neuronavigated biopsy (0, 0)	-		-		-	
Extent of tumour resection (n, %)						
NTR (5, 100.0)	27.42 (17.27)	-	0.91 (0.42)	-	1.56 (0.34)	-
STR (0, 0)	-		-		-	
Postoperative contrast enhancement (n, %)						
Absent (4, 80.0)	32.93 (13.99)	0.177	0.92 (0.48)	0.919	1.58 (0.39)	0.873
Linear (1, 20.0)	5.40		0.86		1.50	
Nodular (0, 0)	-		-		-	
RT + concomitant TMZ (n, %)						
Yes (5, 100.0)	27.42 (17.27)	-	0.91 (0.42)	-	1.56 (0.34)	-
No (0, 0)	-		-		-	
Adjuvant chemotherapy (n, %)						
Yes (4, 80.0)	25.30 (19.18)	0.655	0.76 (0.29)	0.113	1.60 (0.37)	0.665
No (1, 20.0)	35.90		1.50		1.40	

NTR: near total resection; RT: radiotherapy; STR: subtotal resection; TMZ: temozolomide.

Table 11 – Correlation analysis between miR 21-5p, miR 23b-3p and miR 34a-5p plasmatic concentrations 1 month after surgery (FU1) and extent of tumour resection.

	miR 21-5p FU1			**miR 23b-3p FU1**			**Mir 34a-5p FU1**		
	R	R^2	*p* value	R	R^2	*p* value	R	R^2	*p* value
Surgical procedure (craniotomy vs biopsy)	-0.328	0.108	0.215	-0.164	0.027	0.544	-0.103	0.011	0.705
Extent of tumour resection (NTR vs STR)	-0.336	0.113	0.203	-0.238	0.057	0.374	-0.393	0.154	0.132
Extent of tumour resection (percentage)	0.199	0.040	0.459	0.185	0.034	0.492	0.253	0.064	0.344
Volume of postoperative tumour remnant (cc)	-0.153	0.023	0.572	-0.160	0.027	0.553	-0.199	0.040	0.460
Postoperative contrast enhancement (absent vs linear vs nodular)	-0.166	0.028	0.538	0.0	0	1.0	-0.325	0.106	0.219

NTR: near total resection; STR: subtotal resection.

Table 12 – Correlation analysis between miR 21-5p, miR 23b-3p and miR 34a-5p plasmatic concentrations 3 months after surgery (FU3), extent of tumour resection and postoperative concomitant RT and chemotherapy.

	miR 21-5p FU3			**miR 23b-3p FU3**			**Mir 34a-5p FU3**		
	R	R^2	*p* value	R	R^2	*p* value	R	R^2	*p* value
Surgical procedure (craniotomy vs biopsy)	-	-	-	-	-	-	-	-	-
Extent of tumour resection (NTR vs STR)	0.412	0.167	0.310	0.247	0.061	0.555	0.249	0.062	0.552
Extent of tumour resection (percentage)	-0.398	0.158	0.328	-0.495	0.245	0.212	0.016	0.000	0.970
Volume of postoperative tumour remnant (cc)	0.324	0.105	0.434	0.615	0.378	0.105	-0.144	0.021	0.735
Postoperative contrast enhancement (absent vs linear vs nodular)	0.206	0.042	0.625	0.437	0.191	0.279	0.0	0	1.0
RT + concomitant TMZ (yes vs no)	0.0	0	1.0	0.252	0.064	0.547	0.063	0.004	0.881

NTR: near total resection; RT: radiotherapy; STR: subtotal resection; TMZ: temozolomide.

Table 13 – Correlation analysis between miR 21-5p, miR 23b-3p and miR 34a-5p plasmatic concentrations 6 months after surgery (FU6), extent of tumour resection, postoperative concomitant RT and chemotherapy and adjuvant chemotherapy.

	miR 21-5p FU6			**miR 23b-3p FU6**			**Mir 34a-5p FU6**		
	R	R^2	*p* value	R	R^2	*p* value	R	R^2	*p* value
Surgical procedure (craniotomy vs biopsy)	-	-	-	-	-	-	-	-	-
Extent of tumour resection (NTR vs STR)	-0.137	0.019	0.725	-0.137	0.019	0.725	0.413	0.171	0.270
Extent of tumour resection (percentage)	0.152	0.023	0.697	0.127	0.016	0.745	-0.345	0.119	0.363
Volume of postoperative tumour remnant (cc)	-0.198	0.039	0.609	-0.156	0.024	0.689	0.259	0.067	0.500
Postoperative contrast enhancement (absent vs linear vs nodular)	-0.091	0.008	0.815	-0.091	0.008	0.815	0.321	0.103	0.400
RT + concomitant TMZ (yes vs no)	0.414	0.171	0.268	0.414	0.171	0.268	-0.208	0.043	0.591
Adjuvant chemotherapy (yes vs no)	-0.411	0.169	0.272	-0.411	0.169	0.272	0.275	0.076	0.474

NTR: near total resection; RT: radiotherapy; STR: subtotal resection; TMZ: temozolomide.

Table 14 – Correlation analysis between miR 21-5p, miR 23b-3p and miR 34a-5p plasmatic concentrations 12 months after surgery (FU12), extent of tumour resection, postoperative concomitant RT and chemotherapy and adjuvant chemotherapy.

	miR 21-5p FU12			**miR 23b-3p FU12**			**Mir 34a-5p FU12**		
	R	R^2	*p* value	R	R^2	*p* value	R	R^2	*p* value
Surgical procedure (craniotomy vs biopsy)	-	-	-	-	-	-	-	-	-
Extent of tumour resection (NTR vs STR)	-	-	-	-	-	-	-	-	-
Extent of tumour resection (percentage)	0.713	0.508	0.177	0.064	0.004	0.919	0.100	0.010	0.873
Volume of postoperative tumour remnant (cc)	-0.713	0.508	0.177	-0.064	0.004	0.919	-0.100	0.010	0.873
Postoperative contrast enhancement (absent vs linear vs nodular)	-0.707	0.500	0.182	0	0	1.0	0	0	1.0
RT + concomitant TMZ (yes vs no)	-	-	-	-	-	-	-	-	-
Adjuvant chemotherapy (yes vs no)	-0.354	0.125	0.559	-0.707	0.500	0.182	0.354	0.125	0.559

NTR: near total resection; RT: radiotherapy; STR: subtotal resection; TMZ: temozolomide.

Table 15 – Multivariate linear regression analysis between miR 21-5p plasmatic concentrations 1 (FU1), 3 (FU3), 6 (FU6) and 12 months (FU12) after surgery, extent of tumour resection, postoperative concomitant RT and chemotherapy and adjuvant chemotherapy.

FU1: ANOVA: R 0.600; R^2 0.360; adjusted R^2 0.040; F 1.125; *p* value 0.407.
FU3: ANOVA: R 0.962; R^2 0.925; adjusted R^2 0.738; F 4.952; *p* value 0.177.
FU6: ANOVA: R 0.770; R^2 0.592; adjusted R^2 -0.087; F 0.872; *p* value 0.584.
FU12: ANOVA: R 0.719; R^2 0.518; adjusted R^2 0.035; F 1.073; *p* value 0.482.

	OR	95% CI	*p* value
miR 21-5p FU1			
Extent of resection (NTR vs STR)	-976.77	-2343.43 – 389.89	0.142
Extent of resection (percentage)	-29.39	-104.71 – 45.92	0.405
Volume of postoperative tumour remnant (cc)	-0.56	-65.92 – 64.80	0.985
Contrast enhancement (linear vs nodular)	206.53	-98.89 – 511.94	0.163
miR 21-5p FU3			
Extent of resection (NTR vs STR)	-3309.88	-7096.67 – 476.92	0.064
Extent of resection (percentage)	-795.65	-1570.89 – -20.42	0.048
Volume of postoperative tumour remnant (cc)	-1163.49	-2782.72 – 455.75	0.091
Contrast enhancement (linear vs nodular)	-311.35	-905.22 – 282.52	0.153
RT + concomitant TMZ (yes vs no)	174.07	-598.14 – 946.27	0.434
miR 21-5p FU6			
Extent of resection (NTR vs STR)	-2405.07	-8632.84 – 3822.71	0.307
Extent of resection (percentage)	-392.74	-1344.84 – 559.36	0.281
Volume of postoperative tumour remnant (cc)	-	-	-
Contrast enhancement (linear vs nodular)	-532.29	-1786.48 – 721.90	0.270
RT + concomitant TMZ (yes vs no)	191.33	-334.96 – 717.61	0.331
Adjuvant chemotherapy (yes vs no)	-125.28	-651.56 – 401.01	0.504
miR 21-5p FU12			
Extent of resection (NTR vs STR)	-	-	-
Extent of resection (percentage)	-	-	-
Volume of postoperative tumour remnant (cc)	-	-	-
Contrast enhancement (linear vs nodular)	-26.53	-110.83 – 57.76	0.308
RT + concomitant TMZ (yes vs no)	-	-	-
Adjuvant chemotherapy (yes vs no)	-3.97	-88.26 – 80.33	0.858

NTR: near total resection; RT: radiotherapy; STR: subtotal resection; TMZ: temozolomide.

Table 16 – Multivariate linear regression analysis between miR 23b-3p plasmatic concentrations 1 (FU1), 3 (FU3), 6 (FU6) and 12 months (FU12) after surgery, extent of tumour resection, postoperative concomitant RT and chemotherapy and adjuvant chemotherapy.

FU1: ANOVA: R 0.587; R^2 0.345; adjusted R^2 0.107; F 1.448; *p* value 0.283.
FU3: ANOVA: R 0.960; R^2 0.922; adjusted R^2 0.725; F 4.696; *p* value 0.185.
FU6: ANOVA: R 0.650; R^2 0.422; adjusted R^2 -0.542; F 0.438; *p* value 0.804.
FU12: ANOVA: R 0.800; R^2 0.640; adjusted R^2 0.280; F 1.777; *p* value 0.360.

	OR	95% CI	*p* value
miR 23b-3p FU1			
Extent of resection (NTR vs STR)	-46.26	-105.70 – 13.18	0.115
Extent of resection (percentage)	0.23	-0.91 – 1.38	0.665
Volume of postoperative tumour remnant (cc)	0.83	-4.35 – 6.00	0.732
Contrast enhancement (linear vs nodular)	24.68	-0.92 – 50.28	0.057
miR 23b-3p FU3			
Extent of resection (NTR vs STR)	-161.49	-404.65 – 81.66	0.104
Extent of resection (percentage)	-26.95	-76.73 – 22.83	0.145
Volume of postoperative tumour remnant (cc)	2.30	-101.68 – 106.27	0.933
Contrast enhancement (linear vs nodular)	-22.54	-60.67 – 15.59	0.126
RT + concomitant TMZ (yes vs no)	13.03	-36.55 – 62.62	0.375
miR 23b-3p FU6			
Extent of resection (NTR vs STR)	-63.70	-385.76 – 258.37	0.574
Extent of resection (percentage)	-11.01	-60.25 – 38.22	0.528
Volume of postoperative tumour remnant (cc)	-	-	-
Contrast enhancement (linear vs nodular)	-16.24	-81.10 – 48.62	0.484
RT + concomitant TMZ (yes vs no)	8.82	-18.39 – 36.04	0.378
Adjuvant chemotherapy (yes vs no)	-3.93	-31.14 – 23.29	0.677
miR 23b-3p FU12			
Extent of resection (NTR vs STR)	-	-	-
Extent of resection (percentage)	-	-	-
Volume of postoperative tumour remnant (cc)	-	-	-
Contrast enhancement (linear vs nodular)	0.133	-1.64 – 1.90	0.777
RT + concomitant TMZ (yes vs no)	-	-	-
Adjuvant chemotherapy (yes vs no)	-0.773	-2.54 – 1.00	0.201

NTR: near total resection; RT: radiotherapy; STR: subtotal resection; TMZ: temozolomide.

Table 17 – Multivariate linear regression analysis between miR 34a-5p plasmatic concentrations 1 (FU1), 3 (FU3), 6 (FU6) and 12 months (FU12) after surgery, extent of tumour resection, postoperative concomitant RT and chemotherapy and adjuvant chemotherapy.

FU1: ANOVA: R 0.515; R^2 0.266; adjusted R^2 -0.001; F 0.994; *p* value 0.451.
FU3: ANOVA: R 0.817; R^2 0.668; adjusted R^2 -0.163; F 0.803; *p* value 0.636.
FU6: ANOVA: R 0.918; R^2 0.843; adjusted R^2 0.581; F 3.222; *p* value 0.182.
FU12: ANOVA: R 0.317; R^2 0.100; adjusted R^2 -0.799; F 0.111; *p* value 0.900.

	OR	95% CI	*p* value
miR 34a-5p FU1			
Extent of resection (NTR vs STR)	-1.39	-4.68 – 1.90	0.372
Extent of resection (percentage)	0.01	-0.06 – 0.07	0.872
Volume of postoperative tumour remnant (cc)	0.08	-0.21 – 0.37	0.551
Contrast enhancement (linear vs nodular)	-0.57	-1.98 – 0.85	0.398
miR 34a-5p FU3			
Extent of resection (NTR vs STR)	-43.87	-179.62 – 91.88	0.299
Extent of resection (percentage)	-11.68	-39.47 – 16.11	0.212
Volume of postoperative tumour remnant (cc)	-22.32	-80.36 – 35.73	0.240
Contrast enhancement (linear vs nodular)	-3.89	-25.18 – 17.40	0.514
RT + concomitant TMZ (yes vs no)	3.27	-24.42 – 30.95	0.662
miR 34a-5p FU6			
Extent of resection (NTR vs STR)	-69.91	-135.99 – -3.84	0.043
Extent of resection (percentage)	-10.87	-20.97 – -0.77	0.042
Volume of postoperative tumour remnant (cc)	-	-	-
Contrast enhancement (linear vs nodular)	-11.67	-24.97 – 1.64	0.068
RT + concomitant TMZ (yes vs no)	0.73	-4.86 – 6.31	0.707
Adjuvant chemotherapy (yes vs no)	1.23	-4.36 – 6.81	0.535
miR 34a-5p FU12			
Extent of resection (NTR vs STR)	-	-	-
Extent of resection (percentage)	-	-	-
Volume of postoperative tumour remnant (cc)	-	-	-
Contrast enhancement (linear vs nodular)	-0.133	-2.37 – 2.11	0.822
RT + concomitant TMZ (yes vs no)	-	-	-
Adjuvant chemotherapy (yes vs no)	0.233	-2.01 – 2.47	0.698

NTR: near total resection; RT: radiotherapy; STR: subtotal resection; TMZ: temozolomide.

Table 18 – Multivariate linear regression analysis between miR 21-5p, miR 23b-3p and miR 34a-5p plasmatic concentrations at diagnosis.

***miR 21-5p*: ANOVA: R 0.950; R^2 0.902; adjusted R^2 0.893; F 92.341; *p* value <0.001.**

***miR 23b-3p*: ANOVA: R 0.943; R^2 0.889; adjusted R^2 0.878; F 80.079; *p* value <0.001.**

***miR 34a-5p*: ANOVA: R 0.563; R^2 0.317; adjusted R^2 0.249; F 4.649; *p* value 0.022.**

	OR	95% CI	*p* value
miR 21-5p at diagnosis			
miR 23b-3p at diagnosis	**11.50**	**9.53 – 13.47**	**<0.001**
miR 34a-5p at diagnosis	**23.80**	**5.57 – 42.02**	**0.013**
miR 23b-3p at diagnosis			
miR 21-5p at diagnosis	**0.08**	**0.06 – 0.09**	**<0.001**
miR 34a-5p at diagnosis	-1.55	-3.13 – 0.40	0.056
miR 34a-5p at diagnosis			
miR 21-5p at diagnosis	**0.01**	**0.00 – 0.02**	**0.013**
miR 23b-3p at diagnosis	-0.11	-0.23 – 0.00	0.056

Table 19 – Multivariate linear regression analysis between miR 21-5p, miR 23b-3p and miR 34a-5p plasmatic concentrations 1 month (FU1) after surgery with miR 21-5p, miR 23b-3p and miR 34a-5p plasmatic concentrations at diagnosis and 1 month (FU1) after surgery.

***miR 21-5p*: ANOVA: R 0.988; R^2 0.976; adjusted R^2 0.964; F 80.547; *p* value <0.001.**

***miR 23b-3p*: ANOVA: R 0.989; R^2 0.978; adjusted R^2 0.967; F 88.313; *p* value <0.001.**

miR 34a-5p: ANOVA: R 0.696; R^2 0.485; adjusted R^2 0.227; F 1.882; *p* value 0.185.

	OR	95% CI	*p* value
miR 21-5p at FU1			
miR 21-5p at diagnosis	0.132	-0.82 – 1.09	0.763
miR 23b-3p at diagnosis	-2.22	-16.67 – 12.22	0.739
miR 34a-5p at diagnosis	-11.53	-60.99 – 37.94	0.615
miR 23b-3p at FU1	**10.83**	**8.34 – 13.32**	**<0.001**
miR 34a-5p at FU1	11.21	-19.67 – 42.09	0.437
miR 23b-3p at FU1			
miR 21-5p at diagnosis	-0.02	-0.11 – 0.06	0.571
miR 23b-3p at diagnosis	0.53	-0.69 – 1.75	0.353
miR 34a-5p at diagnosis	0.55	-3.84 – 4.93	0.788
miR 21-5p at FU1	**0.08**	**0.06 – 0.10**	**<0.001**
miR 34a-5p at FU1	-0.54	-3.32 – 2.23	0.672
miR 34a-5p at FU1			
miR 21-5p at diagnosis	-0.01	-0.03 – 0.01	0.404
miR 23b-3p at diagnosis	0.05	-0.27 – 0.37	0.737
miR 34a-5p at diagnosis	1.00	0.15 – 1.86	0.025
miR 21-5p at FU1	0.01	-0.01 – 0.02	0.437
miR 23b-3p at FU1	-0.03	-0.21 – 0.14	0.672

Table 20 – Multivariate linear regression analysis between miR 21-5p, miR 23b-3p and miR 34a-5p plasmatic concentrations 3 months (FU3) after surgery and miR 21-5p, miR 23b-3p and miR 34a-5p plasmatic concentrations at diagnosis, 1 (FU1) and 3 months (FU3) after surgery.

miR 21-5p: ANOVA: R 0.999; R^2 0.999; adjusted R^2 0.994; F 214.546; *p* value 0.051.
miR 23b-3p: ANOVA: R 0.999; R^2 0.997; adjusted R^2 0.986; F 88.945; *p* value 0.079.
miR 34a-5p: ANOVA: R 0.992; R^2 0.984; adjusted R^2 0.918; F 14.950; *p* value 0.191.

	OR	95% CI	*p* value
miR 21-5p at FU3			
miR 21-5p at diagnosis	-0.33	-3.13 – 2.46	0.372
miR 21-5p at FU1	-4.62	-9.68 – 0.44	0.055
miR 23b-3p at FU3	121.16	1.55 – 240.77	0.049
miR 34a-5p at FU3	-310.05	-666.09 – 47.99	0.058
miR 23b-3p at FU3			
miR 23b-3p at diagnosis	0.02	-3.06 – 3.10	0.954
miR 23b-3p at FU1	0.39	-0.46 – 1.24	0.109
miR 21-5p at FU3	0.01	-0.09 – 0.10	0.457
miR 34a-5p at FU3	2.35	-4.63 – 9.33	0.146
miR 34a-5p at FU3			
miR 34a-5p at diagnosis	4.23	-16.71 – 25.17	0.237
miR 34a-5p at FU1	-1.82	-13.93 – 10.29	0.307
miR 21-5p at FU3	0.03	-0.05 – 0.10	0.138
miR 23b-3p at FU3	-0.15	-0.86 – 0.57	0.237

Table 21 – Multivariate linear regression analysis between miR 21-5p, miR 23b-3p and miR 34a-5p plasmatic concentrations 6 months (FU6) after surgery and miR 21-5p, miR 23b-3p and miR 34a-5p plasmatic concentrations 3 (FU3) and 6 months (FU6) after surgery.

miR 21-5p: ANOVA: R 0.992; R^2 0.983; adjusted R^2 0.934; F 19.735; *p* value 0.164.

***miR 23b-3p*: ANOVA: R 1.000; R^2 1.000; adjusted R^2 0.999; F 1098.073; *p* value 0.022.**

miR 34a-5p: ANOVA: R 0.992; R^2 0.984; adjusted R^2 0.936; F 20.662; *p* value 0.160.

	OR	95% CI	*p* value
miR 21-5p at FU6			
miR 21-5p at FU3	-0.22	-5.18 – 4.74	0.677
miR 23b-3p at FU6	38.66	-49.83 – 127.15	0.113
miR 34a-5p at FU6	10.24	-535.82 – 556.31	0.851
miR 23b-3p at FU6			
miR 23b-3p at FU3	0.10	-0.08 – 0.28	0.087
miR 21-5p at FU6	**0.02**	**0.01 – 0.03**	**0.022**
miR 34a-5p at FU6	0.05	-0.69 – 0.78	0.581
miR 34a-5p at FU6			
miR 34a-5p at FU3	0.72	-1.83 – 3.27	0.172
miR 21-5p at FU6	-0.06	-0.19 – 0.08	0.116
miR 23b-3p at FU6	1.33	-3.09 – 5.75	0.163

Table 22 – Multivariate linear regression analysis between miR 21-5p, miR 23b-3p and miR 34a-5p plasmatic concentrations 12 months (FU12) after surgery.

miR 21-5p: ANOVA: R 0.472; R^2 0.223; adjusted R^2 -0.554; F 0.287; *p* value 0.777.

miR 23b-3p: ANOVA: R 0.449; R^2 0.202; adjusted R^2 -0.596; F 0.253; *p* value 0.798.

miR 34a-5p: ANOVA: R 0.172; R^2 0.030; adjusted R^2 -0.941; F 0.031; *p* value 0.970.

	OR	95% CI	*p* value
miR 21-5p at FU12			
miR 23b-3p at FU12	18.21	-92.15 – 128.57	0.551
miR 34a-5p at FU12	-7.82	-145.70 – 130.06	0.830
miR 23b-3p at FU12			
miR 21-5p at FU12	0.01	-0.06 – 0.08	0.551
miR 34a-5p at FU12	0.06	-3.38 – 3.50	0.948
miR 34a-5p at FU12			
miR 21-5p at FU12	-0.01	-0.07 – 0.06	0.830
miR 23b-3p at FU12	0.05	-2.64 – 2.73	0.948

Table 23 – Node explorer table for miR 21-5p, miR 23b-3p and miR 34a-5p network analysis (miRNet version 2.0).

ID	Degree	Betweenness
hsa-mir-21-5p	98	3393.358
hsa-mir-34a-5p	89	2679.215
hsa-mir-23b-3p	58	1182.427
E2F1	3	3.134753
TNPO1	3	3.134753
MTAP	3	3.134753
CPEB3	3	3.134753
NUFIP2	3	3.134753

Networks: a) *queries*, miRNA: 3; b) *nodes*, gene: 120, miRNA: 3; c) *edges*, 245.

Table 24 – Node explorer table for miR 21-5p and miR 23b-3p network analysis (miRNet version 2.0).

ID	Degree	Betweenness
hsa-mir-21-5p	36	315
hsa-mir-23b-3p	36	315
ACAT1	2	0.027778
CCNG1	2	0.027778
HAPLN1	2	0.027778
E2F1	2	0.027778
MSH6	2	0.027778
GTF2I	2	0.027778
HNRNPK	2	0.027778
TNPO1	2	0.027778
MARCKS	2	0.027778
MTAP	2	0.027778
PIK3R1	2	0.027778
PTEN	2	0.027778
PTPN14	2	0.027778
RB1	2	0.027778
TGIF1	2	0.027778
TNFAIP3	2	0.027778
TSNAX	2	0.027778
VHL	2	0.027778
ZMYM2	2	0.027778
SOCS6	2	0.027778
DOCK4	2	0.027778
SLC9A6	2	0.027778
CPEB3	2	0.027778
TNRC6B	2	0.027778
RPRD2	2	0.027778
ATXN10	2	0.027778
RNF111	2	0.027778
ETNK1	2	0.027778
ATF7IP	2	0.027778
NUFIP2	2	0.027778
RMND5A	2	0.027778
TMEM170A	2	0.027778
UBR3	2	0.027778
PTPDC1	2	0.027778
PRR14L	2	0.027778
TRIM59	2	0.027778

Networks: a) *queries*, miRNA: 2; b) *nodes*, gene: 36, miRNA: 2; c) *edges*, 72.

Table 25 – Node explorer table for miR 21-5p and miR 34a-5p network analysis (miRNet version 2.0).

ID	Degree	Betweenness
hsa-mir-21-5p	67	1105.5
hsa-mir-34a-5p	67	1105.5
JAG1	2	0.014925
CRYBG1	2	0.014925
APAF1	2	0.014925
FASLG	2	0.014925
BCL2	2	0.014925
BNIP2	2	0.014925
BRCA1	2	0.014925
CALD1	2	0.014925
CASP8	2	0.014925
CDC25A	2	0.014925
CDK6	2	0.014925
CEBPB	2	0.014925
FOXN3	2	0.014925
E2F1	2	0.014925
E2F3	2	0.014925
ERBB2	2	0.014925
MKNK2	2	0.014925
HMGB1	2	0.014925
IGF1R	2	0.014925
TNPO1	2	0.014925
CAPRIN1	2	0.014925
MDM4	2	0.014925
MAP3K1	2	0.014925
MTAP	2	0.014925
MYC	2	0.014925
NFKB1	2	0.014925
PPARA	2	0.014925
RPS7	2	0.014925
SMARCA4	2	0.014925
SOX2	2	0.014925
TGFBR2	2	0.014925
TP53BP2	2	0.014925
TPM1	2	0.014925
VEGFA	2	0.014925
GDF5	2	0.014925
TNFRSF10B	2	0.014925
BCL10	2	0.014925
LRRFIP1	2	0.014925
CLOCK	2	0.014925
CKAP5	2	0.014925
FAM3C	2	0.014925
STAG2	2	0.014925
CPEB3	2	0.014925
NT5C2	2	0.014925
SYNE2	2	0.014925
ADNP	2	0.014925

DDAH1	2	0.014925
GAPVD1	2	0.014925
RDH11	2	0.014925
USP47	2	0.014925
FIGN	2	0.014925
YOD1	2	0.014925
FAM46A	2	0.014925
SAR1A	2	0.014925
TM9SF3	2	0.014925
RTN4	2	0.014925
THOC2	2	0.014925
ESYT2	2	0.014925
NUFIP2	2	0.014925
MOAP1	2	0.014925
NCAPG	2	0.014925
MTMR9	2	0.014925
PROSER1	2	0.014925
LNPK	2	0.014925
KBTBD6	2	0.014925
SOCS4	2	0.014925
GXYLT2	2	0.014925

Networks: a) *queries*, miRNA: 2; b) *nodes*, gene: 67, miRNA: 2; c) *edges*, 134.

Table 26 – Cox regression analysis between miR 21-5p, miR 23b-3p and miR 34a-5p plasmatic concentrations at diagnosis, 1 (FU1), 3 (FU3), 6 (FU6) and 12 months (FU12) after surgery and overall survival.

At diagnosis: chi square 3.044; dof 3; *p* value 0.385
At FU1: chi square 2.637; dof 3; *p* value 0.451
At FU3: chi square 7.841; dof 3; *p* value 0.049
At FU6: chi square 3.304; dof 3; *p* value 0.347
At FU12: chi square 4.886; dof 3; *p* value 0.180

	HR	95% CI	*p* value
miR 21-5p at diagnosis	1.019	0.991 – 1.019	0.503
miR 23b-3p at diagnosis	0.982	0.834 – 1.157	0.829
miR 34a-5p at diagnosis	0.612	0.301 – 1.242	0.174
miR 21-5p at FU1	1.004	0.994 – 1.015	0.405
miR 23b-3p at FU1	0.965	0.865 – 1.076	0.521
miR 34a-5p at FU1	0.715	0.453 – 1.127	0.148
miR 21-5p at FU3	1.005	0.995 – 1.015	0.336
miR 23b-3p at FU3	1.051	0.943 – 1.170	0.370
miR 34a-5p at FU3	0.343	0.064 – 1.834	0.211
miR 21-5p at FU6	1.001	0.984 – 1.018	0.921
miR 23b-3p at FU6	0.809	0.478 – 1.368	0.428
miR 34a-5p at FU6	1.081	0.708 – 1.650	0.719
miR 21-5p at FU12	0.883	0.606 – 1.286	0.517
miR 23b-3p at FU12	27497.812	0.000 – 3.499	0.472
miR 34a-5p at FU12	0.008	0.000 – 8.192	0.869

Table 27 – Cox regression analysis between miR 21-5p, miR 23b-3p and miR 34a-5p plasmatic concentrations at diagnosis, 1 (FU1), 3 (FU3), 6 (FU6) and 12 months (FU12) after surgery and recurrence free survival.

At diagnosis: chi square 2.239; dof 3; *p* value 0.524
At FU1: chi square 1.987; dof 3; *p* value 0.575
At FU3: chi square 3.295; dof 3; *p* value 0.348
At FU6: chi square 2.701; dof 3; *p* value 0.440
At FU12: chi square 4.886; dof 3; *p* value 0.180

	HR	95% CI	*p* value
miR 21-5p at diagnosis	1.005	0.990 – 1.020	0.523
miR 23b-3p at diagnosis	0.945	0.786 – 1.136	0.546
miR 34a-5p at diagnosis	0.606	0.288 – 1.272	0.185
miR 21-5p at FU1	1.006	0.995 – 1.017	0.321
miR 23b-3p at FU1	0.911	0.765 – 1.086	0.298
miR 34a-5p at FU1	0.920	0.619 – 1.367	0.679
miR 21-5p at FU3	1.013	0.993 – 1.034	0.204
miR 23b-3p at FU3	0.801	0.578 – 1.109	0.181
miR 34a-5p at FU3	0.780	0.433 – 1.406	0.409
miR 21-5p at FU6	1.002	0.984 – 1.020	0.823
miR 23b-3p at FU6	0.777	0.434 – 1.392	0.397
miR 34a-5p at FU6	1.268	0.774 – 2.077	0.345
miR 21-5p at FU12	0.883	0.606 – 1.286	0.517
miR 23b-3p at FU12	27497.812	0.000 – 3.499	0.472
miR 34a-5p at FU12	0.008	0.000 – 8.192	0.869

8. REFERENCES

1. Heitzer E, Haque IS, Roberts CES, Speicher MR. Current and future perspectives of liquid biopsies in genomics-driven oncology. *Nat Rev Genet.* 2019;20(2):71-88.
2. Ignatiadis M, Sledge GW, Jeffrey SS. Liquid biopsy enters the clinic - implementation issues and future challenges. *Nat Rev Clin Oncol.* 2021;18(5):297-312.
3. Roth P, Wischhusen J, Happold C, et al. A specific miRNA signature in the peripheral blood of glioblastoma patients. *J Neurochem.* 2011;118(3):449-457.
4. Yu X, Li Z. Serum microRNAs as potential noninvasive biomarkers for glioma. *Tumour Biol.* 2016;37(2):1407-1410.
5. Ma C, Nguyen HPT, Luwor RB, et al. A comprehensive meta-analysis of circulation miRNAs in glioma as potential diagnostic biomarker. *PLoS One.* 2018;13(2):e0189452.
6. Jones J, Nguyen H, Drummond K, Morokoff A. Circulating Biomarkers for Glioma: A Review. *Neurosurgery.* 2021;88(3):E221-E230.
7. Beylerli O, Encarnacion Ramirez MJ, Shumadalova A, et al. Cell-Free miRNAs as Non-Invasive Biomarkers in Brain Tumors. *Diagnostics (Basel).* 2023;13(18).
8. Ohgaki H, Kleihues P. Population-based studies on incidence, survival rates, and genetic alterations in astrocytic and oligodendroglial gliomas. *J Neuropathol Exp Neurol.* 2005;64(6):479-489.
9. Ostrom QT, Gittleman H, Liao P, et al. CBTRUS statistical report: primary brain and central nervous system tumors diagnosed in the United States in 2007-2011. *Neuro Oncol.* 2014;16 Suppl 4(Suppl 4):iv1-63.
10. Stupp R, Mason WP, van den Bent MJ, et al. Radiotherapy plus concomitant and adjuvant temozolomide for glioblastoma. *N Engl J Med.* 2005;352(10):987-996.
11. Stupp R, Hegi ME, Mason WP, et al. Effects of radiotherapy with concomitant and adjuvant temozolomide versus radiotherapy alone on survival in glioblastoma in a randomised phase III study: 5-year analysis of the EORTC-NCIC trial. *Lancet Oncol.* 2009;10(5):459-466.
12. Perry JR, Laperriere N, O'Callaghan CJ, et al. Short-Course Radiation plus Temozolomide in Elderly Patients with Glioblastoma. *N Engl J Med.* 2017;376(11):1027-1037.
13. Weller M, van den Bent M, Preusser M, et al. EANO guidelines on the diagnosis and treatment of diffuse gliomas of adulthood. *Nat Rev Clin Oncol.* 2021;18(3):170-186.
14. Ilhan-Mutlu A, Wagner L, Wohrer A, et al. Plasma MicroRNA-21 concentration may be a useful biomarker in glioblastoma patients. *Cancer Invest.* 2012;30(8):615-621.
15. Ahir BK, Ozer H, Engelhard HH, Lakka SS. MicroRNAs in glioblastoma pathogenesis and therapy: A comprehensive review. *Crit Rev Oncol Hematol.* 2017;120:22-33.
16. Zhao H, Shen J, Hodges TR, Song R, Fuller GN, Heimberger AB. Serum microRNA profiling in patients with glioblastoma: a survival analysis. *Mol Cancer.* 2017;16(1):59.

17. Chen X, Ba Y, Ma L, et al. Characterization of microRNAs in serum: a novel class of biomarkers for diagnosis of cancer and other diseases. *Cell Res.* 2008;18(10):997-1006.
18. Redova M, Sana J, Slaby O. Circulating miRNAs as new blood-based biomarkers for solid cancers. *Future Oncol.* 2013;9(3):387-402.
19. Louis DN, Perry A, Wesseling P, et al. The 2021 WHO Classification of Tumors of the Central Nervous System: a summary. *Neuro Oncol.* 2021;23(8):1231-1251.
20. Molinaro AM, Taylor JW, Wiencke JK, Wrensch MR. Genetic and molecular epidemiology of adult diffuse glioma. *Nat Rev Neurol.* 2019;15(7):405-417.
21. Esquela-Kerscher A, Slack FJ. Oncomirs - microRNAs with a role in cancer. *Nat Rev Cancer.* 2006;6(4):259-269.
22. Guarnieri DJ, DiLeone RJ. MicroRNAs: a new class of gene regulators. *Ann Med.* 2008;40(3):197-208.
23. Croce CM. Causes and consequences of microRNA dysregulation in cancer. *Nat Rev Genet.* 2009;10(10):704-714.
24. Schwarzenbach H, Nishida N, Calin GA, Pantel K. Clinical relevance of circulating cell-free microRNAs in cancer. *Nat Rev Clin Oncol.* 2014;11(3):145-156.
25. Goodall GJ, Wickramasinghe VO. RNA in cancer. *Nat Rev Cancer.* 2021;21(1):22-36.
26. He L, Hannon GJ. MicroRNAs: small RNAs with a big role in gene regulation. *Nat Rev Genet.* 2004;5(7):522-531.
27. Lu J, Getz G, Miska EA, et al. MicroRNA expression profiles classify human cancers. *Nature.* 2005;435(7043):834-838.
28. Calin GA, Croce CM. MicroRNA signatures in human cancers. *Nat Rev Cancer.* 2006;6(11):857-866.
29. Bartel DP. MicroRNAs: target recognition and regulatory functions. *Cell.* 2009;136(2):215-233.
30. Mitchell PS, Parkin RK, Kroh EM, et al. Circulating microRNAs as stable blood-based markers for cancer detection. *Proc Natl Acad Sci U S A.* 2008;105(30):10513-10518.
31. Aili Y, Maimaitiming N, Mahemuti Y, Qin H, Wang Y, Wang Z. Liquid biopsy in central nervous system tumors: the potential roles of circulating miRNA and exosomes. *Am J Cancer Res.* 2020;10(12):4134-4150.
32. Hindson BJ, Ness KD, Masquelier DA, et al. High-throughput droplet digital PCR system for absolute quantitation of DNA copy number. *Anal Chem.* 2011;83(22):8604-8610.
33. Ahmed SP, Castresana JS, Shahi MH. Glioblastoma and MiRNAs. *Cancers (Basel).* 2021;13(7).
34. Sarver AL, Sarver AE, Yuan C, Subramanian S. OMCD: OncomiR Cancer Database. *BMC Cancer.* 2018;18(1):1223.

35. Wang Q, Li P, Li A, et al. Plasma specific miRNAs as predictive biomarkers for diagnosis and prognosis of glioma. *J Exp Clin Cancer Res.* 2012;31(1):97.
36. Visani M, de Biase D, Marucci G, et al. Expression of 19 microRNAs in glioblastoma and comparison with other brain neoplasia of grades I-III. *Mol Oncol.* 2014;8(2):417-430.
37. Toraih EA, Aly NM, Abdallah HY, et al. MicroRNA-target cross-talks: Key players in glioblastoma multiforme. *Tumour Biol.* 2017;39(11):1010428317726842.
38. Matos B, Bostjancic E, Matjasic A, Popovic M, Glavac D. Dynamic expression of 11 miRNAs in 83 consecutive primary and corresponding recurrent glioblastoma: correlation to treatment, time to recurrence, overall survival and MGMT methylation status. *Radiol Oncol.* 2018;52(4):422-432.
39. Jesionek-Kupnicka D, Braun M, Trabska-Kluch B, et al. MiR-21, miR-34a, miR-125b, miR-181d and miR-648 levels inversely correlate with MGMT and TP53 expression in primary glioblastoma patients. *Arch Med Sci.* 2019;15(2):504-512.
40. ParvizHamidi M, Haddad G, Ostadrahimi S, et al. Circulating miR-26a and miR-21 as biomarkers for glioblastoma multiform. *Biotechnol Appl Biochem.* 2019;66(2):261-265.
41. Yan C, Kong X, Gong S, Liu F, Zhao Y. Recent advances of the regulation roles of MicroRNA in glioblastoma. *Int J Clin Oncol.* 2020;25(7):1215-1222.
42. Zhao X, Xiao Z, Li B, et al. miRNA-21 may serve as a promising noninvasive marker of glioma with a high diagnostic performance: a pooled analysis of 997 patients. *Ther Adv Med Oncol.* 2021;13:1758835920987650.
43. Labib EM, Ezz El Arab LR, Ghanem HM, Hassan RE, Swellam M. Relevance of circulating MiRNA-21 and MiRNA-181 in prediction of glioblastoma multiforme prognosis. *Arch Physiol Biochem.* 2022;128(4):924-929.
44. Stepanovic A, Nikitovic M, Stanojkovic TP, et al. Association between microRNAs 10b/21/34a and acute toxicity in glioblastoma patients treated with radiotherapy and temozolomide. *Sci Rep.* 2022;12(1):7505.
45. Chen L, Han L, Zhang K, et al. VHL regulates the effects of miR-23b on glioma survival and invasion via suppression of HIF-1alpha/VEGF and beta-catenin/Tcf-4 signaling. *Neuro Oncol.* 2012;14(8):1026-1036.
46. Loftus JC, Ross JT, Paquette KM, et al. miRNA expression profiling in migrating glioblastoma cells: regulation of cell migration and invasion by miR-23b via targeting of Pyk2. *PLoS One.* 2012;7(6):e39818.
47. Agrawal R, Pandey P, Jha P, Dwivedi V, Sarkar C, Kulshreshtha R. Hypoxic signature of microRNAs in glioblastoma: insights from small RNA deep sequencing. *BMC Genomics.* 2014;15(1):686.
48. Chen L, Zhang K, Shi Z, et al. A lentivirus-mediated miR-23b sponge diminishes the malignant phenotype of glioma cells in vitro and in vivo. *Oncol Rep.* 2014;31(4):1573-1580.

49. Li Y, Guessous F, Zhang Y, et al. MicroRNA-34a inhibits glioblastoma growth by targeting multiple oncogenes. *Cancer Res.* 2009;69(19):7569-7576.
50. Guessous F, Zhang Y, Kofman A, et al. microRNA-34a is tumor suppressive in brain tumors and glioma stem cells. *Cell Cycle.* 2010;9(6):1031-1036.
51. Luan S, Sun L, Huang F. MicroRNA-34a: a novel tumor suppressor in p53-mutant glioma cell line U251. *Arch Med Res.* 2010;41(2):67-74.
52. Yin D, Ogawa S, Kawamata N, et al. miR-34a functions as a tumor suppressor modulating EGFR in glioblastoma multiforme. *Oncogene.* 2013;32(9):1155-1163.
53. Vojdani S, Ghaderian SMH, Zali A, et al. Altered expression of EGFR and miR-34a derived from serum and tumoral tissue was associated with glioblastoma multiform. *Exp Mol Pathol.* 2021;121:104655.
54. van Swieten JC, Koudstaal PJ, Visser MC, Schouten HJ, van Gijn J. Interobserver agreement for the assessment of handicap in stroke patients. *Stroke.* 1988;19(5):604-607.
55. Stummer W, Tonn JC, Goetz C, et al. 5-Aminolevulinic acid-derived tumor fluorescence: the diagnostic accuracy of visible fluorescence qualities as corroborated by spectrometry and histology and postoperative imaging. *Neurosurgery.* 2014;74(3):310-319; discussion 319-320.
56. Kaina B, Christmann M, Naumann S, Roos WP. MGMT: key node in the battle against genotoxicity, carcinogenicity and apoptosis induced by alkylating agents. *DNA Repair (Amst).* 2007;6(8):1079-1099.
57. Aasland D, Gotzinger L, Hauck L, et al. Temozolomide Induces Senescence and Repression of DNA Repair Pathways in Glioblastoma Cells via Activation of ATR-CHK1, p21, and NF-kappaB. *Cancer Res.* 2019;79(1):99-113.
58. Rezaee A, Tehrany PM, Tirabadi FJ, et al. Epigenetic regulation of temozolomide resistance in human cancers with an emphasis on brain tumors: Function of non-coding RNAs. *Biomed Pharmacother.* 2023;165:115187.
59. Lombardi G, De Salvo GL, Brandes AA, et al. Regorafenib compared with lomustine in patients with relapsed glioblastoma (REGOMA): a multicentre, open-label, randomised, controlled, phase 2 trial. *Lancet Oncol.* 2019;20(1):110-119.
60. Pang Y, Chen X, Ji T, et al. The Chromatin Remodeler ATRX: Role and Mechanism in Biology and Cancer. *Cancers (Basel).* 2023;15(8).
61. Al-Khallaf H. Isocitrate dehydrogenases in physiology and cancer: biochemical and molecular insight. *Cell Biosci.* 2017;7:37.
62. Sharma N, Mallela AN, Shi DD, et al. Isocitrate dehydrogenase mutations in gliomas: A review of current understanding and trials. *Neurooncol Adv.* 2023;5(1):vdad053.
63. Brigliadori G, Foca F, Dall'Agata M, et al. Defining the cutoff value of MGMT gene promoter methylation and its predictive capacity in glioblastoma. *J Neurooncol.* 2016;128(2):333-339.

64. Yu W, Zhang L, Wei Q, Shao A. O(6)-Methylguanine-DNA Methyltransferase (MGMT): Challenges and New Opportunities in Glioma Chemotherapy. *Front Oncol.* 2019;9:1547.
65. Karschnia P, Vogelbaum MA, van den Bent M, et al. Evidence-based recommendations on categories for extent of resection in diffuse glioma. *Eur J Cancer.* 2021;149:23-33.
66. Panni P, Colombo E, Donofrio CA, et al. Hemorrhagic burden in poor-grade aneurysmal subarachnoid hemorrhage: a volumetric analysis of different bleeding distributions. *Acta Neurochir (Wien).* 2019;161(4):791-797.
67. Panni P, Donofrio CA, Barzaghi LR, et al. Safety and feasibility of lumbar drainage in the management of poor grade aneurysmal subarachnoid hemorrhage. *J Clin Neurosci.* 2019;64:64-70.
68. Chang L, Zhou G, Soufan O, Xia J. miRNet 2.0: network-based visual analytics for miRNA functional analysis and systems biology. *Nucleic Acids Res.* 2020;48(W1):W244-W251.
69. Fluss R, Faraggi D, Reiser B. Estimation of the Youden Index and its associated cutoff point. *Biom J.* 2005;47(4):458-472.
70. Donofrio CA, Cavalli A, Gemma M, et al. Cumulative intracranial tumour volume prognostic assessment: a new predicting score index for patients with brain metastases treated by stereotactic radiosurgery. *Clin Exp Metastasis.* 2020;37(4):499-508.
71. Zarzuela L, Duran RV, Tome M. Metabolism and signaling crosstalk in glioblastoma progression and therapy resistance. *Mol Oncol.* 2023.
72. Glinge C, Clauss S, Boddum K, et al. Stability of Circulating Blood-Based MicroRNAs - Pre-Analytic Methodological Considerations. *PLoS One.* 2017;12(2):e0167969.
73. Marzi MJ, Montani F, Carletti RM, et al. Optimization and Standardization of Circulating MicroRNA Detection for Clinical Application: The miR-Test Case. *Clin Chem.* 2016;62(5):743-754.
74. Murray MJ, Watson HL, Ward D, et al. "Future-Proofing" Blood Processing for Measurement of Circulating miRNAs in Samples from Biobanks and Prospective Clinical Trials. *Cancer Epidemiol Biomarkers Prev.* 2018;27(2):208-218.
75. Morokoff A, Jones J, Nguyen H, et al. Serum microRNA is a biomarker for post-operative monitoring in glioma. *J Neurooncol.* 2020;149(3):391-400.
76. Dufourd T, Robil N, Mallet D, et al. Plasma or serum? A qualitative study on rodents and humans using high-throughput microRNA sequencing for circulating biomarkers. *Biol Methods Protoc.* 2019;4(1):bpz006.
77. Wu J, Hu S, Zhang L, et al. Tumor circulome in the liquid biopsies for cancer diagnosis and prognosis. *Theranostics.* 2020;10(10):4544-4556.
78. Ban E, Song EJ. Considerations and Suggestions for the Reliable Analysis of miRNA in Plasma Using qRT-PCR. *Genes (Basel).* 2022;13(2).

79. Yang C, Wang C, Chen X, et al. Identification of seven serum microRNAs from a genome-wide serum microRNA expression profile as potential noninvasive biomarkers for malignant astrocytomas. *Int J Cancer.* 2013;132(1):116-127.
80. Xiang M, Zeng Y, Yang R, et al. U6 is not a suitable endogenous control for the quantification of circulating microRNAs. *Biochem Biophys Res Commun.* 2014;454(1):210-214.
81. Occhipinti G, Giulietti M, Principato G, Piva F. The choice of endogenous controls in exosomal microRNA assessments from biofluids. *Tumour Biol.* 2016;37(9):11657-11665.
82. Miotto E, Saccenti E, Lupini L, Callegari E, Negrini M, Ferracin M. Quantification of circulating miRNAs by droplet digital PCR: comparison of EvaGreen- and TaqMan-based chemistries. *Cancer Epidemiol Biomarkers Prev.* 2014;23(12):2638-2642.
83. Li C, Sun J, Xiang Q, et al. Prognostic role of microRNA-21 expression in gliomas: a meta-analysis. *J Neurooncol.* 2016;130(1):11-17.
84. Ivo D'Urso P, Fernando D'Urso O, Damiano Gianfreda C, Mezzolla V, Storelli C, Marsigliante S. miR-15b and miR-21 as Circulating Biomarkers for Diagnosis of Glioma. *Curr Genomics.* 2015;16(5):304-311.
85. Chen M, Medarova Z, Moore A. Role of microRNAs in glioblastoma. *Oncotarget.* 2021;12(17):1707-1723.
86. Behrooz AB, Latifi-Navid H, Nezhadi A, et al. Molecular mechanisms of microRNAs in glioblastoma pathogenesis. *Biochim Biophys Acta Mol Cell Res.* 2023;1870(6):119482.
87. Siegal T, Charbit H, Paldor I, et al. Dynamics of circulating hypoxia-mediated miRNAs and tumor response in patients with high-grade glioma treated with bevacizumab. *J Neurosurg.* 2016;125(4):1008-1015.
88. Margue C, Reinsbach S, Philippidou D, et al. Comparison of a healthy miRNome with melanoma patient miRNomes: are microRNAs suitable serum biomarkers for cancer? *Oncotarget.* 2015;6(14):12110-12127.
89. Regazzo G, Terrenato I, Spagnuolo M, et al. A restricted signature of serum miRNAs distinguishes glioblastoma from lower grade gliomas. *J Exp Clin Cancer Res.* 2016;35(1):124.
90. Alvarado AG, Tessema K, Muthukrishnan SD, et al. Pathway-based approach reveals differential sensitivity to E2F1 inhibition in glioblastoma. *Cancer Res Commun.* 2022;2(9):1049-1060.
91. Zhou J, Tong F, Zhao J, et al. Identification of the E2F1-RAD51AP1 axis as a key factor in MGMT-methylated GBM TMZ resistance. *Cancer Biol Med.* 2023;20(5):385-400.
92. Chkheidze R, Raisanen J, Gagan J, et al. Alterations in the RB Pathway With Inactivation of RB1 Characterize Glioblastomas With a Primitive Neuronal Component. *J Neuropathol Exp Neurol.* 2021;80(12):1092-1098.

93. Hasan H, Afzal M, Castresana JS, Shahi MH. A Comprehensive Review of miRNAs and Their Epigenetic Effects in Glioblastoma. *Cells.* 2023;12(12).
94. Gariboldi MB, Ravizza R, Monti E. The IGFR1 inhibitor NVP-AEW541 disrupts a pro-survival and pro-angiogenic IGF-STAT3-HIF1 pathway in human glioblastoma cells. *Biochem Pharmacol.* 2010;80(4):455-462.
95. Scartozzi M, Bianconi M, Maccaroni E, Giampieri R, Berardi R, Cascinu S. Dalotuzumab, a recombinant humanized mAb targeted against IGFR1 for the treatment of cancer. *Curr Opin Mol Ther.* 2010;12(3):361-371.
96. Genovese G, Ergun A, Shukla SA, et al. microRNA regulatory network inference identifies miR-34a as a novel regulator of TGF-beta signaling in glioblastoma. *Cancer Discov.* 2012;2(8):736-749.
97. Wang J, Zhao YY, Li JF, et al. IDH1 mutation detection by droplet digital PCR in glioma. *Oncotarget.* 2015;6(37):39651-39660.
98. Adachi JI, Shirahata M, Suzuki T, et al. Droplet digital PCR assay for detecting TERT promoter mutations in patients with glioma. *Brain Tumor Pathol.* 2021;38(3):201-209.
99. Abarna R, J R, Chacko G, Pai R. Droplet digital PCR (ddPCR) using FFPE DNA to assess methylation status of MGMT gene among patients with IDH mutant astrocytoma and IDH wild-type glioblastoma. *J Clin Pathol.* 2023;76(12):860-864.
100. Diaz Mendez AB, Sacconi A, Tremante E, et al. A diagnostic circulating miRNA signature as orchestrator of cell invasion via TKS4/TKS5/EFHD2 modulation in human gliomas. *J Exp Clin Cancer Res.* 2023;42(1):66.

List of Publications between November 2021 and January 2024

1. “Anatomical study of the mastoid foramina and mastoid emissary veins: classification and application to localizing the sigmoid sinus” – Chaiyamoon A., Schneider K., Iwanaga J., **Donofrio C.A.,** Badaloni F., Fioravanti A., Tubbs R.S. – Neurosurg Rev. 2023 Dec 19;47(1):16. doi: 10.1007/s10143-023-02229-4.
2. “An anatomical study of the sigmoid sinus artery: Application to the transmastoid approach” – Iwanaga J., Jackson N., Komune N., Johnson K., **Donofrio C.A**., Badaloni F., Fioravanti A., Dumont A.S., Tubbs R.S. – Neurosurg Rev. 2023 Dec 7;47(1):4. doi: 10.1007/s10143-023-02245-4.
3. “Omics sciences and precision medicine in breast and ovarian cancer” – Bonetti G., Madeo G., Michelini S., Ricci M., Cestari M., Michelini S., Gadler M., Benedetti S., Guerri G., Cristofoli F., Generali D., **Donofrio C.A**., Cominetti M., Fioravanti A., Riccio L., Bernini A., Fulcheri E., Stuppia L., Gatta V., Cecchin S., Marceddu G., Bertelli M. – Clin Ter. 2023 Nov-Dec;174(Suppl 2(6)):104-118. doi: 10.7417/CT.2023.2477.
4. “Omics sciences and precision medicine in prostate cancer” – Medori M.C., Micheletti C., Gadler M., Benedetti S., Guerri G., Cristofoli F., Generali D., **Donofrio C.A.,** Cominetti M., Fioravanti A., Riccio L., Bernini A., Fulcheri E., Calogero A.E., Cannarella R., Stuppia L., Gatta V., Cecchin S., Marceddu G., Bertelli M. – Clin Ter. 2023 Nov-Dec;174(Suppl 2(6)):95-103. doi: 10.7417/CT.2023.2476.
5. “Omics sciences and precision medicine in pancreas cancer” – Donato K., Micheletti C., Medori M.C., Maltese P.E., Tanzi B., Tezzele S., Mareso C., Generali D., **Donofrio C.A**., Cominetti M., Fioravanti A., Riccio L., Beccari T., Ceccarini M.R., Iaconelli A., Aquilanti B., Matera G., Ahmed R., Stuppia L., Gatta V., Cecchin S., Marceddu G., Bertelli M. – Clin Ter. 2023 Nov-Dec;174(Suppl 2(6)):85-94. doi: 10.7417/CT.2023.2475.
6. “Omics sciences and precision medicine in glioblastoma” – Micheletti C., Bonetti G., Madeo G., Gadler M., Benedetti S., Guerri G., Cristofoli F., Generali D., **Donofrio C.A**., Cominetti M., Fioravanti A., Riccio L., Manganotti P., Caruso P., Bernini A., Fulcheri E., Stuppia L., Gatta V., Cecchin S., Marceddu G., Bertelli M. – Clin Ter. 2023 Nov-Dec;174(Suppl 2(6)):77-84. doi: 10.7417/CT.2023.2474.
7. “Omics sciences and precision medicine in sarcoma” – Bonetti G., Donato K., Dhuli K., Gadler M., Benedetti S., Guerri G., Cristofoli F., Generali D., **Donofrio C.A**., Cominetti M., Fioravanti A., Riccio L., Bernini A., Fulcheri E., Cavalca D., Stuppia L., Gatta V., Cristoni S., Cecchin S., Marceddu G., Bertelli M. – Clin Ter. 2023 Nov-Dec;174(Suppl 2(6)):68-76. doi: 10.7417/CT.2023.2473.
8. “Omics sciences and precision medicine in colon cancer” – Madeo G., Bonetti G., Gadler M., Benedetti S., Guerri G., Cristofoli F., Generali D., **Donofrio C.A.,** Cominetti M., Fioravanti A., Riccio

L., Bernini A., Fulcheri E., Iaconelli A., Aquilanti B., Matera G., Stuppia L., Gatta V., Cecchin S., Marceddu G., Bertelli M. – Clin Ter. 2023 Nov-Dec;174(Suppl 2(6)):55-67. doi: 10.7417/CT.2023.2472.

9. "Omics sciences and precision medicine in kidney cancer" – Dhuli K., Micheletti C., Medori M.C., Maltese P.E., Tanzi B., Tezzele S., Mareso C., Generali D., **Donofrio C.A.**, Cominetti M., Fioravanti A., Riccio L., Beccari T., Ceccarini M.R., Stuppia L., Gatta V., Cristoni S., Cecchin S., Marceddu G., Bertelli M. – Clin Ter. 2023 Nov-Dec;174(Suppl 2(6)):46-54. doi: 10.7417/CT.2023.2471.

10. "Omics sciences and precision medicine in lung cancer" – Micheletti C., Dhuli K., Donato K., Gadler M., Benedetti S., Guerri G., Cristofoli F., Generali D., **Donofrio C.A.,** Cominetti M., Fioravanti A., Riccio L., Bernini A., Fulcheri E., Stuppia L., Gatta V., Cristoni S., Cecchin S., Marceddu G., Bertelli M. – Clin Ter. 2023 Nov-Dec;174(Suppl 2(6)):37-45. doi: 10.7417/CT.2023.2470.

11. "Omics sciences and precision medicine in melanoma" – Medori M.C., Donato K., Dhuli K., Maltese P.E., Tanzi B., Tezzele S., Mareso C., Miertus J., Generali D., **Donofrio C.A.,** Cominetti M., Fioravanti A., Riccio L., Beccari T., Ceccarini M.R., Gisondi P., Bellinato F., Stuppia L., Gatta V., Cecchin S., Marceddu G., Bertelli M. – Clin Ter. 2023 Nov-Dec;174(Suppl 2(6)):29-36. doi: 10.7417/CT.2023.2469.

12. "Omics sciences and precision medicine in testicular cancer" – Madeo G., Bonetti G., Maltese P.E., Tanzi B., Tezzele S., Mareso C., Agostini F., Generali D., **Donofrio C.A**., Cominetti M., Fioravanti A., Riccio L., Beccari T., Ceccarini M.R., Calogero A.E., Cannarella R., Stuppia L., Gatta V., Nughman M., Cecchin S., Marceddu G., Bertelli M. – Clin Ter. 2023 Nov-Dec;174(Suppl 2(6)):21-28. doi: 10.7417/CT.2023.2468.

13. "Omics sciences and precision medicine in thyroid cancer" – Dhuli K., Medori M.C., Donato K., Maltese P.E., Tanzi B., Tezzele S., Mareso C., Miertus J., Generali D., **Donofrio C.A**., Cominetti M., Fioravanti A., Riccio L., Beccari T., Ceccarini M.R., Stuppia L., Gatta V., Cristoni S., Cecchin S., Marceddu G., Bertelli M. – Clin Ter. 2023 Nov-Dec;174(Suppl 2(6)):11-20. doi: 10.7417/CT.2023.2467.

14. "Omics sciences and precision medicine in Urothelial Carcinoma" – Medori M.C., Micheletti C., Madeo G., Maltese P.E., Tanzi B., Tezzele S., Mareso C., Generali D., **Donofrio C.A**., Cominetti M., Fioravanti A., Riccio L., Beccari T., Ceccarini M.R., Stuppia L., Gatta V., Cristoni S., Ahmed R., Cecchin S., Marceddu G., Bertelli M. – Clin Ter. 2023 Nov-Dec;174(Suppl 2(6)):1-10. doi: 10.7417/CT.2023.2466.

15. "Intrasellar dermoid cyst: case report of a rare lesion and systematic literature review comparing intrasellar, suprasellar and parasellar locations" – **Donofrio C.A.,** Bertazzoni G., Riccio L., Pinacoli A., Pianta L., Generali D., Ungari M., Servadei F., Roncaroli F., Fioravanti A. – World Neurosurg. 2023 Nov 21:S1878-8750(23)01619-4. doi: 10.1016/j.wneu.2023.11.057. Online ahead of print.

16. “Endoscope-Assisted Microvascular Decompression of Cochleo-Vestibular Nerve for Treating Unilateral Pulsatile Tinnitus, Sensorineural Hearing Loss, and Paroxysmal Vertigo: 2-Dimensional Operative Video” – **Donofrio C.A**., Riccio L., Badaloni F., Rosellini E., Servadei F., Fioravanti A. – Oper Neurosurg (Hagerstown). 2023 Nov 1;25(5):e277-e278. doi: 10.1227/ons.0000000000000830. Epub 2023 Jul 11.

17. “Colorectal carcinoma to pituitary tumour: tumour to tumour metastasis” – **Donofrio C.A**.*, Pizzimenti C.*, Djoukhadar I., Kearney T., Gnanalingham K., Roncaroli F. – Br J Neurosurg. 2023 Oct;37(5):1367-1370. doi: 10.1080/02688697.2020.1823937. Epub 2020 Sep 21.

18. “How I do it – The "drum skin" duraplasty technique after foramen magnum decompression for Chiari malformations” – Fioravanti A., Badaloni F., Tubbs R.S., **Donofrio C.A**. – Acta Neurochir (Wien). 2023 Oct;165(10):3045-3050. doi: 10.1007/s00701-023-05576-9. Epub 2023 Apr 15.

19. “The Occipitalis Muscle as an Adjunct Superficial Landmark for the Transverse Sinus and Transverse-Sigmoid Junction: An Anatomical Study With Application to Posterior Cranial Fossa Surgery” – Gilkes A., Rajaram-Gilkes M., Cardona J.J., Reina F., Carrera A., Iwanaga J., Dumont A.S., **Donofrio C.A**., Badaloni F., Fioravanti A., Tubbs R.S. – Cureus. 2023 May 30;15(5):e39723. doi: 10.7759/cureus.39723. eCollection 2023 May.

20. “A Newly Discovered Dural Venous Sinus of the Skull Base: The Anterior Petroclinoid Sinus” – Spencer P.S., Cardona J.J., Reina F., Carrera A., Iwanaga J., Dumont A.S., **Donofrio C.A**., Badaloni F., Fioravanti A., Tubbs R.S. – World Neurosurg. 2023 Apr;172:e581-e584. doi: 10.1016/j.wneu.2023.01.087. Epub 2023 Jan 27.

21. “Transcortical endoportal subchoroidal endoscope-assisted approach to the third ventricle: from virtual reality to anatomical laboratory” **– Donofrio C.A**., Riccio L., Capitanio J.F., Herur-Raman A., Panni P., Gagliardi F., Caputy A.J., Mortini P. – J Neurosurg Sci. 2023 Apr;67(2):175-184. doi: 10.23736/S0390-5616.20.05122-X. Epub 2020 Sep 28

22. “Posterior petrous meningiomas: surgical classification and postoperative outcomes in a case series of 130 patients operated via the retrosigmoid approach” – **Donofrio C.A**., Badaloni F., Riccio L., Morandini A., Bertuccio A., Generali D., Calbucci F., Servadei F., Fioravanti A. – World Neurosurg. 2023 Mar;171:e301-e308. doi: 10.1016/j.wneu.2022.12.022. Epub 2022 Dec 10.

23. “Analysis of PD-L1 and CD3 Expression in Glioblastoma Patients and Correlation with Outcome: A Single Center Report” – Sobhani N., Bouchè V., Aldegheri G., Rocca A., D’Angelo A., Giudici F., Bottin C., **Donofrio C.A**., Pinamonti M., Ferrari B., Panni S., Cominetti M., Aliaga J., Ungari M., Fioravanti A., Zanconati F., Generali D. – Biomedicines. 2023 Jan 22;11(2):311. doi: 10.3390/biomedicines11020311.

24. “A challenging case of sporadic melanocytoma of the jugular foramen.” – **Donofrio C.A.,** Roncaroli F., Riccio L., Pereira M., O’Sullivan J., Mayers H., Potter G.M., Djoukhadar I., Rutherford S.A. – Neurochirurgie 2022 Jul;68(4):453-457. doi: 10.1016/j.neuchi.2021.06.001. Epub 2021 Jun 19.

25. “Classificazione e nomenclatura dei tumori neuroendocrini dell’ipofisi anteriore” – Roncaroli F., **Donofrio C.A.** – L’Endocrinologo 2022. https://doi.org/10.1007/s40619-022-01039-y

26. “Endoscopic sublabial transmaxillary approach to the inferior orbit: pearls and pitfalls – A comparative anatomical study” – **Donofrio C.A**., Riccio L., Pathmanaban O.N., Fioravanti A., Caputy A.J., Mortini P. – Neurosurg Rev 2021 Dec;44(6):3297-3307. doi: 10.1007/s10143-021-01494-5. Epub 2021 Feb 10.

27. “BRAF Signaling Inhibition in Glioblastoma: Which Clinical Perspectives?” – Bouchè V., Aldegheri G., **Donofrio C.A.,** Fioravanti A., Roberts-Thomson S., Fox S.B., Schettini F., Generali D. – Front Oncol. 03 Nov 2021. doi: 10.3389/fonc.2021.772052. eCollection 2021.

28. “Microsurgical endoportal MRI/US-navigated approach for the resection of large intraventricular tumours: a 20-consecutive patients case series.” – Capitanio J.F., **Donofrio C.A.,** Panni P., Barzaghi L.R., Bailo M., Gagliardi F., Mortini P. – Br J Neurosurg. 2021 Oct;35(5):570-577. doi: 10.1080/02688697.2021.1918632. Epub 2021 Aug 5

29. “Malignant behaviour of primary intracranial Rosai Dorfman disease: A rare presentation of a benign disease” – Riccio L.*, **Donofrio C.A**.*, Serio G., Melatini A. – Neurochirurgie 2021 Apr;67(2):205-209. doi: 10.1016/j.neuchi.2020.11.006. Epub 2020 Dec 1. 2.

List of Abstracts, Posters and Oral Presentations between November 2021 and January 2024

1. XXVI Congresso Nazionale e Corso Residenziale dell’Associazione Italiana di Neuro-Oncologia – 23-25 November 2023 – Messina, Italy – “Determination of plasmatic microRNA levels by ddPCR as peripheral glioblastoma biomarkers” – **Donofrio C.A.,** Fioravanti A., Riccio L., Cominetti M., Cappelletti M.R., Ungari M., Generali D., Grossi I., Pelisenco I., De Petro G., Salvi A.

2. 72° Congresso Nazionale SINch 2023 – 12-14 October 2023 – Padua, Italy – “Combined endoscopic transorbital and transmaxillary approach to the infratemporal fossa: anatomical feasibility study” – Corrivetti F., **Donofrio C.A**., Riccio L., Fioravanti A.

3. 72° Congresso Nazionale SINch 2023 – 12-14 October 2023 – Padua, Italy – “Transcranial approaches to tuberculum sellae meningiomas: the ‘dark side of the moon’ in the endoscopic endonasal era” – **Donofrio C.A**., Riccio L., Badaloni F., Bresciani E., Muzzi M., Grappa E., Morandini A., Fioravanti A.

4. 72° Congresso Nazionale SINch 2023 – 12-14 October 2023 – Padua, Italy – “Unilateral pulsatile tinnitus, sensorineural hearing loss and paroxysmal vertigo: endoscopeassisted microvascular decompression of cochleo-vestibular nerve” – **Donofrio C.A**., Riccio L., Badaloni F., Rosellini E., Servadei F., Fioravanti A.

5. 72° Congresso Nazionale SINch 2023 – 12-14 October 2023 – Padua, Italy – “Endoscope-assisted microvascular decompression for trigeminal neuralgia: preliminary results in a cohort of 30 consecutive patients” **– Donofrio C.A**., Riccio L., Bianchini S., Fioravanti A.

6. 72° Congresso Nazionale SINch 2023 – 12-14 October 2023 – Padua, Italy – "Five-aminolevulinic acid-guided glioblastoma surgery: can surgeons rely only on fluorescence? a comparative surgical and histopathological study on 97 patients" – Fioravanti A., Riccio L., Cominetti M., Cappelletti M.R., D'Auria P., Paioli G., Farinaro G., Generali D., Grappa E., Ungari M., **Donofrio C.A.**

7. 72° Congresso Nazionale SINch 2023 – 12-14 October 2023 – Padua, Italy – "The immune microenvironment in glioblastoma: PD-L1 expression and tumour infiltrating lymphocytes – new potential therapeutic targets" – **Donofrio C.A**., Sobhani N., Bouché V., Aldegheri G., Rocca A., D'Angelo A., Giudici F., Bottin C., Pinamonti M., Cominetti M., Beretta E., Riccio L., Ungari M., Zanconati F., Generali D., Fioravanti A.

8. 72° Congresso Nazionale SINch 2023 – 12-14 October 2023 – Padua, Italy – "Combined endoscopic endonasal transclival and contralateral transmaxillary approach to the petrous apex and the petroclival fissure – a reverse translational anatomical study" – **Donofrio C.A.,** Corrivetti F., Riccio L., Fioravanti A., De Notaris M.

9. 72° Congresso Nazionale SINch 2023 – 12-14 October 2023 – Padua, Italy – "Postoperative outcomes in a series of 130 posterior petrous meningiomas operated via the retrosigmoid approach" – **Donofrio C.A**., Badaloni F., Riccio L., Morandini A., Bertuccio A., Generali D., Calbucci F., Servadei F., Fioravanti A.

10. 72° Congresso Nazionale SINch 2023 – 12-14 October 2023 – Padua, Italy – "Vertigini come sintomo d'esordio della sindrome da ipotensione liquorale" – Bianchini S.C.P.G., **Donofrio C.A.,** Ambrosi C., Beretta E., D'Auria P., Morandini A., Muzzi M., Paioli G., Riccio L., Fioravanti A.

11. 72° Congresso Nazionale SINch 2023 – 12-14 October 2023 – Padua, Italy – "Cisti sinoviali della colonna lombare: diagnosi e trattamento. nostra esperienza" – Muzzi M., Morandini A., Paioli G., Bianchini S., **Donofrio C.A**., D'Auria P., Riccio L., Fioravanti A.

12. 72° Congresso Nazionale SINch 2023 – 12-14 October 2023 – Padua, Italy – "Gestione perioperatoria multidiscipilinare e setting intraoperatorio nella "chirurgia da sveglio" per lesioni cerebrali in aree eloquenti" – D'Auria P., **Donofrio C.A**., Grappa E., Subacchi S., Maccabelli G., Bianchini S., Morandini A., Muzzi M., Paioli G., Riccio L., Fioravanti A.

13. 72° Congresso Nazionale SINch 2023 – 12-14 October 2023 – Padua, Italy – ""Hybrid" surgical treatment (open and endovascular) of a vertebral artery thrombosed giant aneurysm: case report and operative video" – Rosellini E., Raspagliesi L., Farinaro G., **Donofrio C.A**., Paioli G., Muzzi M., Fioravanti A.

14. 72° Congresso Nazionale SINch 2023 – 12-14 October 2023 – Padua, Italy – "Exeresi microchirurgica per via suboccipitale retrosigmoidea di un meningioma premeatale della faccia posteriore della rocca petrosa" – Bresciani E., **Donofrio C.A**., Farinaro G., Rosellini E., Morandini A., Bianchini S., Beretta E., Fioravanti A.

15. 72° Congresso Nazionale SINch 2023 – 12-14 October 2023 – Padua, Italy – “Surgical technique resection of a bleeding brainstem cavernoma: case report and operative video” – Farinaro G., Rosellini E., **Donofrio C.A.,** Morandini A., Riccio L., Fioravanti A.

16. 2023 CNS (Congress of Neurological Surgeons) Annual Meeting – 9-13 September 2023 – Washington D.C., U.S.A. – “The Posterior Auricular Muscle as a Superficial Landmark for the Sigmoid Sinus and Transverse-Sigmoid Sinus Junction: An Anatomical Study” – **Donofrio C.A**., Cardona J.J., Riccio L., Chaiyamoon A., Shekhawat D., Iwanaga J., Dumont A.S., Badaloni F., Jackson N., Tubbs R.S., Fioravanti A.

17. 71° Congresso Nazionale SINch 2022 – 13-15 October 2022 – Naples, Italy – “Contralateral transmaxillary approaches: the Caldwell-Luc approach revival for ventral skull base surgery” – **Donofrio C.A**., de Notaris M., Corrivetti F., Morandini A., Riccio L., Fioravanti A.

18. 71° Congresso Nazionale SINch 2022 – 13-15 October 2022 – Naples, Italy – “Endoscopic transorbital approaches: pearls of orbital anatomy for neurosurgeons” – **Donofrio C.A**., Riccio L., Badaloni F., Fioravanti A.

19. EACR (European Association for Cancer Research) Liquid Biopsies – 24-26 May 2022 – Bergamo, Italy – “Determination of plasmatic microRNA levels by ddPCR as peripheral biomarkers for IDH-wild type glioblastomas: a pilot study” – **Donofrio C.A**., Fioravanti A., Riccio L., Cominetti M., Cappelletti M.R., Generali D., Grossi I., De Petro G., Salvi A.

20. 70° Congresso Nazionale SINch 2021 – 14-16 October 2021 – Milan, Italy – “Covid-19 pandemic affected surgical treatment of elderly patients with glioblastoma: the Cremona Hub experience in the ‘Hub-Spokes’ model” – **Donofrio C.A.,** Nodari G., Bianchini S., d’Auria P., Muzzi M., Aliaga Arias J.M., Riccio L., Giudici S., Valtulina C., Morandini A., Fioravanti A.

21. 70° Congresso Nazionale SINch 2021 – 14-16 October 2021 – Milan, Italy – “‘Combined cranio-nasal approach’: transcranial and endoscopic endonasal combined approaches to treat invasive tumours of the anterior cranial fossa” – **Donofrio C.A.,** Riccio L., Nodari G., Paioli G., Grappa E., Morandini A., Fioravanti A.

22. 70° Congresso Nazionale SINch 2021 – 14-16 October 2021 – Milan, Italy – “Surgical treatment of supratentorial meningiomas in elderly patients: safety and efficacy” – **Donofrio C.A.,** d’Auria P., Bianchini S., Nodari G., Ambrosi C., Besana M., Varotti E., Ungari M., Valtulina C., Fioravanti A.

23. 70° Congresso Nazionale SINch 2021 – 14-16 October 2021 – Milan, Italy – “Surgical treatment of glioblastoma in elderly patients: a monocentric and retrospective study” – **Donofrio C.A.,** Cappelletti M., Catenacci E., Aliaga Arias J.M., Subacchi S., Generali D., Maccabelli G., Varotti E., Ungari M., Riccio L., Giudici S., Morandini A., Fioravanti A.

24. 70° Congresso Nazionale SINch 2021 – 14-16 October 2021 – Milan, Italy – “Functional performances in elderly neuro-oncological patients” – Aliaga Arias J.M., Subacchi S., **Donofrio C.A.,** Catenacci E., Paioli G., Grappa E., Muzzi M., Morandini A., Fioravanti A.

25. eEANS 2021: Neurosurgery in translation – 03-07 October 2021 – Virtual Congress – “Meningiomas of the posterior petrous bone: surgical anatomy and postoperative results of 130 consecutive patients” – **Donofrio C.A**., Badaloni F., Nodari G., Paioli G., d’Auria P., Muzzi M., Calbucci F., Fioravanti A.

26. eEANS 2021: Neurosurgery in translation – 03-07 October 2021 – Virtual Congress – “Haemorrhagic brainstem cavernous malformation: early and long term functional outcomes after microsurgical resection” – **Donofrio C.A**., Badaloni F., Aliaga Arias J.M., Valtulina C., Bianchini S., Catenacci E., Morandini A., Calbucci F., Fioravanti A.

27. eEANS 2021: Neurosurgery in translation – 03-07 October 2021 – Virtual Congress – “Degenerative cervical myelopathy: the preoperative Nurick score as predictor of surgical outcomes” – **Donofrio C.A**., Muzzi M., Catenacci E., Paioli G., Nodari G., Valtulina C., Morandini A., Fioravanti A.